Appendix 1

Physical Environmental Study for the Northeaster Grand Banks

Physical Environmental Study for the Northeaster Grand Banks

Submitted To:
LGL Limited
388 Kenmount Road
St. John's, NL A1B 4A5

Submitted By;
Oceans Ltd.
85 LeMarchant Road
St. John's, NL
A1C 2H1

April 2005

Table of Contents

1 Climatology

The climatology presented in this report has been prepared from two data sources. They are:

- AES-40 wind and wave hindcast dataset covering the North Atlantic Ocean that was developed by Oceanweather Inc. of Cos Cob, Connecticut under contract to the Meteorological Service of Canada (MSC), and
- Comprehensive Ocean-Atmosphere Data Set (COADS) Long Marine Report (LMR) dataset consisting of marine weather and sea state observations from vessels and platforms at sea obtained from MSC.

In its earlier versions, the AES-40 data set consisted of 40, then 42, continuous years of hindcast wind and wave data. The results of the NCAR/NCEP (U.S. National Centers for Environmental Prediction) global re-analysis for 1958-97 wind fields were used as input to a third generation deep water wave model (Berek et al., 2000). The winds were first modified by adding measured winds from buoys and platforms. Tropical cyclone wind fields were generated and added to the background winds. The wind fields were then refined using Oceanweather's Interactive Objective Kinematic Analysis System. The model grid spacing was 0.625º latitude by 0.833º longitude.

Currently, the AES-40 hindcast dataset provides wind velocity and sea state parameter data at 6-hour intervals for the 49 year period from July 01, 1954 through June 30, 2003. The wind and wave statistics presented in this report are based on the hindcast data for AES-40 grid point 5622, at location 46.88° N, 48.33° W. Data were extracted from the dataset using Oceanweather's OSMOSIS software. Some of the statistics presented were output directly by OSMOSIS, others were computed using in-house developed software. No quality control of this dataset was necessary.

The temperature and visibility statistics presented in this report were developed from the COADS LMR observational dataset for the period 1950 through 1995. Reports from the area bounded by latitudes 46.50° N and 47.25° N and longitudes 47.50° W and 48.50° W were incorporated in the statistics. The COADS dataset is noisy and contains observation and position errors, as well as coding mistakes. For this work, positions were assumed to be correct. Otherwise, software filters were used to quality control the data in an effort to reduce the number of erroneous reports. The software to select COADS LMR observations, carry out the quality control, and prepare the statistics was developed in-house at Oceans Ltd.

Location map

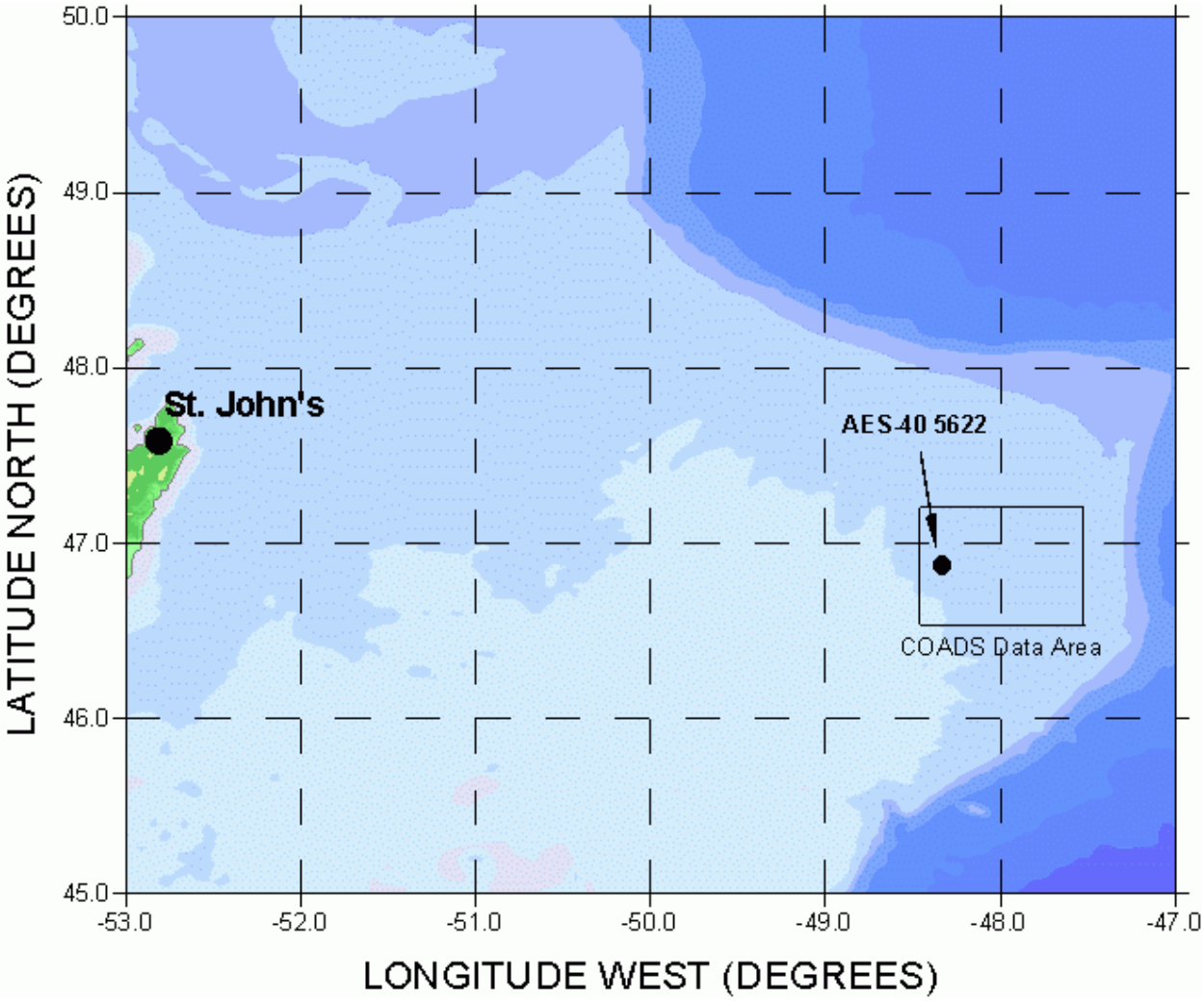

Figure 1.1 General Location Map showing the position of AES-40 grid point 5622 and the COADS data area.

1.1 Wind Climatology

The wind climatology for AES-40 grid point 5622 and vicinity is summarized below in a series of tables and plots. Table 1.1 provides basic descriptive statistics for winds at a 10 m level above the surface on a monthly basis and for the full 49-year period. The table shows that the mean or most frequent wind direction is from the west to west-southwest during the winter season, while southwesterly winds prevail during the summer months. Monthly wind speeds are lowest during the months of June, July, and August as expected. Average wind speeds are notably higher during the winter months, with maximum monthly winds having exceeded 30 m/s in February. Standard deviations, a measure of the variability about the monthly means, are smallest during the summer and larger in the cold season, typical of the Grand Banks climatology.

Table 1.1 Monthly 10 m Wind Direction and Speed Statistics.

Monthly and Annual 10 m Wind Statistics at AES-40 Grid Point 5622						
Month	Wind Direction (degrees True)	Wind Speed (metres / second)				
	Mean	Min	Max	Mean	Std Dev.	Median
January	261	0.5	26.9	10.7	4.5	10.5
February	264	0.8	30.1	10.7	4.5	10.5
March	265	0.4	28.9	9.7	4.3	9.5
April	248	0.4	26.8	8.2	3.9	7.9
May	239	0.2	21.1	7.0	3.5	6.7
June	229	0.3	21.8	6.5	3.2	6.3
July	222	0.2	20.2	6.2	2.9	6.1
August	228	0.3	21.6	6.5	3.1	6.3
September	251	0.3	23.3	7.4	3.6	7.1
October	260	0.3	26.3	8.7	3.9	8.4
November	255	0.5	25.9	9.4	4.2	9.0
December	260	0.6	29.3	10.4	4.5	10.2
Annual	247	0.2	30.1	8.5	4.2	8.0

Source: Grid point 5622, AES-40 wind and wave hindcast dataset (July 01, 1954 through June 30, 2003)

Table 1.2 presents maximum wind speeds (at 10 m above sea level) by direction for each month and for the full 49-year period. The highest winds are from the southwest through northern sectors. High wind speeds during the late summer months may be caused by tropical cyclones or their remnants, or by energetic extra-tropical low pressure systems.

Table 1.2 Monthly 10 m Wind Speed Statistics by Direction.

Monthly and Annual Maximum 10 m Wind Speeds										
	(metres / second)									
	True Wind Direction (center of 45 degree sector)									
Month	NE	E	SE	S	SW	W	NW	N	All Directions	
	045	090	135	180	225	270	315	360	Lowest	Highest
January	20.0	23.1	24.2	26.9	26.0	26.7	25.2	22.7	20.0	26.9
February	26.4	21.7	25.7	25.2	30.1	26.7	26.7	29.3	21.7	30.1
March	21.5	20.8	23.5	21.6	23.5	24.2	28.9	26.1	20.8	28.9
April	22.4	21.0	21.1	26.8	22.6	21.6	23.6	23.9	21.0	26.8
May	16.6	16.7	18.1	19.3	20.1	19.0	21.1	20.6	16.6	21.1
June	15.0	18.7	19.0	20.0	19.0	21.5	21.8	13.9	13.9	21.8
July	15.6	19.1	15.9	18.2	20.2	17.0	16.4	14.8	14.8	20.2
August	18.3	17.0	18.7	21.2	17.9	19.8	18.1	21.6	17.0	21.6
September	21.9	20.6	18.6	23.3	22.3	22.1	22.7	22.1	18.6	23.3
October	21.6	18.2	20.4	23.9	25.5	26.3	22.5	25.0	18.2	26.3
November	23.0	22.0	20.9	25.8	21.5	24.0	24.8	25.9	20.9	25.9
December	20.5	21.5	23.7	21.6	26.7	28.6	29.3	28.2	20.5	29.3
Annual	26.4	23.1	25.7	26.9	30.1	28.6	29.3	29.3	21.7	30.1

Source: Grid point 5622, AES-40 wind and wave hindcast dataset (July 01, 1954 through June 30, 2003)

1.1.1 Wind Rose Plots

Table 1.3 shows the percent frequency of occurrence of wind speed by 45-degree direction sector for all months and years. Again, this shows the prevalence of southwest and west winds with the highest winds from the southwest and northwest quadrants. A graphic representation of these data in the form of a wind rose plot is shown as Figure 1.2.

Monthly tables of the percent frequency of occurrence wind speed by direction and corresponding wind rose diagrams are contained in Appendix A.

Table 1.3 Percentage Occurrence of Wind Speed by Direction for all Months and All Years.

Wind Speed Range (m/s)	Center of 45 Degree Direction Bins								
	045	**090**	**135**	**180**	**225**	**270**	**315**	**360**	**Totals**
0.0 - < 5.0	1.67	1.79	2.38	3.54	4.60	3.70	2.44	1.90	22.02
5.0 - < 10.0	2.48	2.28	3.25	6.74	11.96	9.22	5.96	3.59	45.48
10.0 - < 15.0	1.04	0.87	1.56	3.41	5.19	6.33	4.53	1.92	24.85
15.0 - < 20.0	0.25	0.20	0.45	1.03	1.12	1.92	1.27	0.46	6.70
20.0 - < 25.0	0.04	0.02	0.04	0.10	0.13	0.29	0.19	0.08	0.88
25.0 - < 30.0	0.00	0.00	0.00	0.01	0.01	0.02	0.01	0.01	0.07
30.0 - < 35.0	0.00	0.00	0.00	0.00	0.00	0.00	0.00	0.00	0.00
Totals	5.48	5.16	7.68	14.82	23.01	21.48	14.40	7.96	100.00

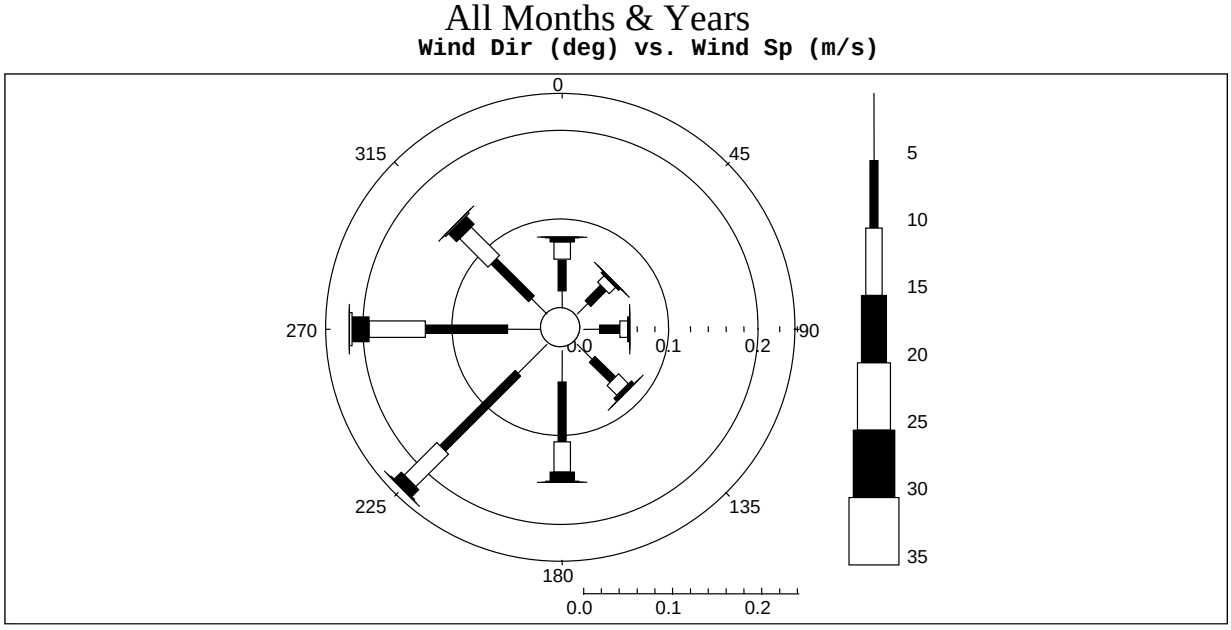

Source: Grid point 5622, AES-40 wind and wave hindcast dataset (July 01, 1954 through June 30, 2003)

Figure 1.2 Wind Rose for All Months and Years, July 1954 through June 2003.

1.1.2 Monthly Percent Exceedance of the 10 m Wind Speed

Table 1.4 shows the percentage exceedance of the 10 m wind speed for each month of the year computed from the entire 49-year dataset. The exceedance values are plotted in Figures 1.3 and 1.4. Figure 1.3, which shows curves for the months of January through to July, illustrates the progression from winter conditions to the more benign summer conditions. Figure 1.4 shows the monthly progression from the summer (July) through to the winter season as conditions become more boisterous. Gale and storm force wind speed limits are also shown on the plots. Winds are gale force between 34 to less than 48 knots (17.5 m/s - 24.7 m/s) and storm force wind when 48 knots (24.7 m/s) or more.

Table 1.4 Percentage Exceedances of 10 m Wind Speeds

Wind Speed (m/s)	Percentage Exceedance of Wind Speed (%)											
	Jan	Feb	Mar	Apr	May	Jun	Jul	Aug	Sep	Oct	Nov	Dec
0	100.0	100.0	100.0	100.0	100.0	100.0	100.0	100.0	100.0	100.0	100.0	100.0
1	99.9	99.9	99.5	99.6	98.1	98.1	97.5	98.6	99.0	99.7	99.7	99.8
2	98.9	98.9	97.7	97.1	93.1	93.4	92.6	94.5	96.0	97.5	98.4	98.7
3	96.7	97.3	94.7	92.3	87.1	86.5	85.3	87.7	90.8	94.0	95.7	96.2
4	93.7	94.2	90.6	85.9	78.8	77.6	75.8	77.2	83.4	88.7	91.5	92.9
5	89.3	90.0	85.5	77.9	69.4	66.3	64.2	65.8	73.1	81.4	85.1	88.5
6	84.1	84.1	78.8	69.2	57.5	54.3	51.5	53.1	61.9	72.9	77.4	82.7
7	78.4	78.1	71.7	58.5	46.7	42.3	39.0	40.2	51.2	63.3	69.0	75.7
8	70.9	70.7	64.3	48.6	35.9	30.5	26.8	28.6	40.3	54.3	60.2	67.9
9	63.4	62.6	55.3	39.0	26.6	21.7	16.0	19.0	30.3	44.6	50.4	60.0
10	54.4	54.3	46.0	30.7	19.3	14.6	9.3	12.8	21.9	34.8	41.8	51.4
11	46.0	45.6	37.0	23.4	13.2	8.5	5.2	7.9	15.2	26.4	33.6	43.1
12	37.8	37.0	29.1	16.9	9.1	5.3	2.9	5.3	10.3	19.2	26.7	35.3
13	30.2	29.1	22.5	12.0	5.9	3.2	1.7	3.5	7.2	13.6	20.4	28.3
14	23.4	22.6	16.5	7.9	3.3	1.8	0.9	2.0	4.6	9.0	14.9	21.9
15	17.5	17.5	11.4	5.3	2.1	0.8	0.5	1.2	3.0	6.2	10.2	16.6
16	13.0	12.4	7.9	3.6	1.3	0.5	0.2	0.7	1.9	4.1	6.9	11.8
17	9.1	8.8	5.2	2.1	0.6	0.3	0.1	0.3	1.4	2.6	4.5	7.7
18	6.4	6.2	3.3	1.3	0.3	0.2	0.0	0.2	1.0	1.7	2.9	5.3
19	4.3	4.3	1.6	0.7	0.2	0.1	0.0	0.1	0.6	0.9	1.7	3.5
20	3.0	3.1	1.0	0.5	0.1	0.0	0.0	0.0	0.3	0.6	1.0	1.9
21	2.0	2.2	0.6	0.4	0.0	0.0	0.0	0.0	0.2	0.3	0.6	1.3
22	1.0	1.5	0.3	0.2	0.0	0.0	0.0	0.0	0.1	0.1	0.3	0.8
23	0.6	0.9	0.2	0.1	0.0	0.0	0.0	0.0	0.0	0.1	0.2	0.6
24	0.3	0.6	0.1	0.0	0.0	0.0	0.0	0.0	0.0	0.0	0.1	0.3
25	0.2	0.4	0.0	0.0	0.0	0.0	0.0	0.0	0.0	0.0	0.0	0.2
26	0.1	0.2	0.0	0.0	0.0	0.0	0.0	0.0	0.0	0.0	0.0	0.1
27	0.0	0.1	0.0	0.0	0.0	0.0	0.0	0.0	0.0	0.0	0.0	0.1
28	0.0	0.1	0.0	0.0	0.0	0.0	0.0	0.0	0.0	0.0	0.0	0.0
29	0.0	0.1	0.0	0.0	0.0	0.0	0.0	0.0	0.0	0.0	0.0	0.0
30	0.0	0.0	0.0	0.0	0.0	0.0	0.0	0.0	0.0	0.0	0.0	0.0

Source: Grid point 5622, AES-40 wind and wave hindcast data set (July 01, 1954 through June 30, 2003)

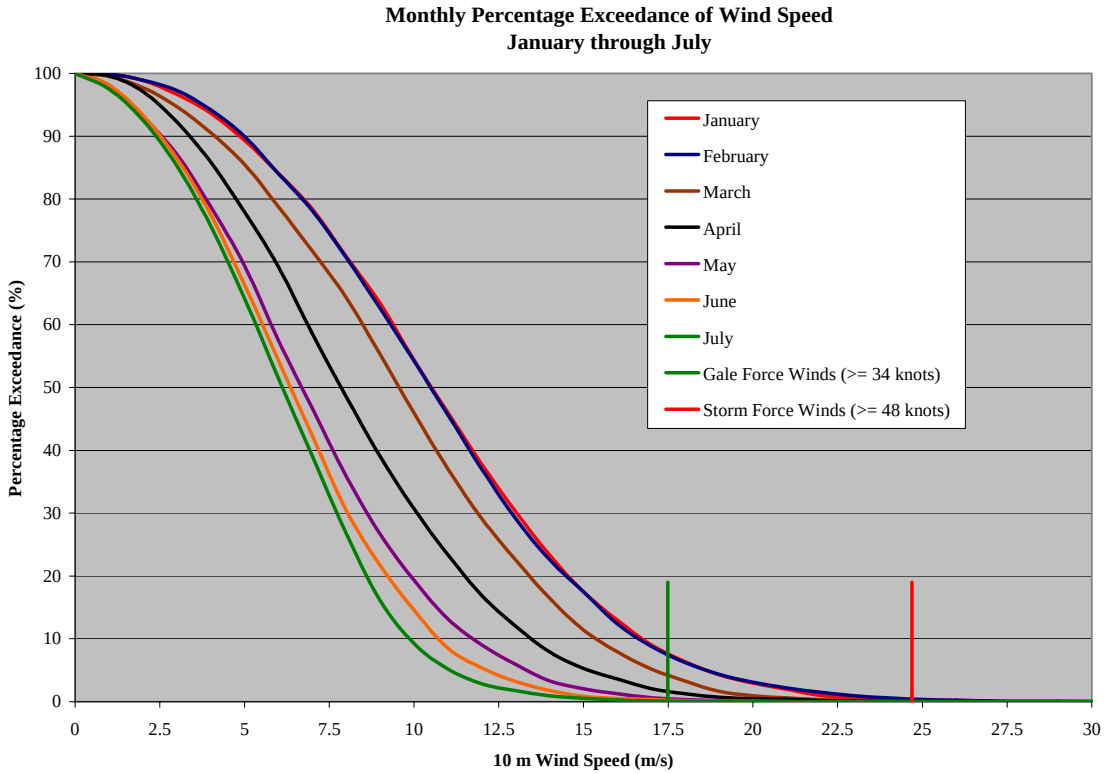

Source: Grid point 5622, AES-40 wind and wave hindcast dataset (July 01, 1954 through June 30, 2003)

Figure 1.3 Monthly Percentage Exceedances of 10 m Wind Speed - January through July

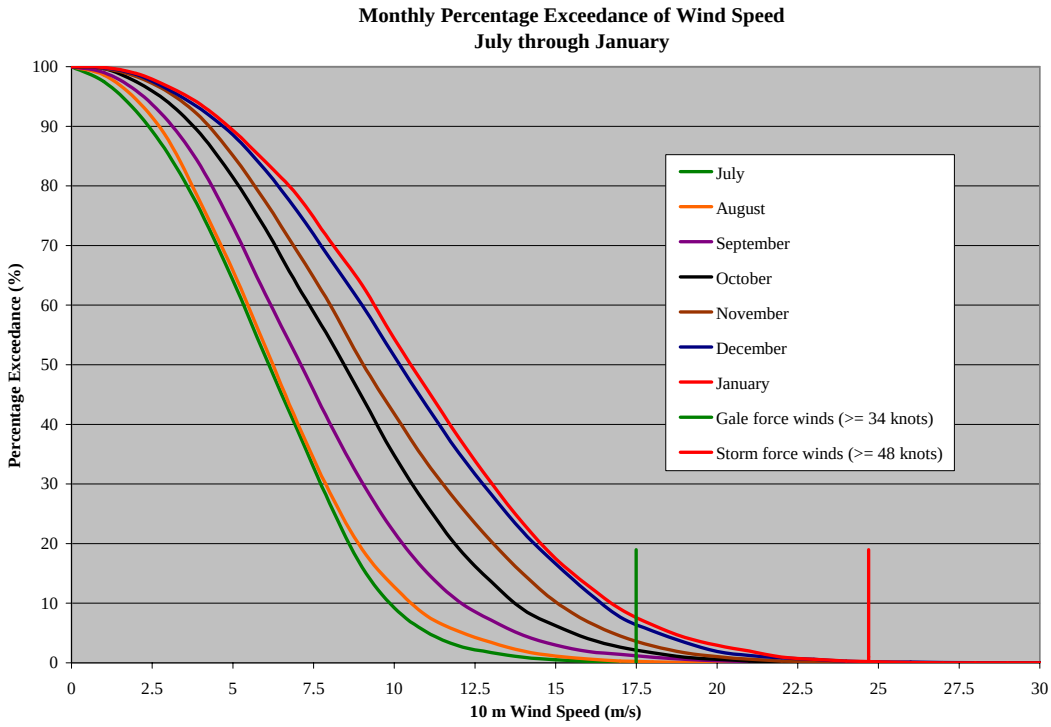

Source: Grid point 5622, AES-40 wind and wave hindcast dataset (July 01, 1954 through June 30, 2003)

Figure 1.4 Monthly Percentage Exceedance of 10 m Wind Speed – July through January

1.2 Wave Climate

The wave climate in the exploration area includes the affects of locally generated wind-waves and swell that propagates into the area from both nearby and distant locations. The highest sea states occur during severe storm systems that track through the region, mainly during October through March. Occasionally, severe storms may occur outside these months. Storms of tropical origin occur most often from late August through October. Hurricanes are usually reduced to tropical storm strength or evolve into extra-tropical storms by the time they reach the Grand Banks, but occasionally these storms still retain hurricane force winds and hence produce high waves.

Sea state conditions at AES-40 grid point 5622 in the Husky exploration area are described in terms of significant wave height and spectral peak period statistics. Table 1.5 contains basic descriptive statistics for significant wave height on a monthly basis. The lowest monthly mean significant wave height occurs in July (1.7 m), while the highest average occurs in January (4.1 m). Standard deviations are smaller in the summer months than during the winter months. Monthly maximum values of significant wave height have ranged from near 6 m in July and August to 13 to 14 m in the winter months. Table 1.6 provides basic descriptive statistics for spectral peak period, the period at which wave energy is highest.

Table 1.5 Monthly Statistics of Significant Wave Height.

Monthly Statistics of Significant Wave Height					
	Significant wave Height (metres)				
Month	**Min**	**Max**	**Mean**	**Std Dev.**	**Median**
January	0.7	13.0	4.1	1.6	3.7
February	0.9	13.7	3.8	1.6	3.5
March	0.6	11.1	3.4	1.4	3.1
April	0.5	10.8	2.9	1.1	2.7
May	0.5	10.1	2.2	0.9	2.0
June	0.6	9.0	1.9	0.7	1.8
July	0.6	6.0	1.7	0.6	1.6
August	0.4	5.8	1.8	0.7	1.6
September	0.8	10.1	2.3	1.0	2.1
October	0.9	11.1	2.9	1.2	2.6
November	0.6	11.6	3.3	1.4	3.0
December	1.1	13.4	3.9	1.5	3.6

Source: Grid point 5622, AES-40 wind and wave hindcast dataset (July 01, 1954 through June 30, 2003)

Table 1.6 Monthly Statistics of Spectral Peak Period.

Monthly Statistics of Spectral Peak Period					
	Peak Period (seconds)				
Month	Min	Max	Mean	Std Dev.	Median
January	4.8	15.9	10.5	1.9	10.6
February	4.2	17.0	10.2	2.1	10.3
March	3.5	17.2	10.0	2.0	10.0
April	3.4	15.7	9.6	1.8	9.6
May	3.6	15.6	8.5	1.7	8.4
June	3.5	17.5	8.0	1.6	7.9
July	3.8	18.7	7.7	1.6	7.4
August	3.8	17.1	7.8	1.7	7.5
September	4.2	15.9	8.7	2.0	8.5
October	3.9	15.7	9.3	1.9	9.1
November	4.0	15.9	9.8	1.9	9.8
December	4.7	16.1	10.4	1.9	10.4

Source: Grid point 5622, AES-40 wind and wave hindcast dataset (July 01, 1954 through June 30, 2003)

1.2.1 Monthly Percentage Exceedance of Significant Wave Height

Table 1.7 shows the percentage exceedance of significant wave height for each month of the year. Figures 1.5 and 1.6 are exceedance plots of the data for January to July and for July to January, respectively, showing the progression through the seasons. During the winter and spring months, sea ice incursion at grid point 5622 is indicated in the dataset by zero values for significant wave height. Thus, exceedance values of less than 100 percent for zero significant wave height occur in the months of January through May. Table 1.8 shows the percent frequency of occurrence of sea ice during the winter and spring for the 49-year period from the AES-40 dataset.

Table 1.7 Monthly Percentage Exceedance of Significant Wave Height.

Percentage Exceedance of Significant Wave Height (Hs)												
Hs	(%)											
(m)	Jan	Feb	Mar	Apr	May	Jun	Jul	Aug	Sep	Oct	Nov	Dec
0.0	95.92	93.91	83.66	95.80	99.97	100.00	100.00	100.00	100.00	100.00	100.00	100.00
0.5	95.92	93.91	83.66	95.78	99.95	100.00	100.00	99.88	100.00	100.00	100.00	100.00
1.0	95.85	93.82	83.16	95.36	98.03	95.99	94.29	96.02	98.64	99.82	99.76	100.00
1.5	95.06	91.78	80.68	89.39	78.85	68.13	57.72	59.30	84.08	94.45	96.67	99.29
2.0	91.97	86.07	73.29	73.52	49.05	34.85	24.90	27.86	55.17	77.65	86.04	95.06
2.5	84.51	75.61	60.01	54.13	28.18	15.44	8.82	12.67	31.07	56.04	69.54	85.60
3.0	71.59	62.27	45.59	35.60	14.63	6.94	3.44	6.25	16.65	36.41	51.70	70.74
3.5	55.38	47.53	32.36	22.36	7.50	3.55	1.50	3.11	9.49	22.00	35.43	52.81
4.0	40.80	33.72	22.99	13.50	4.15	1.51	0.69	1.63	5.82	12.66	23.33	37.97
4.5	29.26	23.77	15.40	8.30	2.27	0.66	0.35	0.72	3.23	7.57	15.37	26.30
5.0	19.96	16.76	10.20	4.64	1.23	0.34	0.20	0.28	1.90	4.79	9.98	18.43
5.5	13.56	11.29	6.44	2.26	0.59	0.12	0.03	0.10	1.11	3.11	6.79	12.82
6.0	9.45	7.62	4.23	1.33	0.30	0.05	0.02	0.00	0.80	2.02	4.64	8.89
6.5	6.73	5.20	2.63	0.94	0.16	0.05	0.00	0.00	0.54	1.33	3.03	6.19
7.0	4.99	4.05	1.71	0.61	0.10	0.05	0.00	0.00	0.41	0.91	1.97	4.20
7.5	3.82	3.31	1.20	0.41	0.07	0.05	0.00	0.00	0.29	0.66	1.36	3.13
8.0	2.90	2.71	0.82	0.29	0.05	0.03	0.00	0.00	0.20	0.54	1.00	2.37
8.5	2.49	2.11	0.54	0.12	0.05	0.02	0.00	0.00	0.19	0.33	0.75	1.60
9.0	1.97	1.63	0.38	0.10	0.03	0.00	0.00	0.00	0.12	0.23	0.51	1.20
9.5	1.45	1.17	0.31	0.05	0.03	0.00	0.00	0.00	0.09	0.13	0.36	0.81
10.0	0.94	0.83	0.10	0.03	0.02	0.00	0.00	0.00	0.02	0.07	0.20	0.59
10.5	0.61	0.49	0.03	0.03	0.00	0.00	0.00	0.00	0.00	0.03	0.14	0.36
11.0	0.41	0.33	0.02	0.00	0.00	0.00	0.00	0.00	0.00	0.02	0.07	0.23
11.5	0.20	0.33	0.00	0.00	0.00	0.00	0.00	0.00	0.00	0.00	0.02	0.13
12.0	0.16	0.18	0.00	0.00	0.00	0.00	0.00	0.00	0.00	0.00	0.00	0.05
12.5	0.05	0.09	0.00	0.00	0.00	0.00	0.00	0.00	0.00	0.00	0.00	0.03
13.0	0.00	0.04	0.00	0.00	0.00	0.00	0.00	0.00	0.00	0.00	0.00	0.03
13.5	0.00	0.02	0.00	0.00	0.00	0.00	0.00	0.00	0.00	0.00	0.00	0.00
14.0	0.00	0.00	0.00	0.00	0.00	0.00	0.00	0.00	0.00	0.00	0.00	0.00

Source: Grid point 5622, AES-40 wind and wave hindcast dataset (July 01, 1954 through June 30, 2003)

Table 1.8 Percentage Frequency of Occurrence of Sea Ice at Grid Point 5622.

Percentage Occurrence of Sea Ice*	
Month	**(%)**
January	4.08
February	6.09
March	16.34
April	4.20
May	0.03

* Source: Grid point 5622, AES-40 wind and wave hindcast dataset (July 01, 1954 through June 30, 2003

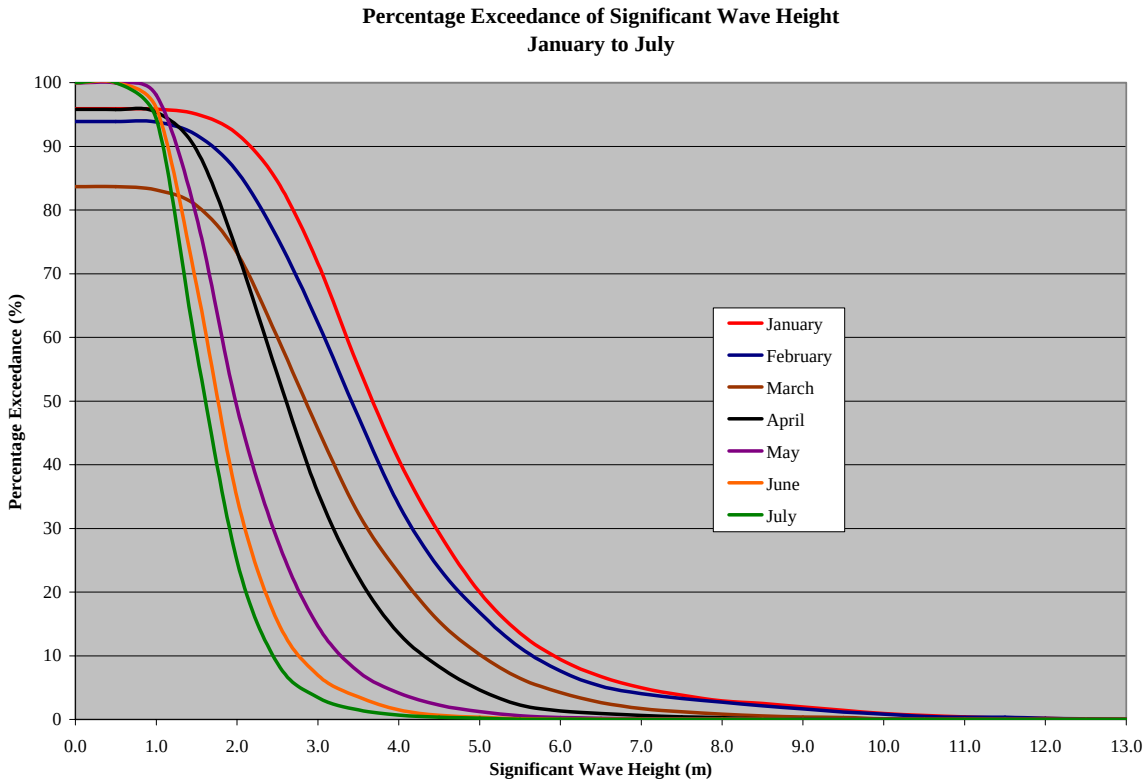

Source: Grid point 5622, AES-40 wind and wave hindcast dataset (July 01, 1954 through June 30, 2003)

Figure 1.5 Monthly Percent Exceedance of Significant Wave Height - January to July.

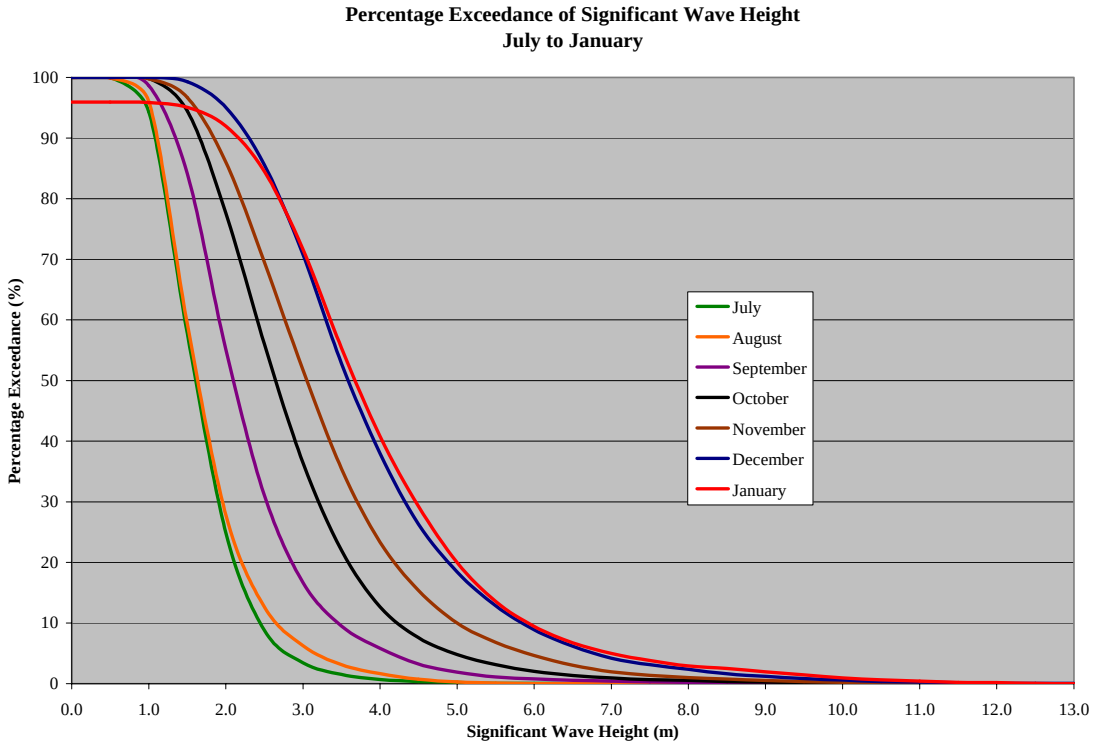

Source: Grid point 5622, AES-40 wind and wave hindcast dataset (July 01, 1954 through June 30, 2003)

Figure 1.6 Monthly Percent Exceedance of Significant Wave Height - July to January.

1.2.2 Monthly Percentage Occurrence of Spectral Peak Period

Table 1.9 provides percent frequency of occurrence of spectral peak periods for each month of the year. Again, the percent frequency for zero peak periods indicates the occurrence of sea ice at the grid point location. During the warm season, the most frequent peak period is in the 7 to 8 second range; during the winter, the peak periods of the higher sea states are more frequent in the 9 to 12 second range.

Table 1.9 Monthly Percent Frequency of Occurrence of Spectral Peak Periods.

Monthly Percent Frequency of Occurrence of Spectral Peak Period (Tp)												
Tp (s)	**Jan**	**Feb**	**Mar**	**Apr**	**May**	**Jun**	**Jul**	**Aug**	**Sep**	**Oct**	**Nov**	**Dec**
0	4.1	6.1	16.3	4.2	0.0	0.0	0.0	0.0	0.0	0.0	0.0	0.0
> 0.0 - < 1.0	0.0	0.0	0.0	0.0	0.0	0.0	0.0	0.0	0.0	0.0	0.0	0.0
1.0 - < 2.0	0.0	0.0	0.0	0.0	0.0	0.0	0.0	0.0	0.0	0.0	0.0	0.0
2.0 - < 3.0	0.0	0.0	0.0	0.0	0.0	0.0	0.0	0.0	0.0	0.0	0.0	0.0
3.0 - < 4.0	0.0	0.0	0.0	0.0	0.1	0.0	0.0	0.1	0.0	0.0	0.0	0.0
4.0 - < 5.0	0.0	0.1	0.4	0.2	0.7	0.9	0.9	1.2	0.4	0.3	0.2	0.1
5.0 - < 6.0	0.7	1.7	1.5	1.9	4.7	8.1	10.0	10.2	4.7	2.3	1.5	0.6
6.0 - < 7.0	3.1	4.8	4.9	5.9	12.3	19.1	24.2	23.9	14.4	7.9	5.8	2.8
7.0 - < 8.0	6.1	7.9	7.5	10.5	21.5	26.1	29.2	28.9	20.5	15.2	9.9	6.8
8.0 - < 9.0	11.4	12.8	11.0	18.8	26.3	24.4	19.4	18.1	20.9	22.3	17.3	12.9
9.0 - <10.0	16.1	15.4	16.3	21.5	17.9	12.8	9.4	8.0	15.2	20.1	21.7	19.4
10.0 - <11.0	18.9	17.4	16.3	17.9	9.3	4.9	3.6	4.9	10.4	13.6	19.5	21.7
11.0 - <12.0	17.4	16.1	13.0	11.2	4.5	1.7	1.2	2.5	6.7	9.9	12.2	16.9
12.0 - <13.0	12.6	9.3	7.5	4.1	1.6	0.9	0.7	1.3	3.5	4.4	6.1	10.3
13.0 - <14.0	6.3	5.3	3.2	2.7	0.8	0.5	0.4	0.4	2.3	2.5	3.9	5.3
14.0 - <15.0	2.7	2.3	1.5	1.1	0.2	0.4	0.3	0.5	0.8	1.2	1.5	2.6
15.0 - <16.0	0.5	0.7	0.4	0.1	0.0	0.1	0.4	0.1	0.2	0.3	0.4	0.6
16.0 - <17.0	0.0	0.1	0.1	0.0	0.0	0.0	0.1	0.0	0.0	0.0	0.0	0.0
17.0 - <18.0	0.0	0.0	0.0	0.0	0.0	0.1	0.1	0.0	0.0	0.0	0.0	0.0
18.0 - <19.0	0.0	0.0	0.0	0.0	0.0	0.0	0.0	0.0	0.0	0.0	0.0	0.0

Source: Grid point 5622, AES-40 wind and wave hindcast dataset (July 01, 1954 through June 30, 2003)

1.2.3 Percent Frequency of Significant Wave Height and Spectral Peak Period

Table 1.10 presents the percent frequency of the joint occurrence of significant wave height and spectral peak period for the full 49-year period of the hindcast dataset. Ice is seen to be present at the location 2.55 percent of the time during this period.

Table 1.10 Percent Frequency of the Joint Occurrence of Significant Wave Height and Spectral Peak Period.

Percent Frequency of Joint Occurrence of Significant Wave Height and Spectral Peak Period															
	Ice	Significant Wave Height (m)													
Spectral Peak Period (s)	0	> 0.0 to < 1.0	1 to < 2.0	2 to < 3.0	3 to < 4.0	4 to < 5.0	5 to < 6.0	6 to < 7.0	7 to < 8.0	8 to < 9.0	9 to <10.0	10 to <11.0	11 to <12.0	12 to <13.0	13 to <14.0	Totals
0	2.55															**2.55**
> 0.0 to < 1.0																**0.00**
1.0 to < 2.0																**0.00**
2.0 to < 3.0																**0.00**
3.0 to < 4.0		0.01	0.02													**0.03**
4.0 to < 5.0		0.03	0.41	0.02												**0.46**
5.0 to < 6.0		0.20	3.27	0.54	0.02											**4.03**
6.0 to < 7.0		0.63	5.55	4.26	0.34	0.01										**10.79**
7.0 to < 8.0		0.44	7.57	5.35	2.38	0.16										**15.90**
8.0 to < 9.0		0.07	7.58	4.60	4.17	1.47	0.09									**17.98**
9.0 to <10.0		0.10	3.87	5.97	2.95	2.38	0.82	0.06								**16.15**
10.0 to <11.0		0.05	1.65	4.98	3.18	1.57	1.24	0.43	0.06	0.01						**13.17**
11.0 to <12.0		0.02	0.79	2.23	3.16	1.48	0.79	0.57	0.27	0.09	0.01					**9.41**
12.0 to <13.0		0.01	0.36	0.84	1.47	1.12	0.54	0.27	0.20	0.21	0.14	0.02				**5.18**
13.0 to <14.0			0.19	0.43	0.56	0.62	0.40	0.21	0.08	0.07	0.11	0.09	0.02			**2.78**
14.0 to <15.0			0.12	0.18	0.26	0.26	0.17	0.11	0.05	0.02	0.02	0.03	0.03	0.02		**1.27**
15.0 to <16.0			0.05	0.04	0.04	0.06	0.04	0.04	0.01	0.01			0.01	0.01		**0.31**
16.0 to <17.0					0.01	0.01										**0.02**
17.0 to <18.0				0.01												**0.01**
Totals	**2.55**	**1.56**	**31.43**	**29.45**	**18.54**	**9.14**	**4.09**	**1.69**	**0.67**	**0.41**	**0.28**	**0.14**	**0.06**	**0.03**	**0.00**	**100**

Source: Grid point 5622, AES-40 wind and wave hindcast dataset (July 01, 1954 through June 30, 2003)

1.3 Air and Sea Surface Tempertures

Air and surface temperature data for the Husky exploration area were extracted from the COADS LMR dataset as summarized above. Monthly mean values were computed and these statistics are presented in Figure 1.7. In the winter season, average sea surface temperatures are warmer than the mean air temperatures; the opposite is the case during the summer season. Because of this, the lower portion of the atmosphere is generally unstable during the winter months and stable in the spring and summer months. Monthly average air temperatures are evidently just below zero Celsius at the coldest time of the year and about 13.5° C in August, the warmest month. The range of sea surface temperatures is smaller than that for air temperatures, an artifact of the higher heat capacity of the ocean.

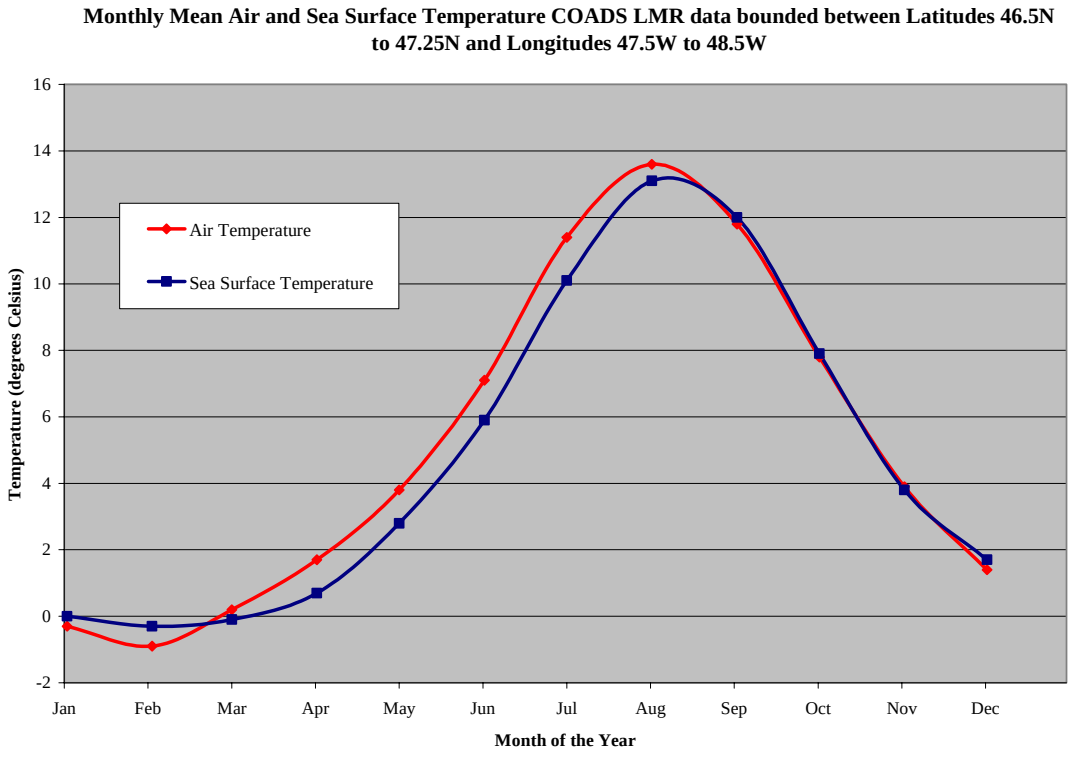

Figure 1.7 Monthly Average Air and Sea Surface Temperature.

Table 1.11 Monthly Air and Sea Surface Temperature Statistics.

Air and Sea Surface Temperatures													
		Monthly Means and Standard Deviations											
		Jan	Feb	Mar	Apr	May	Jun	Jul	Aug	Sep	Oct	Nov	Dec
Air	Mean	-0.3	-0.9	0.2	1.7	3.8	7.1	11.4	13.6	11.8	7.8	3.9	1.4
	Standard Deviation	3.0	3.1	2.7	2.2	2.4	2.2	2.2	2.4	2.5	2.8	2.6	3.1
Sea Surface	Mean	0.0	-0.3	-0.1	0.7	2.8	5.9	10.1	13.1	12.0	7.9	3.8	1.7
	Standard Deviation	1.0	0.9	1.0	1.3	1.9	1.7	2.0	2.1	2.4	2.3	2.0	1.8

Table 1.11 contains monthly mean air and sea surface temperatures along with the corresponding standard deviations for the specified COADS area.

1.4 Visibility and Causes of Restricted Visibility

Visibility data were extracted from the COADS observational dataset for this review and summarized in Table 1.12. The data were combined to correspond with visibility criteria used in marine weather forecasts, with the ranges expressed in kilometers. Figure 1.8 illustrates these statistics in the form of a bar chart with one additional range; it includes the percent occurrence of visibility reports of less than 1 km. During the warmer months visibility is restricted by mist and fog; in the winter season snow or snow showers also cause reduced visibility.

Table 1.12 Percentage Frequency of Occurrence of Visibility Reports.

Percent Frequency of Occurrence of Visibility Reports													
Visibility		Month											
Classification	Range	Jan	Feb	Mar	Apr	May	Jun	Jul	Aug	Sep	Oct	Nov	Dec
Poor	< 2 km	15.0	16.1	20.2	28.5	38.9	43.5	55.4	30.4	17.0	11.6	14.4	13.9
Fair	2 km to < 10 km	13.3	16.1	15.2	13.4	14.9	11.8	11.4	12.1	11.2	9.7	12.6	15.5
Good	>= 10 km	71.7	67.9	64.6	58.0	46.3	44.7	33.2	57.5	71.8	78.7	73.0	70.6

The lowest visibility conditions occur in July with poor visibility being reported in 55% of reports. This is largely due to fog (visibility less than 1 km) as indicated the Figure 1.8. Primarily, the type of fog is advection fog, which is formed as relatively warm, moist air is advected over the colder water surface. The reports for July indicate that visibility was reduced in either fog or mist for 66.8 % of the observations. Good visibility (no restriction) was reported in only 33.2 % of the observations. October has the highest percentage of good visibility reports with a value of 78.7%.

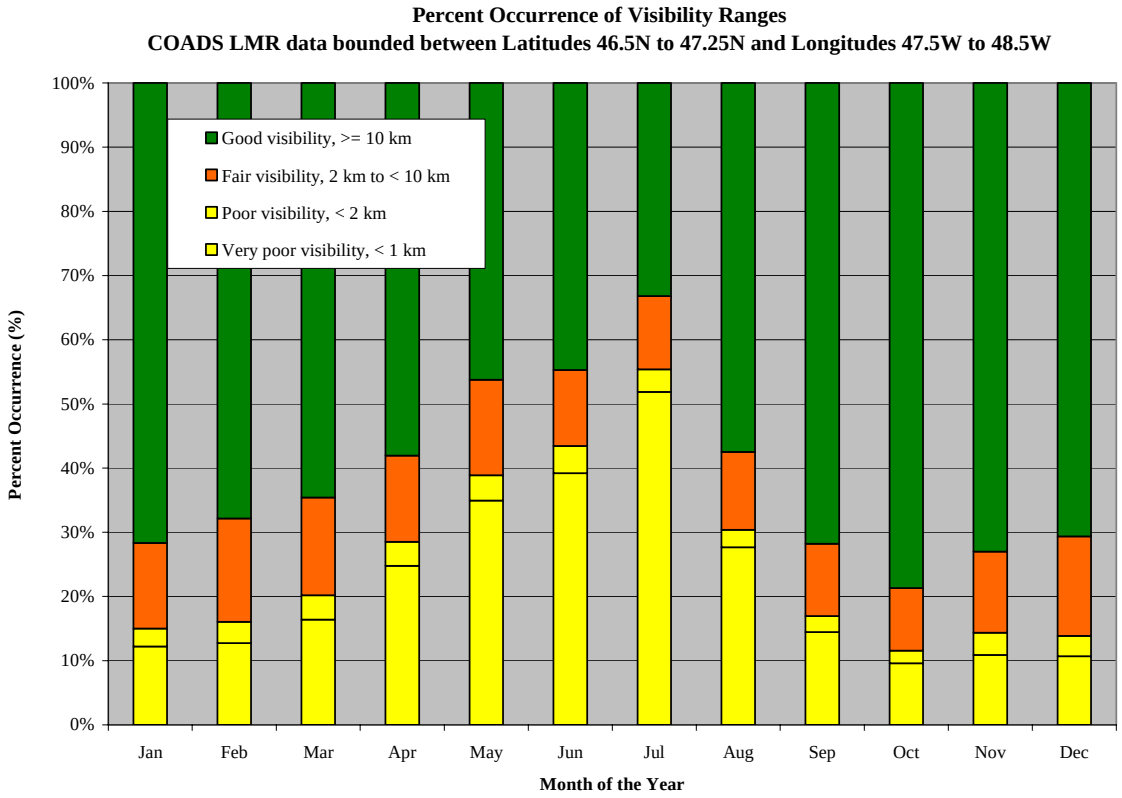

Figure 1.8 Percent Frequency of Occurrence of Visibility Ranges.

2 Wind and Wave Extreme Analysis

The wind and wave extreme analysis was carried out from the AES-40 data set at grid point 5622 for 49 years of data between July 1, 1954 and June 30, 2003. Grid point 5622 is located at 46.88°N; 48.33°w, the closed grid point to the study area. The AES-40 wind and wave hindcast data set for the North Atlantic Ocean was prepared by Oceanweather Inc of Cos. Cob, Connecticut under contract to the Meteorological Service of Canada. The AES-40 data set is a hindcast data set using the National Center for Atmospheric Research (NCEP-CSAR) global re-analysis surface marine wind fields, and further re-analyzed by Oceanweather Inc. with corrections to the original data set. The corrections included adjusting all observed winds to the standard reference level of 10 m above the sea surface, intensifying extratropical storms as necessary and including tropical cyclone boundary layer winds. The waves were then hindcast by Oceanweather using their third-generation wave model. The hindcast wind fields closely resembled the waves measured at offshore buoys and observations from offshore platforms, thus validating the data set. The data has been generated using time steps of 6 hours. In some storms, particularly those of short duration, the peak winds may get missed due to the length of the sampling period. A shorter sampling period would be more desirable. However, the AES-40 data set has been a major improvement over previous data sets because of the many years of continuous data.

The extreme values for wind and waves were calculated using the peak-over-threshold method; and after considering four different distributions, the Gumbel Distribution was chosen as the most appropriate because it gave the best fit to the data. A sensitivity analysis was carried out to determine how many storms to use in the analysis, because the extreme values can vary depending on how well the data fits the distribution function. The sensitivity analysis showed that the Gumbel Distribution had a good fit using 245 storms when all the data was considered in calculating the yearly extremes. For monthly extremes the top 60 storms were used in the analysis. Sixty storms were chosen in order to give a consistent threshold value for waves during the winter months as compared to all months combined. This represents a significant wave height threshold value of 7.75 m. A plot of the correlation coefficient versus the number of storms is shown in Figure 2.1.

2.1 Extreme Value Estimates for Winds from a Gumbel Distribution

The extreme value estimates for wind were calculated using Oceanweather's software programs for return periods of 1-year, 10-years, 25-years, 50-years and 100-years. The values calculated for each month and all months combined are given in Table 2.1. The extreme value analysis used hourly wind values for the reference height of 10-metres above sea level. The 10-minute and 1-minute winds were calculated from the 1-hour mean values using a constant ratio of 1.06 and 1.22 respectively. The 100-year extreme wind speed was 31.2 m/s. The 1-year, 10-year, 25-year, and 50-year extreme wind speeds were 24.4 m/s,

27.9 m/s, 29.2 m/s, and 30.2 m/s, respectively. These values may be slightly under estimated due to the 6-hour time interval in the data. It is highly probable that some of the peaks in the wind speed have been missed by the hindcasting methodology. The distribution fits for the wind data values using the 245 storms in 3 different distributions are presented in Figure 2.2.

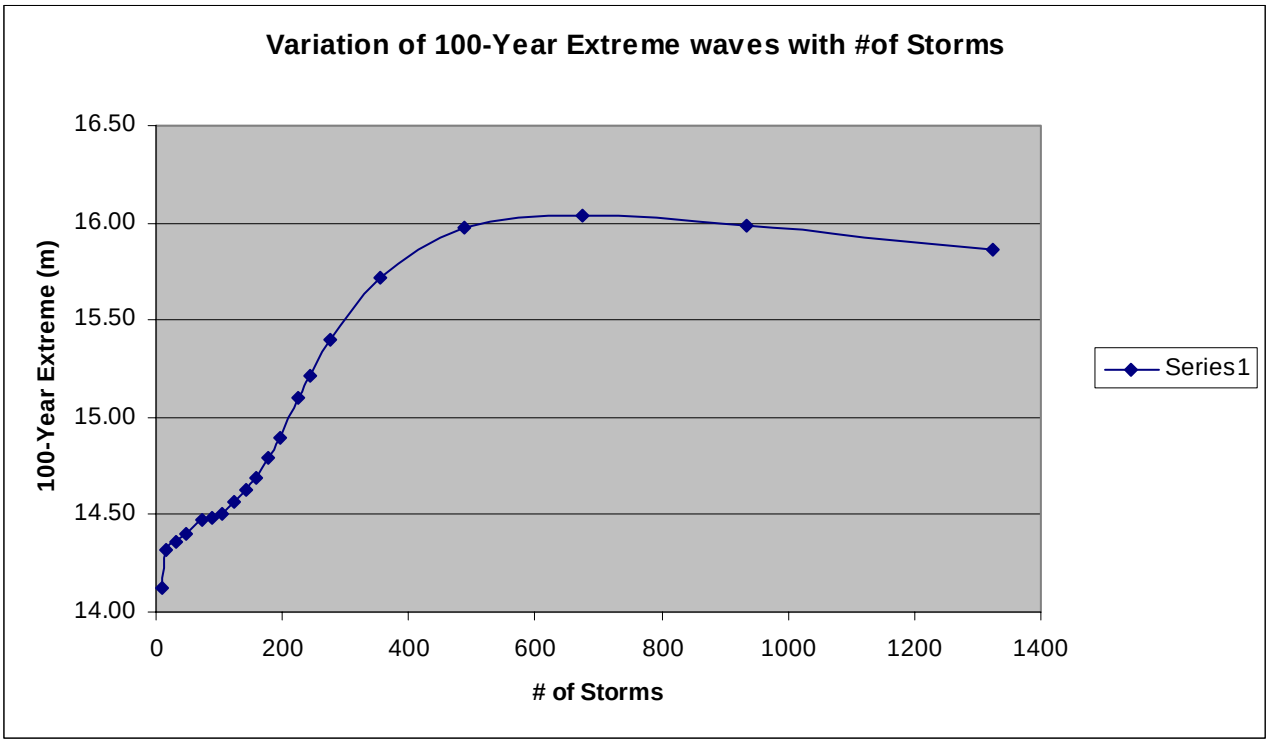

Figure 2.1 Correlation Coefficient for Significant Wave Height using a Gumbel Distribution.

Table 2.1 Extreme Wind Estimates for Return Periods of 1, 10, 25, 50 and 100 Years.

Monthly Wind Speed Extremes at Grid Point # 5622 (46.88N 48.33W)

	Wind Speed 1-hr (m/s)				
Month	**1.0**	**10.0**	**25.0**	**50.0**	**100.0**
JAN	21.5	25.4	26.7	27.6	28.5
FEB	21.6	26.8	28.5	29.7	31.0
MAR	19.2	24.0	25.5	26.6	27.7
APR	17.4	22.7	24.3	25.6	26.8
MAY	15.6	19.3	20.5	21.4	22.3
JUN	14.4	18.6	20.0	21.0	22.0
JUL	13.2	17.2	18.5	19.4	20.4
AUG	14.5	18.9	20.4	21.4	22.4
SEP	16.6	22.0	23.7	24.9	26.2
OCT	17.7	22.6	24.2	25.3	26.5
NOV	19.4	23.8	25.2	26.2	27.2
DEC	20.6	26.0	27.7	29.0	30.2
ALL	24.4	27.9	29.2	30.2	31.2
	Wind Speed 10-min (m/s)				
Month	**1.0**	**10.0**	**25.0**	**50.0**	**100.0**
JAN	22.8	26.9	28.2	29.2	30.2
FEB	22.9	28.5	30.2	31.5	32.8
MAR	20.3	25.4	27.0	28.2	29.4
APR	18.4	24.0	25.8	27.1	28.4
MAY	16.5	20.5	21.7	22.7	23.6
JUN	15.2	19.7	21.2	22.2	23.3
JUL	13.9	18.2	19.6	20.6	21.6
AUG	15.3	20.1	21.6	22.7	23.8
SEP	17.6	23.3	25.1	26.4	27.7
OCT	18.7	24.0	25.6	26.9	28.1
NOV	20.6	25.2	26.7	27.8	28.9
DEC	21.8	27.5	29.3	30.7	32.0
ALL	25.8	29.5	30.9	32.0	33.1
	Wind Speed 1-min (m/s)				
Month	**1.0**	**10.0**	**25.0**	**50.0**	**100.0**
JAN	26.2	31.0	32.5	33.6	34.7
FEB	26.3	32.7	34.8	36.3	37.8
MAR	23.4	29.3	31.1	32.5	33.8
APR	21.2	27.6	29.7	31.2	32.7
MAY	19.0	23.6	25.0	26.1	27.2
JUN	17.5	22.7	24.4	25.6	26.8
JUL	16.1	21.0	22.5	23.7	24.8
AUG	17.7	23.1	24.8	26.1	27.4
SEP	20.3	26.8	28.9	30.4	31.9
OCT	21.6	27.6	29.5	30.9	32.3
NOV	23.7	29.0	30.7	32.0	33.2
DEC	25.1	31.7	33.8	35.3	36.8
ALL	29.7	34.0	35.6	36.8	38.1

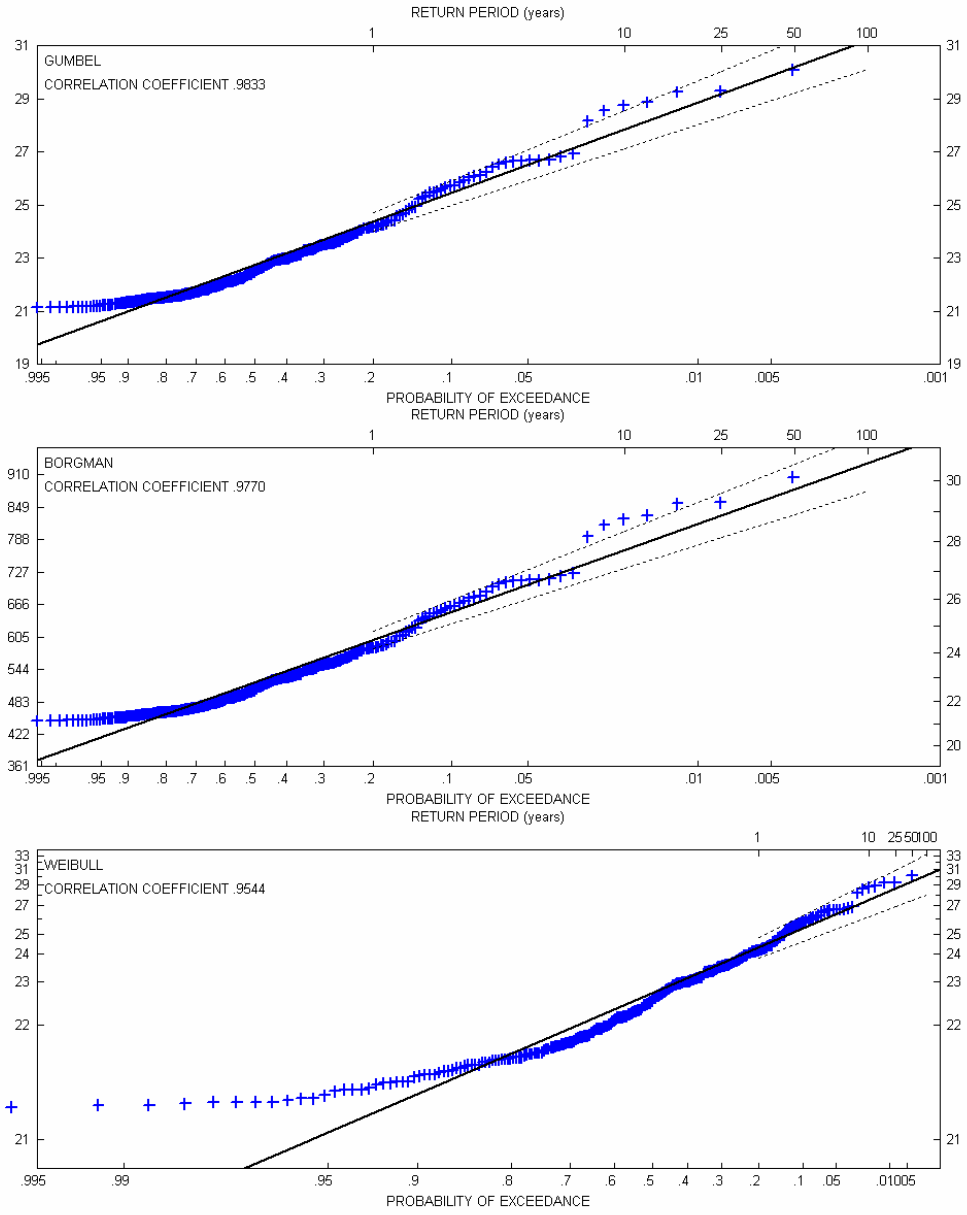

AE GPT 5622: Wind Speed (m/s) (Peak values)
Top 245 storms in 49 years

Gumbel Parameters: Location 22.21018, Scale 1.446421
Borgman Parameters: Location 22.21018, Scale 1.446421
Weibull Parameters: Location 20.727, Scale 2.544741, Shape 1.386085

Period	Prob.	Gumbel	lcl	ucl	Borgman	lcl	ucl	Weibull	lcl	ucl	Galton
1.0	0.2000000	24.38	24.03	24.73	24.48	24.14	24.82	24.31	23.84	24.86	24.48
10.0	0.0200000	27.85	27.14	28.57	27.72	27.09	28.35	27.54	26.16	29.26	26.84
25.0	0.0080000	29.19	28.33	30.05	28.87	28.14	29.59	28.65	26.92	30.87	27.57
50.0	0.0040000	30.19	29.22	31.16	29.71	28.90	30.50	29.46	27.45	32.06	28.08
100.0	0.0020000	31.20	30.12	32.28	30.52	29.65	31.37	30.23	27.96	33.22	28.57

oceanweather Inc.

Figure 2.2 Distribution fits for Wind Data using the 245 Storms.

2.1 Extreme Value Estimates for Waves from a Gumbel Distribution

The Extreme value estimates for waves for return periods of 1-year, 10-years, 25-years, and 50-years and 100-years are given in Table 2.2. Similar to winds, the values were calculated for each month considered separately and for all months combined. The 100-year extreme significant wave height was 15.2 m. The 1-year, 10-years, 25years, and 50-years extreme significant wave heights were 10.4 m, 12.9 m, 13.8 m, and 14.5 m respectively. The highest extreme significant wave height is expected to occur during February. Extreme value estimates were also calculated for the maximum wave heights and for the spectral peak periods associated with the significant wave heights. The maximum wave heights are calculated values of the median values of the probability distribution of maximum individual wave heights. The extreme significant wave heights, maximum wave heights, and associated peak periods are presented in Table 2.2. Graphs of how well the Gumbel, Borgman, and Weibull Distribution fit the significant wave height data for selected 245 storms are presented in Figure 2.3

2.2 Joint Probability of Extreme Wave Heights and Spectral Peak Periods

In order to examine the period ranges of storm events, an environmental contour plot was produced showing the probability of the joint occurrence of significant wave heights and the spectral peak periods using the methodology of Winterstein et al. (1993). The environmental contour plot is presented in Figure 2.4. The wave heights were fitted to a Weibull Distribution and the peak periods to a lognormal distribution. The wave data was divided into bins of 1 metre for significant wave heights and 1 second for peak periods. Since the lower wave values were having too much of an impact on the wave extremes, the wave heights below 2 metres were modeled separately in a Weibull Distribution. The two Weibull curves were combined at 2 metres, the point where both functions had the same probability.

Three-parameter Weibull Distributions were used with a scaling parameter α, shape parameter β, and location parameter γ. The three parameters were solved by using a least square method, the maximum log likelihood, and the method of moments. The following equation was minimized to get the coefficients

$$LS(\alpha,\beta,\gamma) := \sum_{i=0}^{13} \left[\ln\left(-\ln\left(1 - FP_i\right)\right) - \beta \cdot \ln\left[\frac{\left(h_i - \gamma\right)}{\alpha}\right]\right]^2$$

where h_i is the endpoint of the height bin (0.5, 1.5, …) and FP_i is the cumulative probability of the height bin. Using a minimizing function the three parameters α, β and γ were calculated.

Table 2.2 Extreme Wave Estimates for Return Periods of 1, 10, 25, 50, and 100 Years.
Monthly Wave Extremes at Grid Point # 5622 (46.88N 48.33W)

Significant Wave Height (m)					
Month	**1.0**	**10.0**	**25.0**	**50.0**	**100.0**
JAN	8.6	11.9	12.9	13.7	14.4
FEB	8.0	11.9	13.1	14.1	15.0
MAR	6.5	9.5	10.5	11.2	11.9
APR	5.3	8.4	9.3	10.0	10.7
MAY	4.2	6.8	7.6	8.2	8.8
JUN	3.5	5.9	6.6	7.1	7.7
JUL	3.2	5.0	5.6	6.0	6.4
AUG	3.7	5.3	5.8	6.2	6.6
SEP	4.6	8.1	9.2	10.0	10.8
OCT	5.6	9.1	10.2	11.0	11.9
NOV	6.8	10.3	11.4	12.2	13.0
DEC	8.2	11.4	12.4	13.1	13.9
ALL	10.4	12.9	13.8	14.5	15.2
Maximum Wave Height (m)					
Month	**1.0**	**10.0**	**25.0**	**50.0**	**100.0**
JAN	16.2	22.2	24.1	25.5	26.9
FEB	15.3	22.7	25.1	26.8	28.5
MAR	12.3	18.2	20.1	21.4	22.8
APR	10.3	15.7	17.4	18.6	19.9
MAY	8.1	13.5	15.2	16.4	17.7
JUN	6.9	11.1	12.4	13.4	14.3
JUL	6.2	9.5	10.6	11.4	12.1
AUG	7.2	10.1	11.1	11.8	12.4
SEP	9.0	15.1	17.0	18.4	19.8
OCT	10.7	17.1	19.1	20.6	22.0
NOV	12.8	19.2	21.2	22.7	24.1
DEC	15.3	21.2	23.1	24.5	25.8
ALL	19.6	24.3	26.1	27.5	28.8
Associated Peak Period (sec)					
Month	**1.0**	**10.0**	**25.0**	**50.0**	**100.0**
JAN	12.4	14.4	14.9	15.3	15.7
FEB	12.3	14.0	14.5	14.8	15.1
MAR	11.8	13.1	13.4	13.7	13.9
APR	10.8	12.4	12.9	13.2	13.5
MAY	10.0	11.4	11.8	12.1	12.3
JUN	8.5	10.6	11.1	11.5	11.9
JUL	8.2	10.2	10.8	11.2	11.5
AUG	8.9	10.4	10.9	11.2	11.5
SEP	10.1	12.0	12.4	12.8	13.1
OCT	10.9	12.5	13.0	13.3	13.6
NOV	11.7	13.4	13.9	14.2	14.5
DEC	12.5	14.1	14.5	14.8	15.1
ALL	13.5	14.7	15.1	15.5	15.7

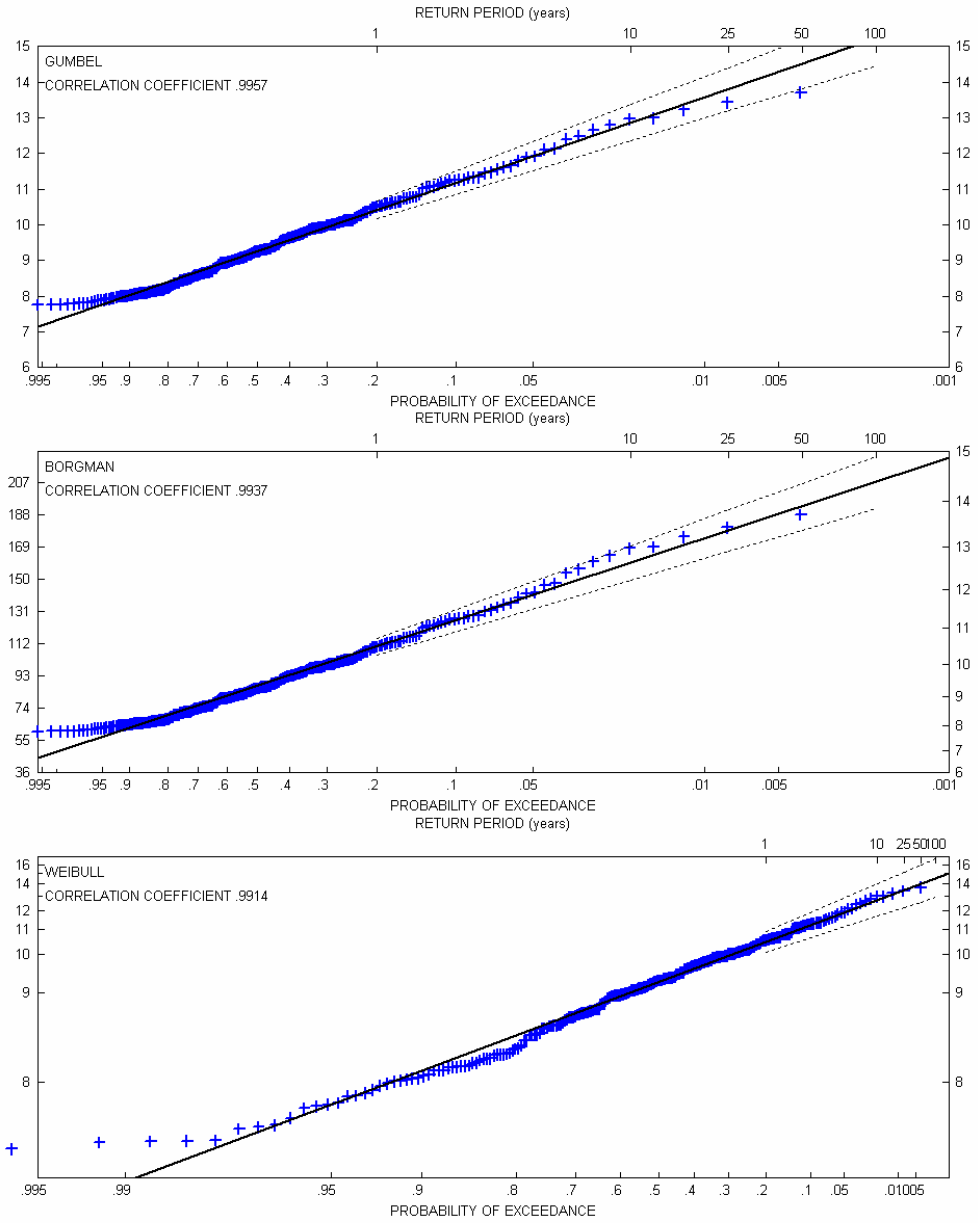

AE GPT 5622: Significant Wave Height (m) (Peak values)
Top 245 storms in 49 years

Gumbel Parameters: Location 8.887468, Scale 1.017884
Borgman Parameters: Location 8.887468, Scale 1.017884
Weibull Parameters: Location 7.60186, Scale 2.068963, Shape 1.505236

Period	Prob.	Gumbel	lcl	ucl	Borgman	lcl	ucl	Weibull	lcl	ucl	Galton
1.0	0.2000000	10.41	10.17	10.66	10.50	10.27	10.73	10.44	10.07	10.87	10.48
10.0	0.0200000	12.86	12.36	13.36	12.63	12.22	13.03	12.72	11.69	14.02	12.28
25.0	0.0080000	13.80	13.19	14.40	13.36	12.89	13.81	13.49	12.20	15.14	12.86
50.0	0.0040000	14.51	13.82	15.19	13.88	13.38	14.37	14.04	12.56	15.96	13.28
100.0	0.0020000	15.21	14.45	15.97	14.38	13.84	14.91	14.57	12.90	16.75	13.68

oceanweather Inc.

Figure 2.3 Distribution Fits for Wave Data Using the 245 Storms.

A lognormal distribution was fitted to the spectral peak periods in each wave height bin. The coefficient of the lognormal distribution was then calculated. Using the coefficients and the two distribution functions, the joint wave height and period combinations were calculated for the various return periods. The values were plotted and contours produced as shown in Figure 2.4 for return periods of 1-year, 10-years, 25-years, 50-years, and 100- years.

The values for the significant wave height estimates and the associated spectral peak periods are given in Table 1.3. The 100-year extreme wave height using the Weibull Distribution on the complete data set was 15.6 m as compared to 15.2 m using a Gumbel Distribution on a selected number of storms. The extreme wave estimates for significant wave height together with their spectral peak periods for each month for return periods of 1-year, 10-years, 25-years, 50-years and 100 years are given in tables 2.4 to 2.16. The environmental contour plots for each month are given in Appendix B. Tables 2.3 to 2.15 also give the range of spectral peak periods associated with the maximum significant wave height for each return period.

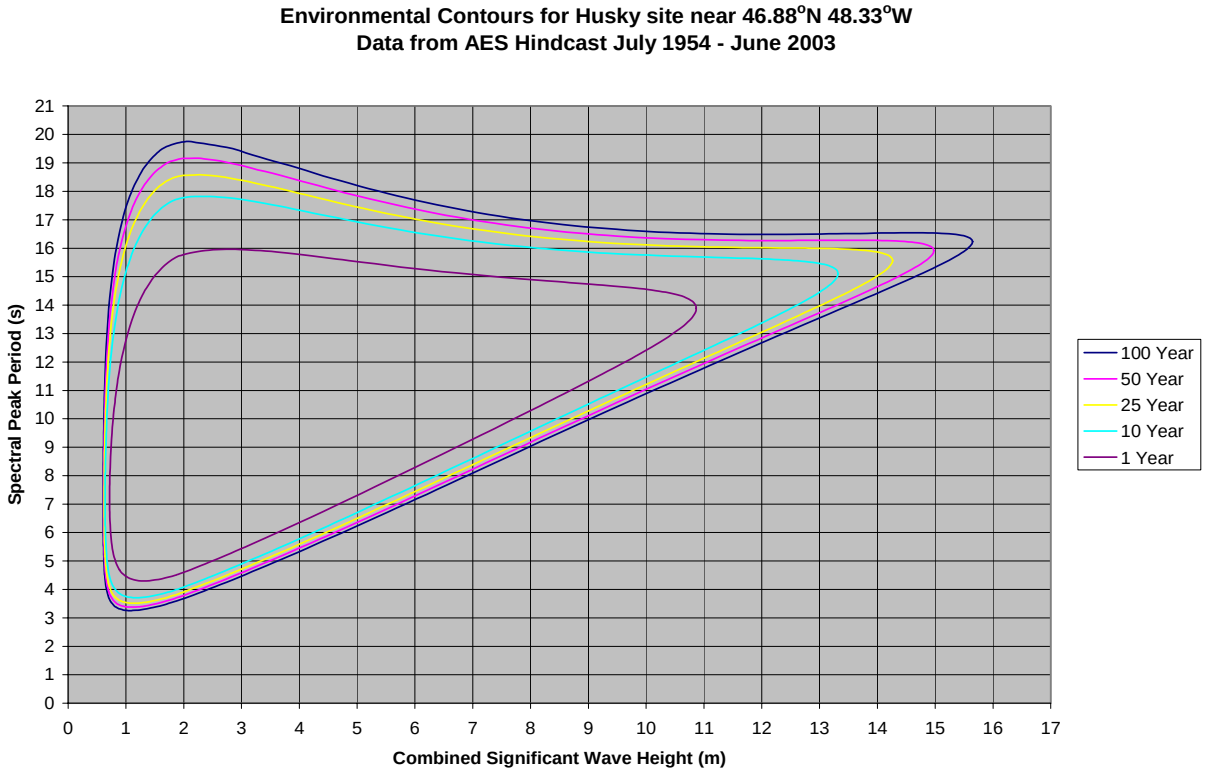

.

Figure 2.4 Environmental Contour Plot for White Rose Delineation Wells.

Table 2.3 Extreme Wave Estimates and Spectral Peak Periods for all Months Combined.

Return Period (years)	*Significant Wave Height (m)*	*Spectral Peak Period(s) Median Value*	*Peak Period(s) Lower limit*	*Peak Periods (s) Upper Limit*
1	10.9	13.9	11.9	16.2
10	13.3	15.1	13.5	16.9
25	14.3	15.6	14.1	17.1
50	15.0	15.9	14.6	17.4
100	15.6	16.2.	15.0	17.6

Table 2.4 Extreme Wave Estimates and Spectral Peak Periods for January.

Return Period (years)	*Significant Wave Height (m)*	*Spectral Peak Period(s) Median Value*	*Peak Period(s) Lower limit*	*Peak Periods (s) Upper Limit*
1	9.7	13.3	11.2	15.7
10	12.2	14.6	13.0	16.3
25	13.1	15.1	13.7	16.6
50	13.8	15.5	14.2	16.9
100	14.5	15.8	14.6	17.1

Table 2.5 Extreme Wave Estimates and Spectral Peak Periods for February.

Return Period (years)	*Significant Wave Height (m)*	*Spectral Peak Period(s) Median Value*	*Peak Period(s) Lower limit*	*Peak Periods (s) Upper Limit*
1	9.6	13.1	11.0	15.7
10	12.5	14.7	13.1	16.5
25	13.5	15.3	13.9	16.9
50	14.3	15.8	14.5	17.2
100	15.1	16.3	15.1	17.5

Table 2.6 Extreme Wave Estimates and Spectral Peak Periods for March.

Return Period (years)	*Significant Wave Height (m)*	*Spectral Peak Period(s) Median Value*	*Peak Period(s) Lower limit*	*Peak Periods (s) Upper Limit*
1	7.9	12.3	9.6	15.7
10	10.1	13.3	11.0	16.0
25	10.9	13.6	11.5	16.1
50	11.5	13.8	11.8	16.2
100	12.0	14.1	12.2	16.2

Table 2.7 Extreme Wave Estimates and Spectral Peak Periods for April.

Return Period (years)	*Significant Wave Height (m)*	*Spectral Peak Period(s) Median Value*	*Peak Period(s) Lower limit*	*Peak Periods (s) Upper Limit*
1	6.9	11.7	9.2	14.8
10	8.8	12.5	10.5	14.9
25	9.5	12.8	10.9	15.0
50	10.1	13.0	11.3	15.0
100	10.6	13.2	11.6	15.1

Table 2.8 Extreme Wave Estimates and Spectral Peak Periods for May.

Return Period (years)	*Significant Wave Height (m)*	*Spectral Peak Period(s) Median Value*	*Peak Period(s) Lower limit*	*Peak Periods (s) Upper Limit*
1	5.6	10.6	8.3	13.5
10	7.6	11.9	10.0	14.2
25	8.5	12.4	10.7	14.5
50	9.1	12.8	11.2	14.7
100	9.7	13.2	11.7	15.0

Table 2.9 Extreme Wave Estimates and Spectral Peak Periods for June.

Return Period (years)	*Significant Wave Height (m)*	*Spectral Peak Period(s) Median Value*	*Peak Period(s) Lower limit*	*Peak Periods (s) Upper Limit*
1	4.6	9.8	7.4	13.0
10	6.4	11.2	9.2	13.6
25	7.2	11.8	10.0	13.9
50	7.7	12.2	10.6	14.2
100	8.3	12.7	11.1	14.5

Table 2.10 Extreme Wave Estimates and Spectral Peak Periods for July.

Return Period (years)	*Significant Wave Height (m)*	*Spectral Peak Period(s) Median Value*	*Peak Period(s) Lower limit*	*Peak Periods (s) Upper Limit*
1	4.0	9.1	6.7	12.4
10	5.1	9.9	7.7	12.7
25	5.5	10.2	8.1	12.9
50	5.8	10.4	8.4	13.0
100	6.2	10.7	8.7	13.1

Table 2.11 Extreme Wave Estimates and Spectral Peak Periods for August.

Return Period (years)	*Significant Wave Height (m)*	*Spectral Peak Period(s) Median Value*	*Peak Period(s) Lower limit*	*Peak Periods (s) Upper Limit*
1	4.3	9.5	6.8	13.2
10	5.6	10.8	8.2	14.2
25	6.1	11.4	8.8	14.7
50	6.5	11.8	9.3	15.1
100	6.9	12.3	9.8	15.5

Table 2.12 Extreme Wave Estimates and Spectral Peak Periods for September.

Return Period (years)	*Significant Wave Height (m)*	*Spectral Peak Period(s) Median Value*	*Peak Period(s) Lower limit*	*Peak Periods (s) Upper Limit*
1	6.5	11.2	8.7	14.3
10	8.5	12.3	10.3	14.7
25	9.3	12.8	10.9	15.0
50	9.9	13.1	11.4	15.1
100	10.5	13.4	11.8	15.3

Table 2.13 Extreme Wave Estimates and Spectral Peak Periods for October.

Return Period (years)	*Significant Wave Height (m)*	*Spectral Peak Period(s) Median Value*	*Peak Period(s) Lower limit*	*Peak Periods (s) Upper Limit*
1	7.2	11.6	9.3	14.5
10	9.4	12.8	10.9	15.0
25	10.2	13.3	11.5	15.3
50	10.9	13.6	11.9	15.5
100	11.5	14.0	12.4	15.7

Table 2.14 Extreme Wave Estimates and Spectral Peak Periods for November.

Return Period (years)	*Significant Wave Height (m)*	*Spectral Peak Period(s) Median Value*	*Peak Period(s) Lower limit*	*Peak Periods (s) Upper Limit*
1	8.1	12.4	10.1	15.3
10	10.3	13.5	11.6	15.7
25	11.1	13.9	12.1	15.9
50	11.7	14.2	12.5	16.0
100	12.3	14.4	12.9	16.2

Table 2.15 Extreme Wave Estimates and Spectral Peak Periods for December.

Return Period (years)	*Significant Wave Height (m)*	*Spectral Peak Period(s) Median Value*	*Peak Period(s) Lower limit*	*Peak Periods (s) Upper Limit*
1	9.2	13.1	10.8	15.8
10	11.7	14.2	12.4	16.3
25	12.6	14.6	13.0	16.5
50	13.2	14.9	13.3	16.6
100	13.9	15.2	13.7	16.8

3 Physical Oceanography

3.1 Water Masses

Temperature and salinity data from historical measurements was extracted from the Bedford Institute of Oceanography (BIO) archive. This archive in addition to maintaining the data collected by BIO and the Department of Fisheries and Oceans (DFO), also contains data collected by Marine Environmental Data Service in Ottawa, the National Oceanographic Center (NODC) in Washington, universities, consulting firms, and other groups. The geographic limits used for this study are 46.7°N to 46.97°N, and 48.17°W to 47.55°W. The data was sorted into depth bins from 0 to 100 m in steps of 10 $\pm$5 m, and from 125 to 200 m in steps of 25 $\pm$5 m.

3.1.1 Historical Data

There are two water masses on the eastern Newfoundland Shelf; the cold intermediate layer water (CIL) and the Labrador Current Water (LCW) (Figure 3.1).

The Cold Intermediate Layer is a low salinity, colder intermediate layer water. The Cold Intermediate Layer water is measured on the Shelf from late spring to fall with temperatures ranging from 0°C to -1.84^{o}C and salinities ranging from 32% to 33.5 ‰ (Petrie et al., 1988; Colbourne, 2004). The Cold Intermediate Layer is a low salinity and colder water mass than underlying waters. The waters above the cold intermediate layer are warmed in late spring and summer due to solar heating and have a lower salinity due to fresh water run-off from James Bay, Labrador rivers and other sources. The Cold Intermediate Layer can extend from shore to over 200 km, and to a depth of 200 m with inter-annually variations (Colbourne, 2004). The Cold Intermediate Layer forms in the winter through heat loss at the surface and salt releases during ice formation. On the Slope the water is warmer and more saline. The Cold Intermediate Layer remains isolated between the seasonally heated upper layer of the Shelf and the warmer Slope water near the bottom. The Cold Intermediate Layer water is separated from the warmer saltier water of the continental Slope by a frontal region denoted by a strong horizontal temperature and salinity gradient near the edge of the Shelf (Colbourne and Fitzpatrick, 2002).

The Labrador Current Water (Figure 3.1) is also present on the Shelf. The Labrador Current Water is a combination of outflow waters from Baffin Bay and Hudson Strait, mixed together with remnants of the West Greenland Current. The Labrador Current originates from the Hudson Strait at 60^{o}N and flows southward over the Labrador and Newfoundland Shelf and Slope to the tail end of the Grand Banks at 43^{o}N (Lazier and Wright, 1993). The Labrador Current becomes two branches on the southern Labrador Shelf; an inshore branch with approximately 15% of the transport and a main slope branch with approximately 85% of the transport (Lazier and Wright, 1993). The offshore Labrador Current typically flows along the continental slope between the 300 m and 1500 m isobath (Lazier and Wright, 1993).

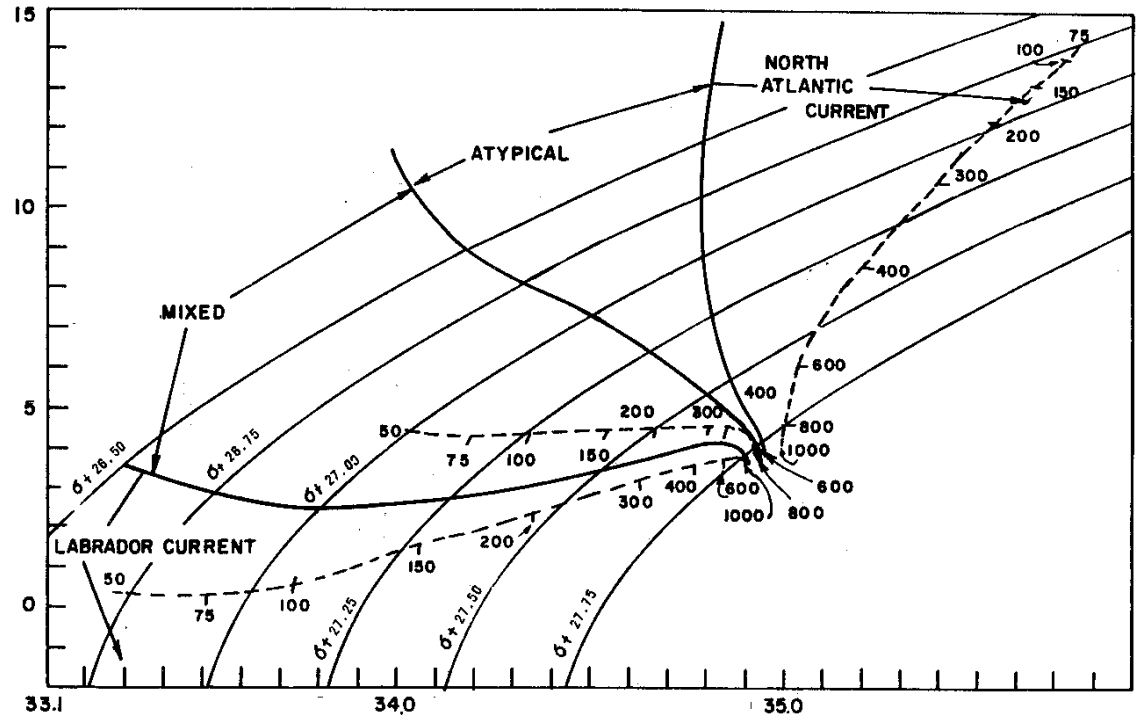

Figure 3.1 The T–S water masses of NW Atlantic zone.

Source: (Hayes et al., 1977).
Note: Dashed lines represent 20 year mean for each water mass.

The Labrador Current Water has seasonal and vertical variability giving it a fairly large range of properties (Figure 3.2). Lazier (1982) demonstrated that the temperature and salinity of the water masses of the Labrador Shelf undergo seasonal modification, with its properties mirroring the cycle of heating and cooling, ice formation and melt. Hinrichsen and Tomczak (1993) give a general value of -0.28°C (potential temperature) and 33.33 ‰ salinity for Labrador Current water properties. Lazier (1982) gives a range of properties for the inshore branch (over the Shelf) of -1.0°C to 2.0°C and 32 ‰ to 33.5 ‰, and for the offshore branch (over the Slope) a range of 3°C to 4°C and 34% to 35 ‰. Over the Slope the Labrador Current Water is generally warmer and saltier than over the Shelf. Hendry et al. (1998) plotted the Labrador Current Water T-S curve for June and July (Figure 3.2) and shows that the properties vary from a minimum temperature of approximately -1.44°C with a corresponding salinity near 32.9 ‰ and maximum temperatures and salinities near 7°C and 35 ‰, respectively.

3.1.2 Summary of Water Masses

The temperature and salinity contour plots and T-S curve for the study region is shown in Figures 3.3 and 3.4, and a comparison with different water masses is shown in Figure 3.5.

The T-S curve is determined by combining all available data at each depth interval and calculating the average temperature and salinity. There is no data for the periods of January and August. The upper 50 m temperature and salinity is highly variable and represents the mixed layer. In the temperature contour plot the blue area represents the cold intermediate layer from May to November and the vertical homogeneity during the winter months. In this area the cold intermediate layer appears to extend to the sea bottom. The T-S diagram (Figure 3.4) shows the inshore Labrador Current Water and Cold Intermediate Layer according to the given ranges from Lazier (1982) and Petrie et al. **(**1988), respectively. At a depth of over 30 m the Shelf water average T-S curve is within the range of the Labrador Current Water properties, and over 50 m it is in the range of the Cold Intermediate Layer properties. From approximately 70 m to 125 m the average T-S curve changes and represents a different water mass from that of the mixed layer. This water mass is the Labrador Current Water.

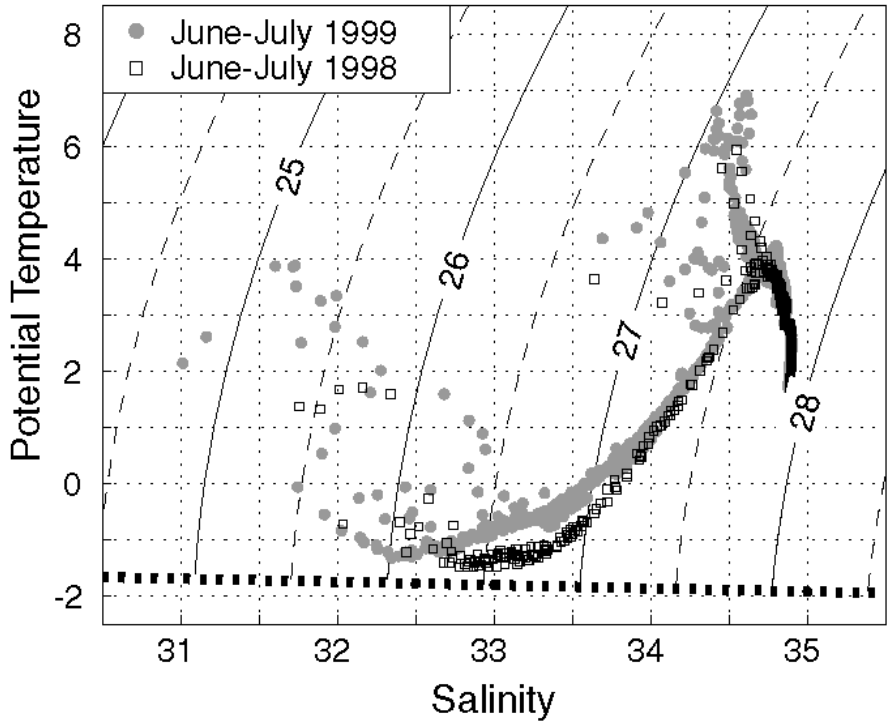

Figure 3.2 Potential temperature vs salinity for the Labrador Current for 1998 and 1999.

Source: Adapted from Hendry et al. (1998).
Note: Potential temperature is defined as the temperature of a parcel of water at the sea surface after it has been raised adiabatically from some depth in the ocean to remove the influence of compressibility.

Figure 3.5 compares the average T-S curve for the study area with the average T-S curve for the Newfoundland Shelf (47°N to 47.80°N; 49.25°W to 47.65°W), the average T-S curve from the BIO database from 1900-2004 for the Slope region just north of the study area, the average for Labrador waters from International Ice Patrol for 1948-1958 (Mamayev, 1975) and the stations from the IV cruise of the R.V. Mikhail Lomonsov (Mamayev, 1975). The North Atlantic T-S curve is warmer and saltier than the all other curves. The T-S curve for station 290 on the Newfoundland Shelf is very similar to the curve for the two regions on the Newfoundland Shelf.

The two T-S curves for the Newfoundland Shelf are very similar, however the curve for the study area which is further south, has slightly higher temperatures.

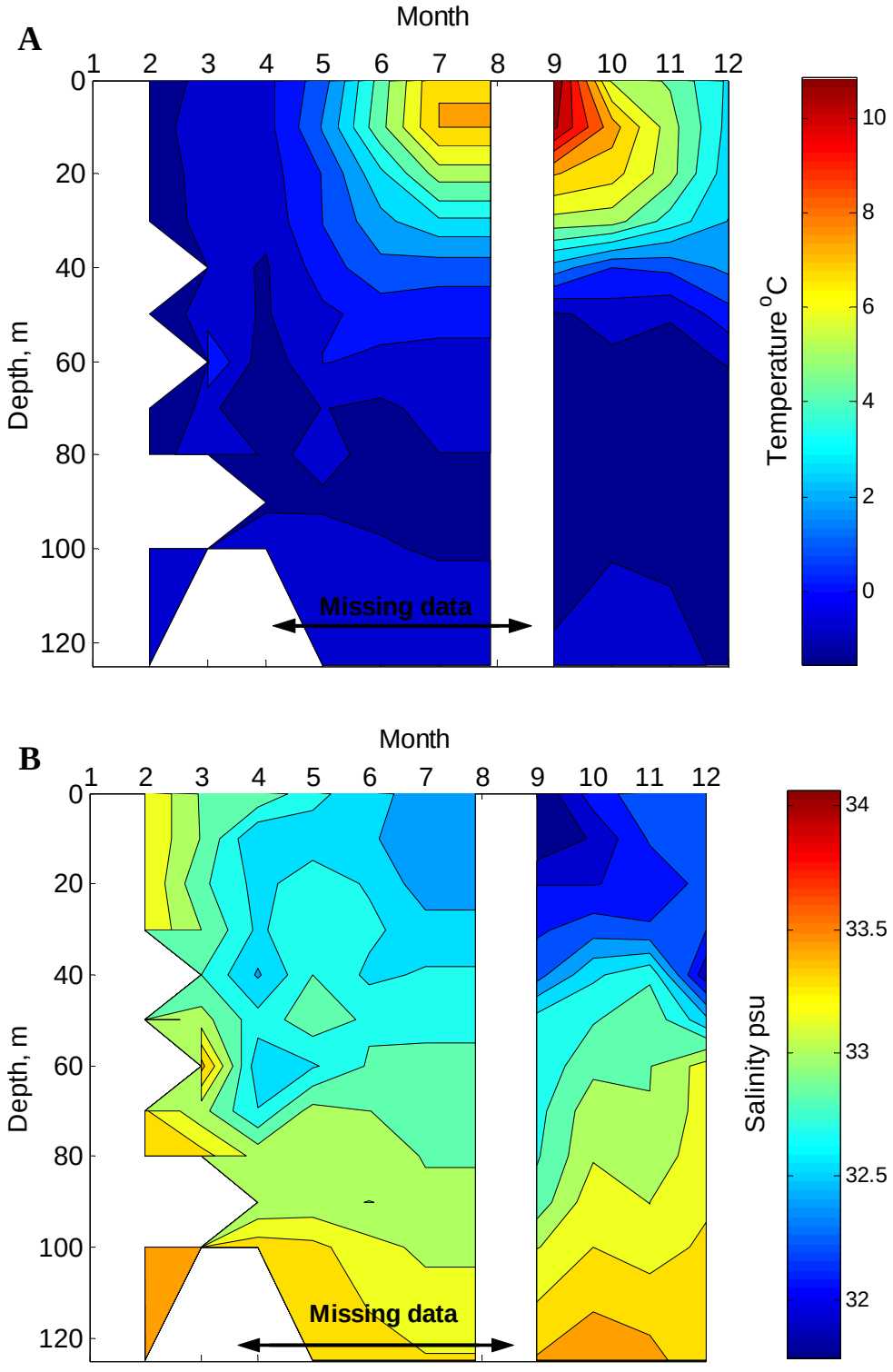

Figure 3.3 Monthly mean A)temperature and B) salinity from BIO database, 1900-2004 from the surface to 125 m for the region on the Newfoundland Shelf defined by; 46.7°N to 46.97°N and 48.17°W to 47.55°W.

Note: White areas are missing data.

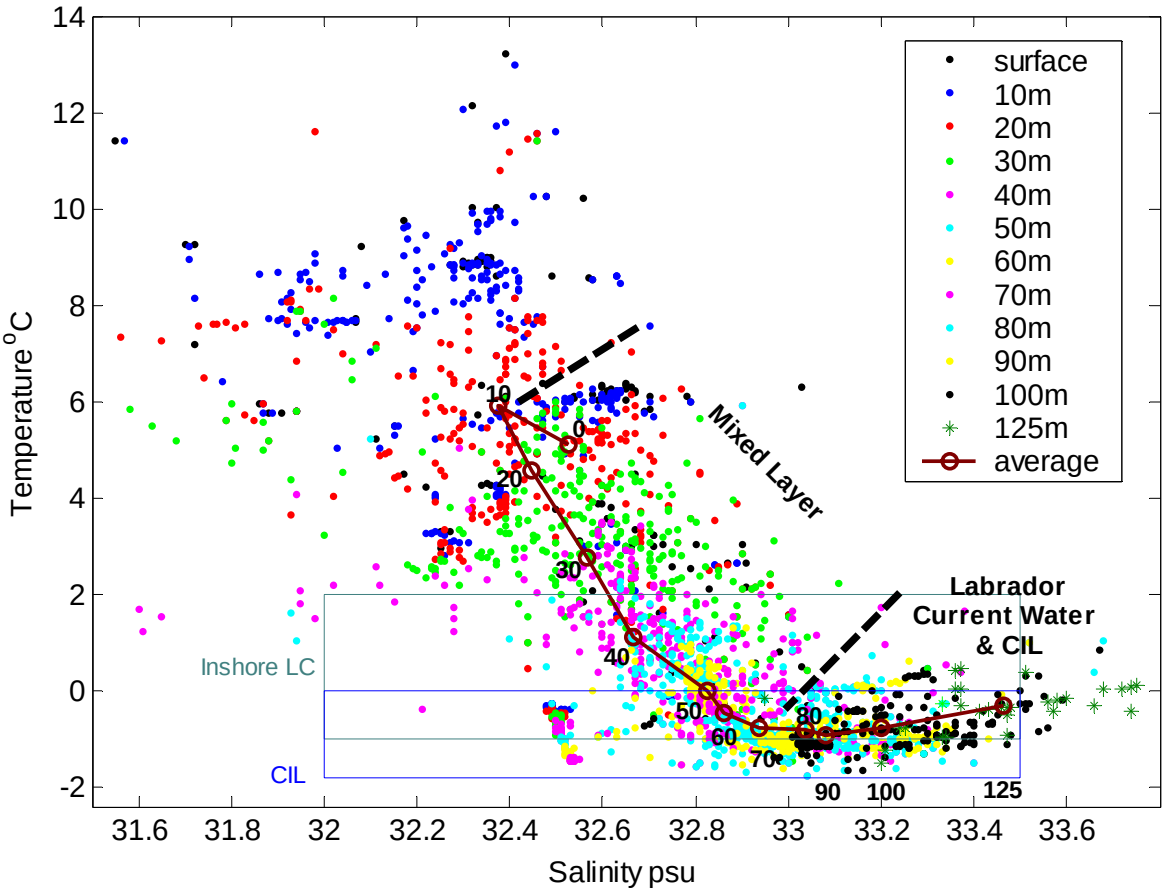

Figure 3.4 T-S Curve from BIO database, 1900-2004 for the region on the Newfoundland Shelf defined by; 46.7°N to 46.97°N, and 48.17°W to 47.55°W.

Note: Each coloured point depicts a different depth and the line is the average. The boxes are the ranges of different water masses, Labrador Current water ranges are from Lazier (1982) and the Cold Intermediate Layer water from Petrie et al. (1988).

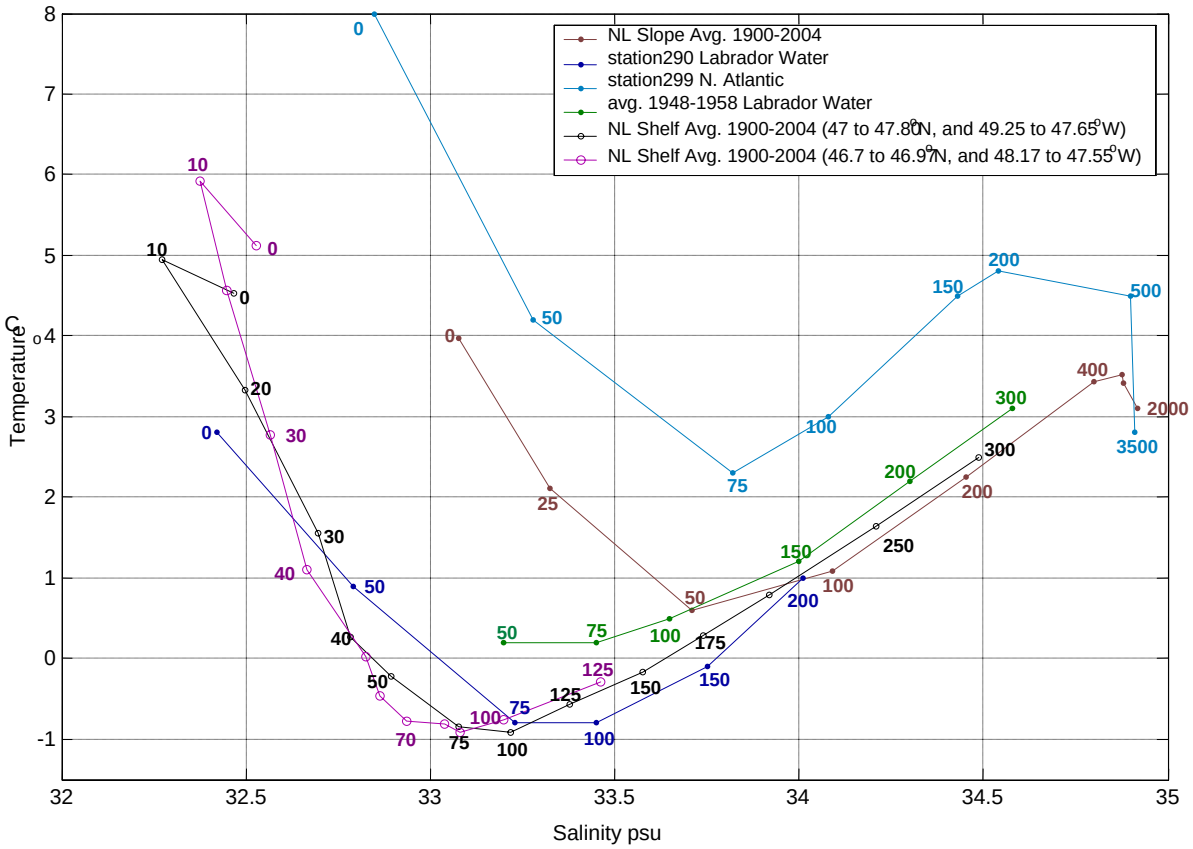

Figure 3.5 T-S Curves for the Newfoundland Shelf (46.7°N to 46.97°N, and 48.17°W to 47.55°W); Newfoundland Shelf (47°N to 47.80°N, and 49.25°W to 47.65°W) Continental Slope, Labrador Sea, and North Atlantic.

Note: The Slope and Shelf average is from the BIO database from 1900-2004 (brown, purple and black line). The average for the Labrador waters is from International Ice Patrol for 1948-1958 (Mamayev, 1975) (Green line). The station data is from the IV cruise of the R.V. Mikhail Lomonsov (Mamayev, 1975) (blue lines).

3.2 *Currents*

The large scale circulation off Atlantic Canada is dominated by well established currents that flow along the margins of the continental shelf. The main circulatory feature near the study area is the Labrador Current, which transports sub-polar water to lower latitudes along the continental shelf of eastern Canada (Figure 3.6). Oceanographic studies show a strong western boundary current following the shelf break with relative low variability compared to the mean flow. Over the Grand Banks a weaker current system is observed. For this area the magnitude of the variability often exceeds that of the mean flow (Colbourne, 2000).

The Labrador Current consists of two major branches. The inner branch is located on the inner half of the shelf and its core is steered by the local underwater topography. The stronger offshore branch flows along the shelfbreak over the upper portion of the continental slope, to the north of the area of interest, between the 300 m and 1500 m isobath This branch of the Labrador Current divides between 48°N and 50°W, resulting in one sub-branch flowing to the east or northeast and the other flowing south around the eastern edge of the Grand Banks and through the Flemish Pass. Characteristic current speeds on the Slope are in the order of 25 cm/sec to 40 cm/sec, while those of the inner branch and on the shallow waters of the Grand Banks are generally much lower.

The outer branch of the Labrador Current exhibits a distinct seasonal variation in flow speeds (Lazier and Wright, 1993), in which the mean flows from September to October are nearly twice as large as the mean flows in March and April. This annual cycle is reported to be the result of the large annual variation in the steric height over the continental shelf in relation to the much less variable internal density characteristic of the adjoining deep waters.

Figure 3.2 shows a summarized analysis of the existing data from drifter buoys carried out by Colbourne et al. (1997). This figure illustrates the general pattern of the spatial distribution of the surface currents to the northeast of the Newfoundland shelf. The intensified flow near the study area can be seen in the form of relatively large vectors and convergence of the paths of the drifter buoys.

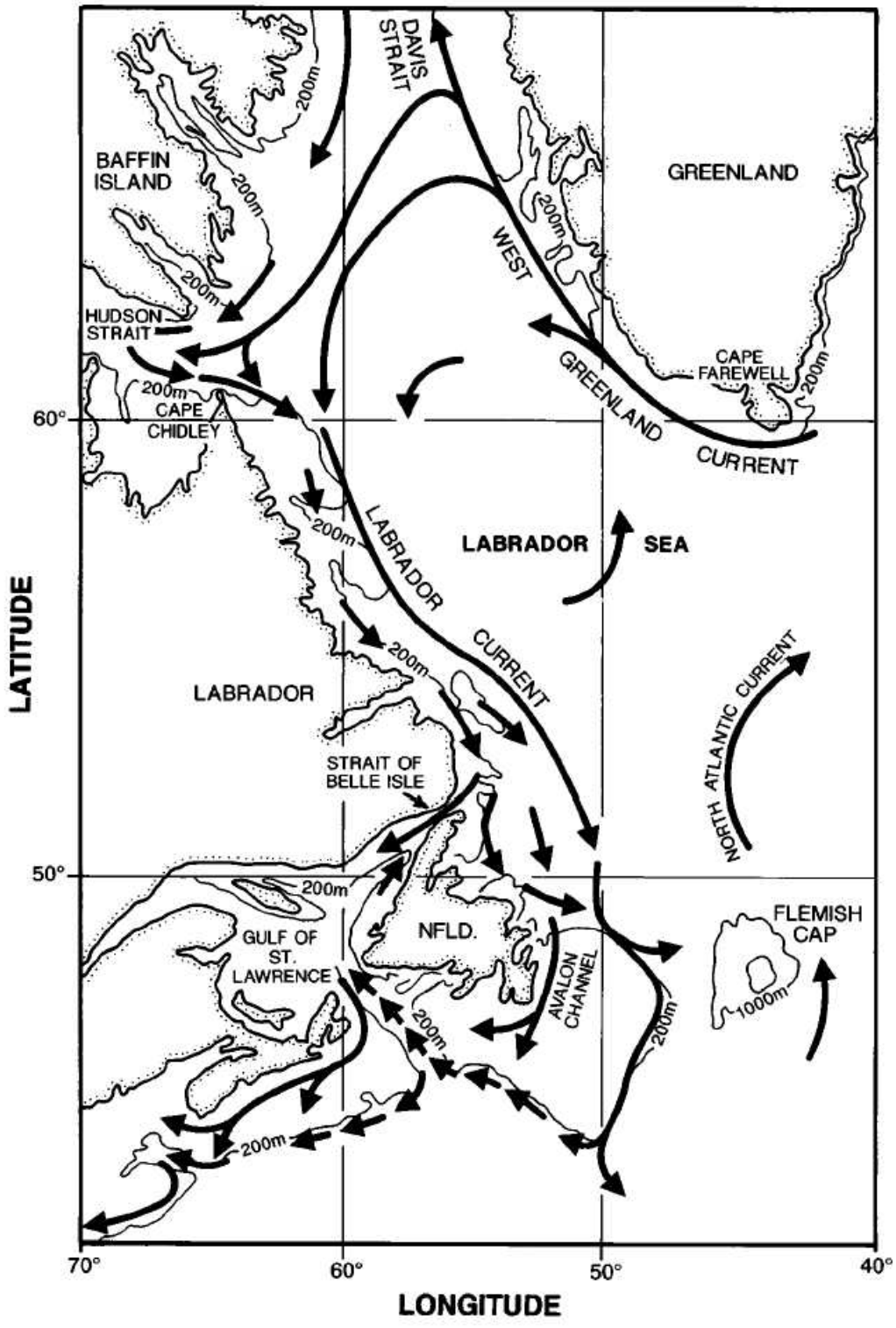

Figure 3.6 Mayor Ocean Circulation Features in the Northwest Atlantic.
Source: Colbourne et al., 1997

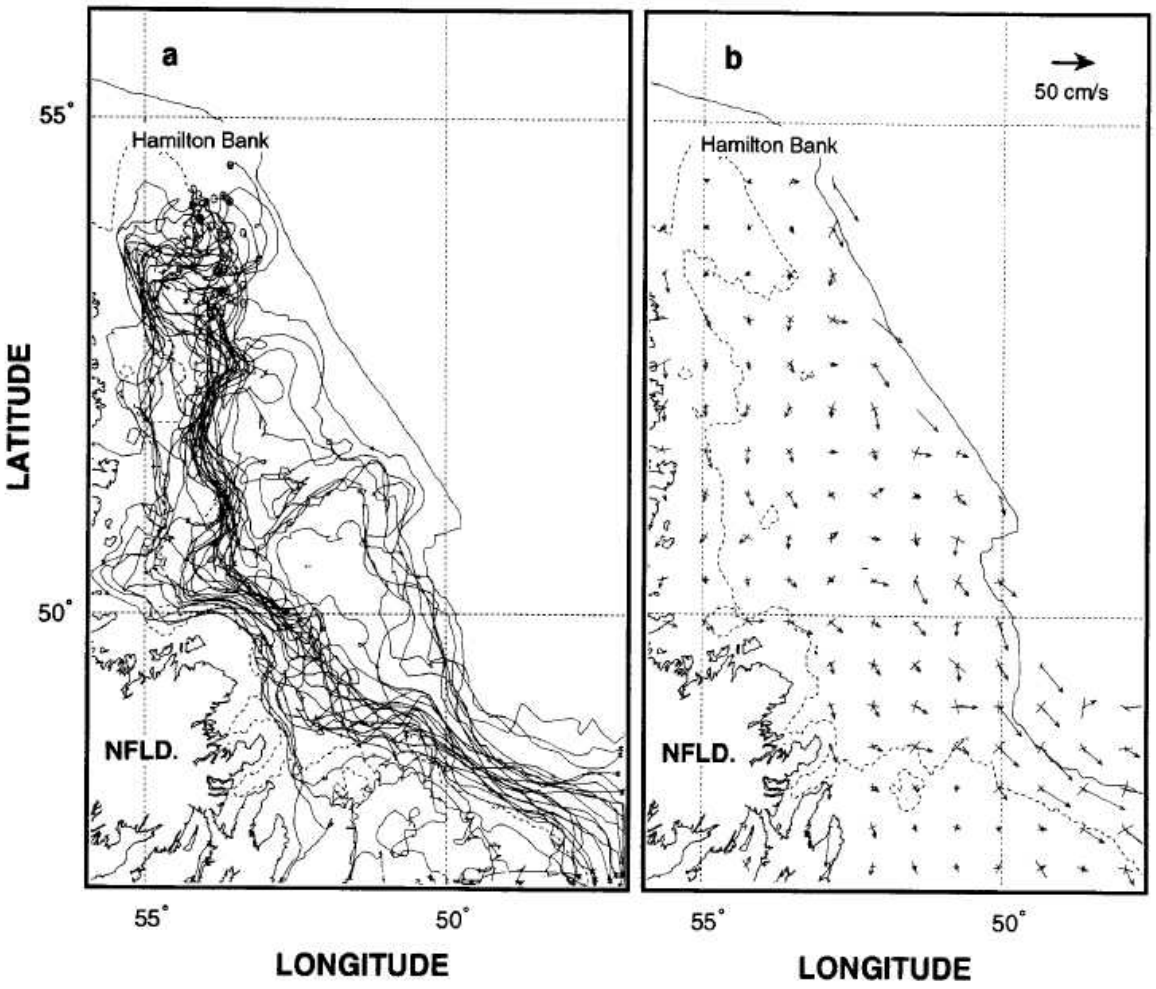

Figure 3.7 Currents on the northeast Newfoundland shelf as inferred from 149 drifting buoys.

Source: Colbourne et al. (1997).

Note: (a) Low-pass-filtered drifting buoy tracks. Drop locations are indicated by circles and terminal positions by asterisks.
(b) Mean surface currents derived from spatial averages of all drifting buoy tracks. The principal axes of variation are indicated by crosses.

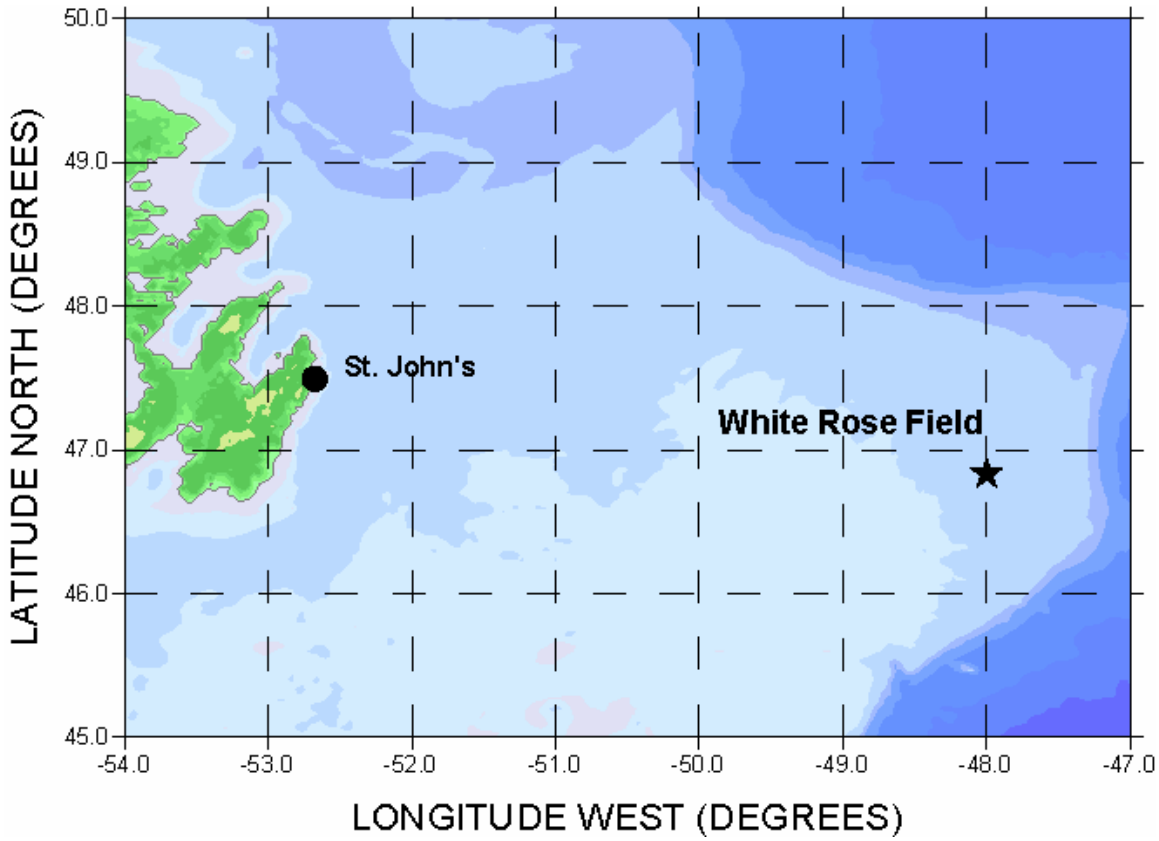

Figure 3.8 General location of the study area.

The oceanic properties of the Labrador Current water over the Newfoundland continental shelf are primarily determined by meteorological wind forcing and solar heat exchange of the Northwest Atlantic including the arctic regions **(**Colbourne et al., 1997**).** Wind stress is an important driving force for the surface currents on the continental shelf, with a distinct annual cycle of comparatively strong winds in winter and weaker, more variable winds in summer.

The White Rose field is located near the northeastern edge of the Newfoundland shelf, thus corresponding to an area of transition between the strong offshore branch of the Labrador Current and the weaker, less organized flow characteristic of the shallow waters of the Grand Banks.

In this area, factors other than wind and tides play a dominant role in the general circulation picture. Currents on the shelf edge can be generated by several different mechanisms. De Tracey et al. (1996) suggest that currents at the edge of the Grand Banks are the result of the interaction between factors like meandering and eddy formation in the Labrador Current, and the propagation of continental shelf waves generated up-stream by distant storms.

3.2.1 Current Data

In order to assess the characteristics of the marine currents in the immediate vicinity of the study area, the data was analyzed from moored current meters from 1984 to 2002, and upward looking moored ADCP units from 2002 to 2004. The depth at which the current meters were deployed varied but they were in general, grouped within certain depth intervals. For that reason, and to simplify the presentation of the results, the discussion that follows will deal with the currents in a water column divided in three layers: subsurface, mid-water and near the bottom depths. To keep the consistency in the discussion, ADCP data bins corresponding to these three layers were selected for analysis.

The results presented in this report do not intend to be definitive, since each data set represents a snapshot of the current behavior at the moment of the observations. However, given that all the climatic seasons are present and all the three layers of the water column's vertical structure were sampled, the discussion that follows qualifies as a reasonable approximation of what one could expect in terms of marine currents, in the White Rose area.

Later in this text, the different data sets will usually be referred to by the name of the wells being drilled during the data collection period. This information is provided in Table 1, together with the spatial and temporal coverage of the discussed data. The geographic location of the different moorings is shown in Figures 3.9 to 3.11.

In Table 3.4 "White Rose NBS" corresponds to a study of the currents in the bottom boundary layer measured by Oceans Ltd. for Husky Energy in 2002. In this study two instruments were deployed at 10 m (depth 110 m) and 3 m (depth 117 m) above the ocean floor.

The information contained in these data sets was used to obtain overall and monthly rose plots and, if the data quality was appropriate, the corresponding progressive vector diagrams. Some information on the tidal currents was determined by means of harmonic tidal analysis of the longer data series.

Table 3.1 Location and Sampling Periods of Current Data.

Site	Period	Depths (m), data type(*)	Geographic Coordinates
White Rose N-30	Aug. 16 – Sep. 29, 1999	20 CM	46°49'48"N; 48°03'47”W
White Rose N-30	Aug. 19 – Oct. 14, 1999	59 CM	46°50'13"N; 48°05'20"W
White Rose L-08	Mar. 31 – Jun. 22, 1999	20 CM	46°47'46"N; 48°02'48"W
White Rose L-08	Mar. 31 – Jun. 22, 1999	62 CM	46°47'46"N; 48°02'48"W
White Rose L-08	Mar. 31 – Jun. 22, 1999	111 CM	46°47'48"N; 48°02'48"W
White Rose A-17	Jun. 23 – Aug. 6, 1999	20 CM	46°00'46"N; 48°00'03"W
White Rose E-09	May 14 – July 5, 1988	98 CM	46°51'48"N; 48°03'56"W
White Rose NBS	Apr. 15 – Jun. 18, 2002	110 CM	46°48'00"N; 48°01'48"W
White Rose NBS	Apr. 15 – Aug. 22, 2002	117 CM	46°48'00"N; 48°02'00"W
Cape Race N-68	Jul. 8 – Aug. 4, 2000	24 DD	46°37'45"N; 48°24'46"W
Cape Race N-68	Jul. 8 – Aug. 4, 2000	48 DD	46°37'45"N; 48°24'46"W
White Rose E-09	Sep. 1 – Oct. 22, 1987	53 CM	46°48'26"N; 48°01'23"W
White Rose E-09	Sep. 1 – Nov. 19, 1987	98 CM	46°48'26"N; 48°01'23"W
White Rose E-09	Jan. 19 – Feb. 20, 1988	49 CM	46°48'26"N; 48°01'23"W
White Rose E-09	Jan. 18 – Feb. 19, 1988	99 CM	46°48'26"N; 48°01'23"W
Cape Race N-68	Jul. 8 – Aug. 4, 2000	80 DD	46°37'45"N; 48°24'46"W
Gros Morne C-17	Sep. 4 – Sep. 18, 2002	24 DD	46°36'14"N; 48°02'25"W
Gros Morne C-17	Sep. 4 – Sep. 18, 2002	56 DD	46°36'14"N; 48°02'25"W
Gros Morne C-17	Sep. 4 – Sep. 18, 2002	96 DD	46°36'14"N; 48°02'25"W
Trepassey J-91	Jul. 25 – Aug. 27, 2002	28 DD	46°40'35"N; 47°58'57"W
Trepassey J-91	Jul. 25 – Aug. 27, 2002	60 DD	46°40'35"N; 47°58'57"W
Trepassey J-91	Jul. 25 – Aug. 27, 2002	100 DD	46°40'35"N; 47°58'57"W

Table 3.1(cont'd). Current Data Sets. Their depths, time coverage and geographic location.

White Rose H-20	May 15 – Jul. 8, 2000	27 DD	46°49'30"N; 48°01'38"W
White Rose H-20	May 15 – Jul. 8, 2000	59 DD	46°49'30"N; 48°01'38"W
White Rose H-20	May 15 – Jul. 8, 2000	107 DD	46°49'30"N; 48°01'38"W
White Rose J-49	Aug. 10 – Nov. 11, 1985	14 CM	46°48'33"N; 48°06'27"W
White Rose J-49	Aug. 10 – No. 19, 1985	57 CM	46°48'33"N; 48°06'27"W
White Rose J-49	Aug. 10 – Nov. 19, 1985	97 CM	46°48'33"N; 48°06'27"W
White Rose N-22	Jul. 5 – Oct. 16, 1984	18 CM	46°51'48"N; 48°03'57"W
White Rose N-22	Jul. 5 – Nov. 10, 1984	80 CM	46°51'48"N; 48°03'57"W
White Rose A-90	Jul. 13 – Aug. 11, 1988	12 CM	46°49'11"N; 47°57'19"W
White Rose A-90	Jul. 13 – Aug. 11, 1988	58 CM	46°49'11"N; 47°57'19"W
White Rose A-90	Jul. 13 – Aug. 11, 1988	110 CM	46°49'11"N; 47°57'19"W
White Rose L-61	Dec. 19 – Feb. 15, 1985	13 CM	46°50'36"N; 48°10'28"W

(*) CM: Current meter data, DD: Acoustic Doppler Current Profiler data.

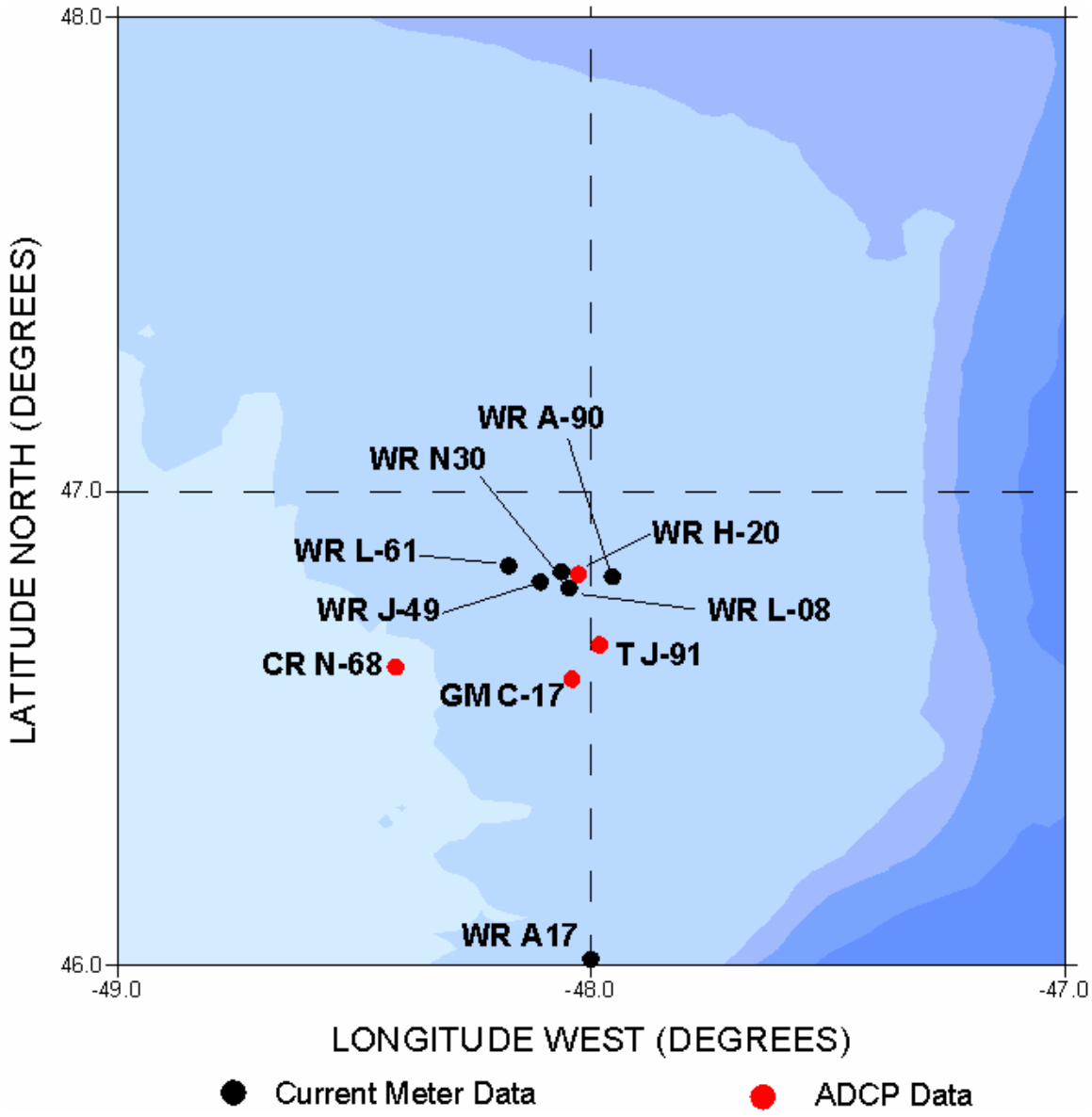

Figure 3.9 Location of the Current Meters and ADCP Moorings in the Near Surface Layer.

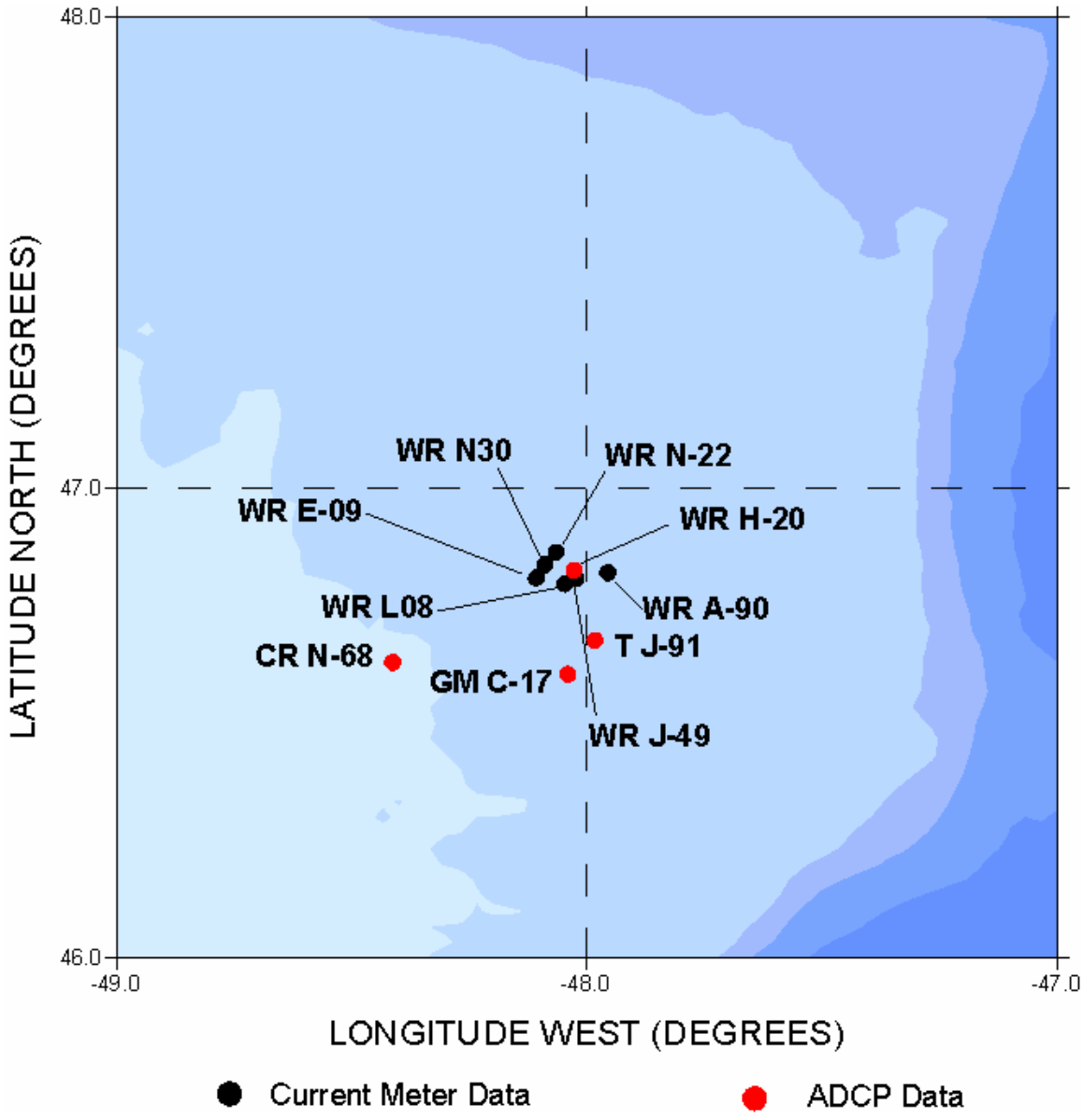

Figure 3.10 Location of the Current Meter and ADCP Moorings in the Mid-Water Layer.

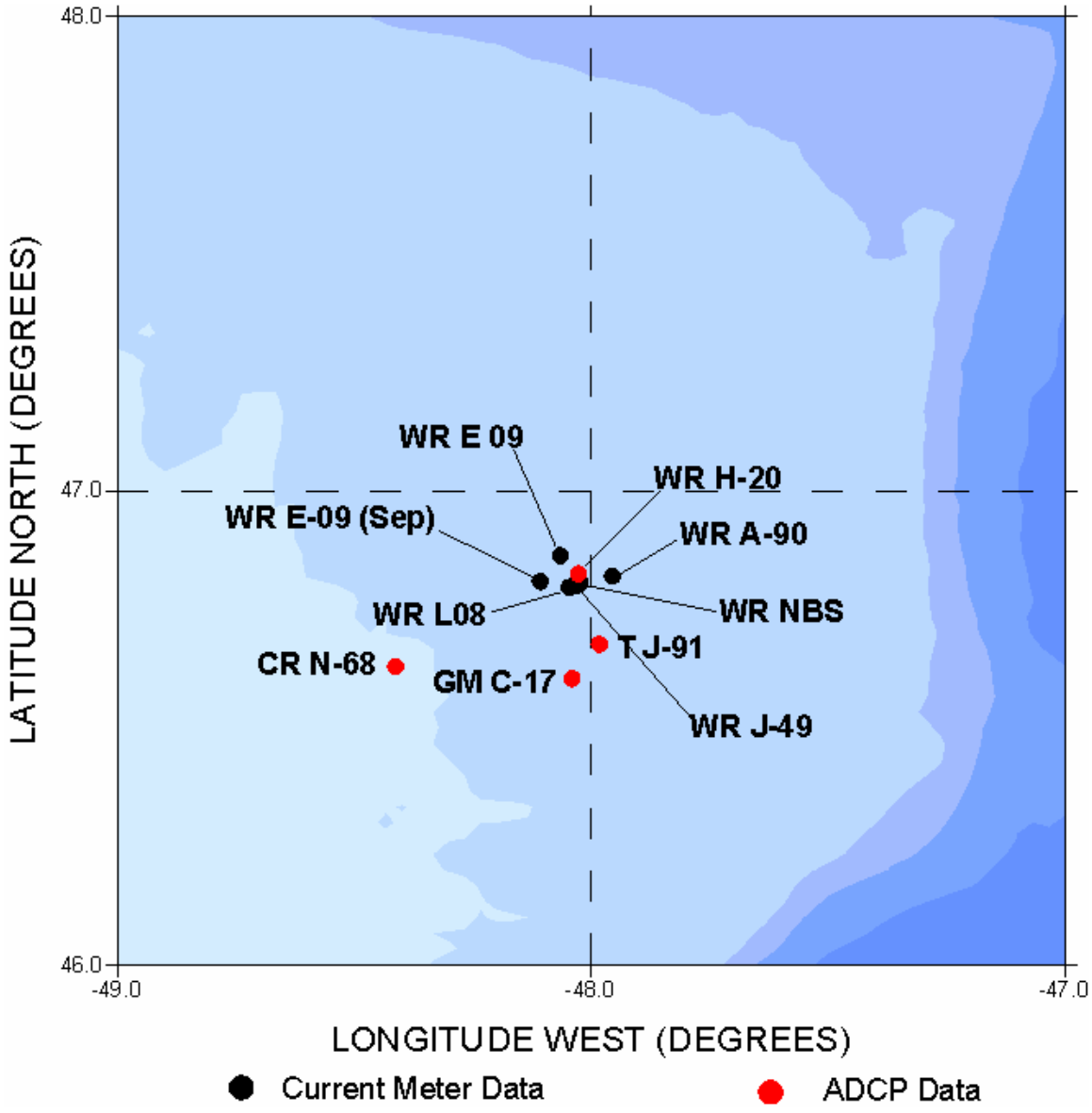

Figure 3.11 Location of the Current Meters and ADCP Moorings in the Near Bottom Layer.

3.2.2 Histograms of Speed and Direction and Progressive Vector Diagrams

Speed histograms and rose plots are presented in Figures 3.12 to 3.14. Rose plots are a graphic representation of the percent occurrence of direction in specified direction intervals. Rose plots show at a glance the most probable direction the current will follow according to a given data set. Speed histograms give a distribution of the probability of occurrence of different speed values.

Progressive vector diagrams (see Appendix C) show the distance and direction a particle of water would travel if the flow was spatially uniform. They are helpful in determining the main velocity of the currents over the whole sampling period. The mean velocity is not to be confused with the mean speed, which is a mere average of the speed values, regardless of the vector orientation. The mean velocity tells us about the distance a water particle will travel under the given conditions. Progressive vector diagrams are shown in Appendix C. The predominant direction of the currents in the study area is between the east and southeast directions. This is consistent with the presence to the north, of the offshore branch of the Labrador Current.

Subsurface currents
The available data suggests a high level of variability associated with the currents in the subsurface layer. The analysis of the progressive vector diagrams shows that the currents were directed mainly to the south at the White Rose N-30, L-61, J-49 and H-20, and Trepassey J-91 well locations. Velocities in this area ranged between 1 cm/sec and 8 cm/sec. At White Rose A-17, L-61 and A-90 the residual current was flowing to the northeast with velocities ranging between 6.4 cm/sec and 10.8 cm/sec at the time of the measurements.

The overall rose plots for these locations (Figure 3.12) showed similar information and little variability from month to month. However, the annual availability was considerable.

Mid-water levels
In the mid-water portion of the water column, the progressive vector diagrams showed a similar circulation pattern as in the subsurface waters in terms of the direction of the flows. Southward or southeastward currents were measured at Gros Morne C-17, Trepassey J-91, and White Rose L-08, A-90, J-49, N-22 and H-20. Similar to the upper layer currents, there were northly currents during some periods. Northeastward and northwestward currents occurred at White Rose N-30 and Cape Race N-68 respectively. Mean velocities at White Rose N-30 were relatively high and reached 10.6 cm/sec. At White Rose E-09 during autumn 1987 the current was in a westerly direction with a mean velocity of 9 cm/sec.

The rose plots for these depths (Figure 3.13) show similar information. They also show that, even though the predominance of some current directions is evident, the currents can cover a wide range of possible directions.

Near bottom depths
Near the bottom, the currents appeared to be in better agreement with the bottom topography of the northeast corner of the Grand Banks. Southeastwards flows occurred at all the White Rose sites. The currents were to the south at Trepassey J-91 and at Gros Morne C-17 and Cape Race N-68. The mean velocities were below 4 cm/sec for all the sampled locations except for White

Rose at A-90 where the mean velocity was 4.1 cm/sec. Speed histogram and rose plots are presented in Figures 3.12 to 3.14. Rose plots are graphic representations of the percent occurrence of direction in specified direction intervals.

The overall rose plots (Figure 3.14) show a high occurrence of currents to the northwest at Cape Race N-68, to the west at Gros Morne C-17, southwest at Trepassey J-91 and southeast at all the White Rose locations. In general, the currents are in all directions showing a rotation tidal circulation. The three data sets with predominant currents to the northwest, west and southwest were very short since the measurements at Cape Race N-68 and Trepassey J-91 was approximately for one month and Gros Morne C-17 was for only two weeks. A longer data set would probably show the resultant currents to be in a southeast direction.

3.2.3 Statistical Summaries of Current Speed

Statistical summaries of current speed for each location and depth are presented in Tables 3.2 to 3.4. In the subsurface waters, very high speeds of 89.9 cm/sec and 82.0 cm/sec occurred at White Rose N-30 and White Rose N-22, respectively. At White Rose N-30 the high speed occurred in September 1999, and at White Rose N-22 the high occurred in September 1984 during the season of tropical storms on the Grand Banks

At mid-depth the highest current speeds occurred at White Rose N-30 with a value of 40.8 cm/sec, and at White Rose J-49 with a value of 43.7 cm/sec. At White Rose N-30 the maximum speed occurred in September 1999, and at White Rose J-49 the maximum speed occurred in November 1985.

The highest speed in the near-bottom waters occurred in November 1985 at White Rose J-49 with a value of 50.6 cm/sec.

Table 3.2 Statistical summary of the current speeds collected at the near-surface depths.

Site ID	Duration	Depth(m)	Mean (cm/sec)	St. Dev (cm/sec)	Max. Speed (cm/sec)
WR N-30	Aug-Sep 1999	20	27.0	16.92	89.9
WR A-17	Jun-Aug 1999	20	11.4	7.89	42.1
CR N-68	Jul-Aug 2000	24	9.9	5.62	37.0
GM C-17	Sep 2002	24	14.7	7.91	41.0
T J-91	Jul-Aug 2002	28	11.7	5.97	33.0
WR H-20	May-Jul 2000	27	12.5	7.57	67.0
WR J-49	Aug-Nov, 1985	14	14.7	7.37	61.7
WR L-08	Mar-Jun 1999	20	10.4	7.53	45.7
WR N-22	Jul-Oct,1984	18	19.6	11.82	82.0
WR A-90	Jul-Aug,1988	12	10.6	1.19	12.6
WR L-61	Dec–Feb, 1985	13	13.0	7.11	36.0

Table 3.3 Statistical summary of the current speeds collected at mid-water depths.

Site ID	Duration	Depth(m)	Mean (cm/sec)	St. Dev (cm/sec)	Max. Speed (cm/sec)
WR N-30	Aug-Sep 1999	59	11.2	7.32	40.8
WR L-08	Mar-Jun 1999	62	12.1	5.02	29.4
CR N-68	Jul-Aug 2000	48	10.6	5.17	31.0
GM C-17	Sep 2002	56	11.4	5.24	24.0
T J-91	Jul-Aug 2002	60	9.0	5.14	31.0
WR H-20	May-Jul 2000	59	9.3	4.96	25.0
WR J-49	Aug-Nov, 1985	57	11.8	5.46	43.7
WR N-22	Jul-Nov, 1984	80	9.6	4.79	31.0
WR E-09	Sep-Oct, 1987	53	10.0	4.91	32.6
WR E-09	Jan-Feb, 1988	49	10.4	5.97	35.0
WR A-90	Jul-Aug, 1988	58	8.9	5.45	24.7

Table 3.4 Statistical summary of the current speeds collected at the near-bottom depths.

Site ID	Duration	Depth(m)	Mean (cm/sec)	St. Dev (cm/sec)	Max. Speed (cm/sec)
WR L-08	Aug-Sep 1999	111	9.5	5.21	27.6
WR E-09	May-Jul 1988	98	10.9	6.97	38.8
WR NBS	Apr-Jun 2002	110	9.5	5.21	31.8
WR NBS	Apr-Aug 2002	117	6.7	3.58	23.6
CR N-68	Jul-Aug 2000	80	8.2	4.45	24.0
GM C-17	Sep 2002	96	10.2	5.56	30.0
T J-91	Jul-Aug 2002	100	8.7	4.83	30.0
WR H-20	May-Jul 2000	107	9.1	4.65	25.0
WR J-49	Aug-Nov, 1985	97	10.7	5.76	50.6
WR E-09	Sep-Nov, 1987	98	10.9	7.09	36.2
WR E-09	Jan-Feb, 1988	99	13.0	6.27	34.5
WR A-90	Jul-Aug, 1988	110	8.9	4.68	25.2

White Rose N-30

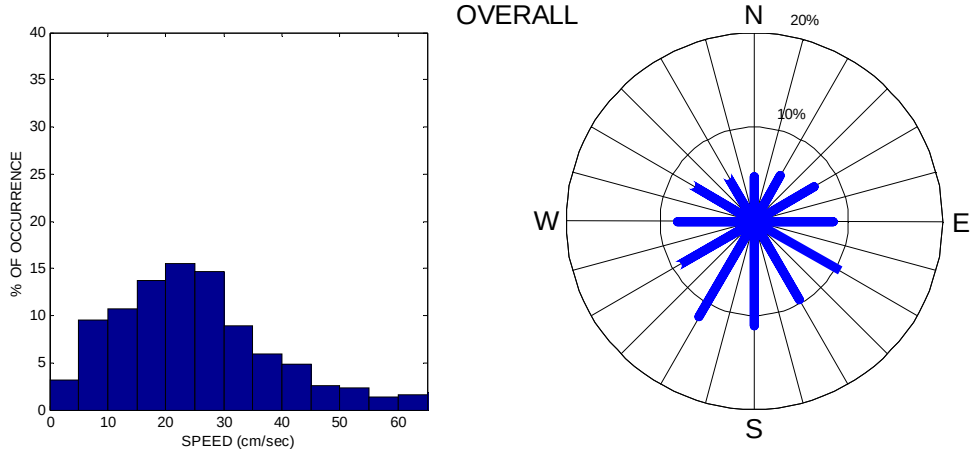

White Rose A-17

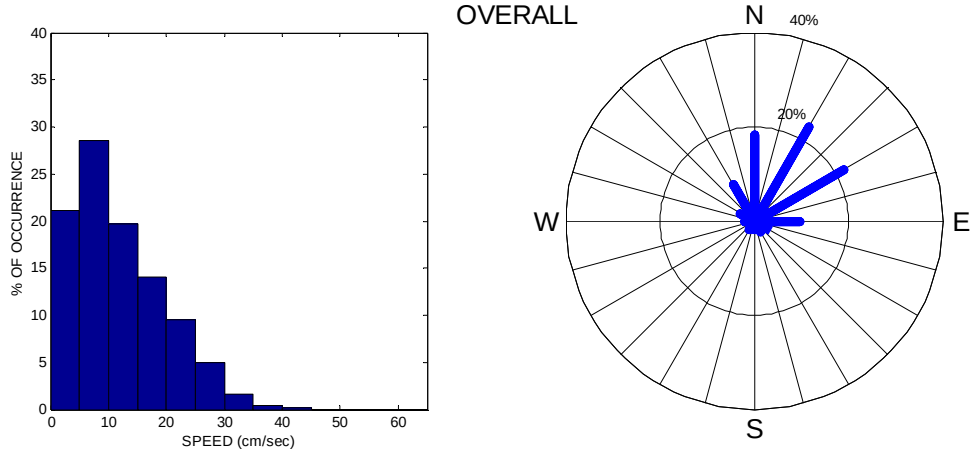

Cape Race N-68

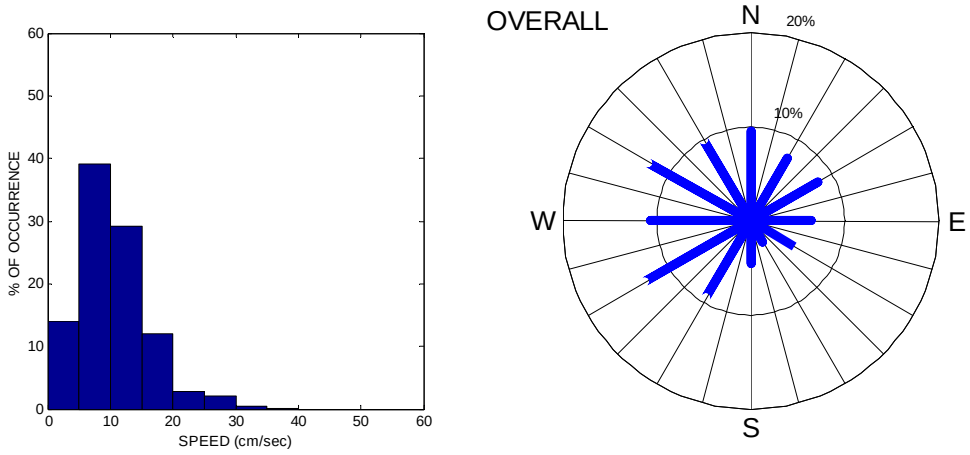

Figure 3.12 Histograms of Speed and Direction for the Subsurface Depths.

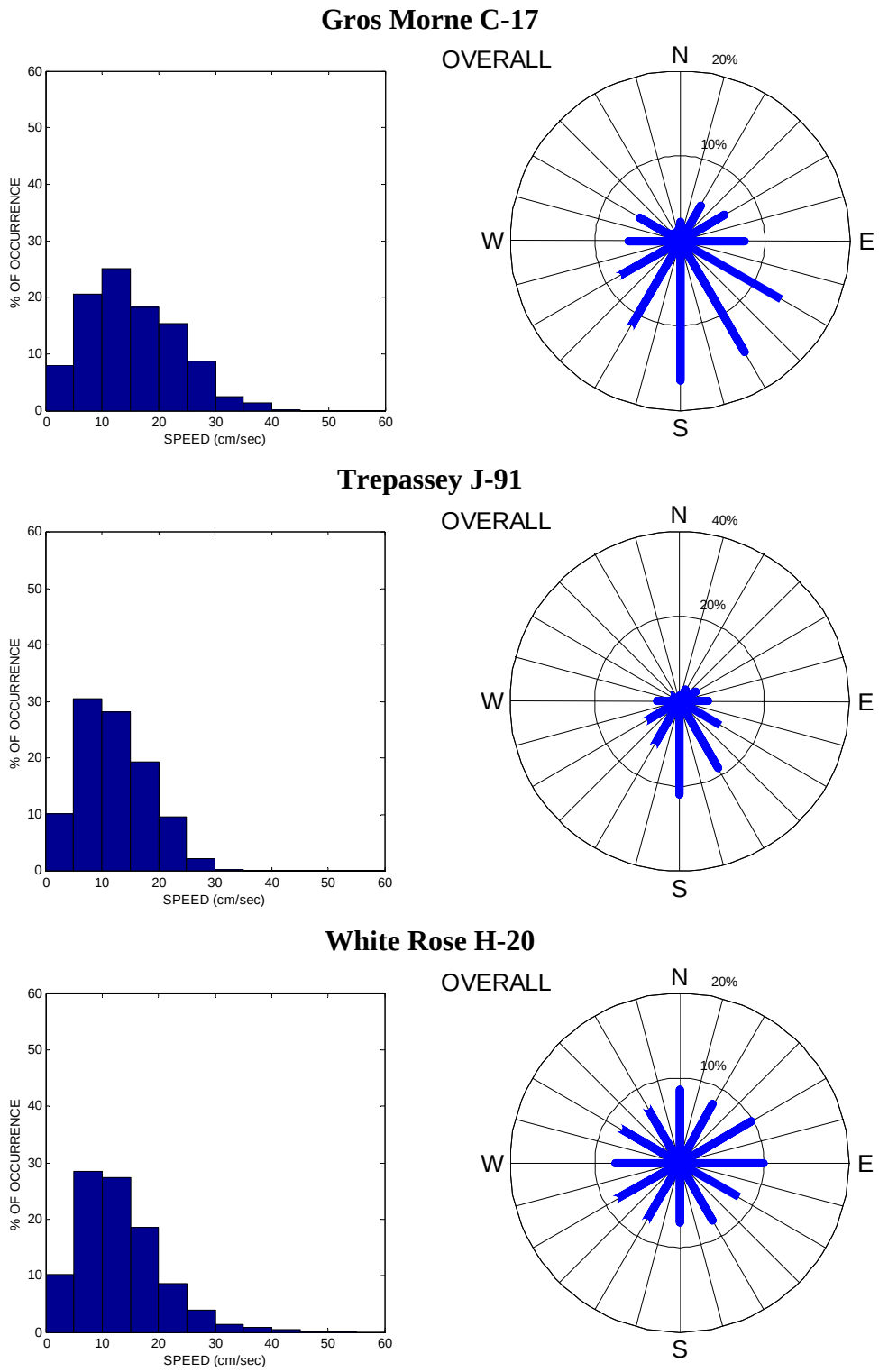

Figure 3.12 (cont'd) Histograms of Speed and Direction for the Subsurface Depths.

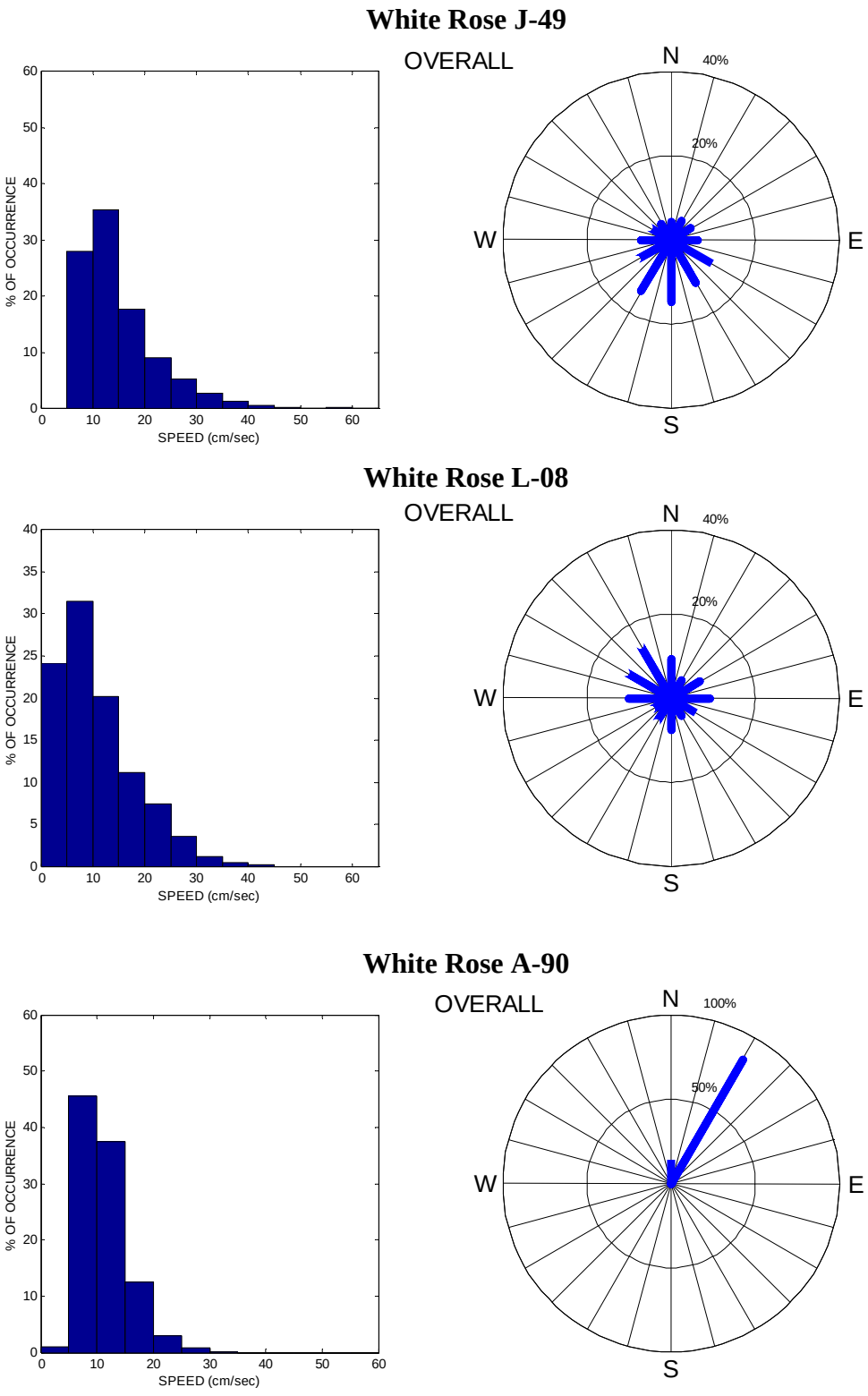

Figure 3.12(cont'd) Histograms of Speed and Direction for the Subsurface Depths.

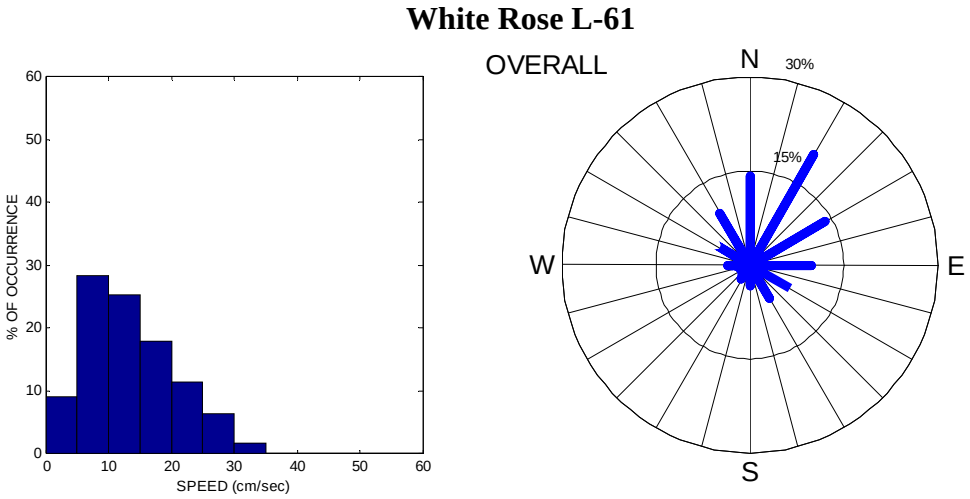

Figure 3.12 (cont'd) Histograms of Speed and Direction for the Subsurface Depths.

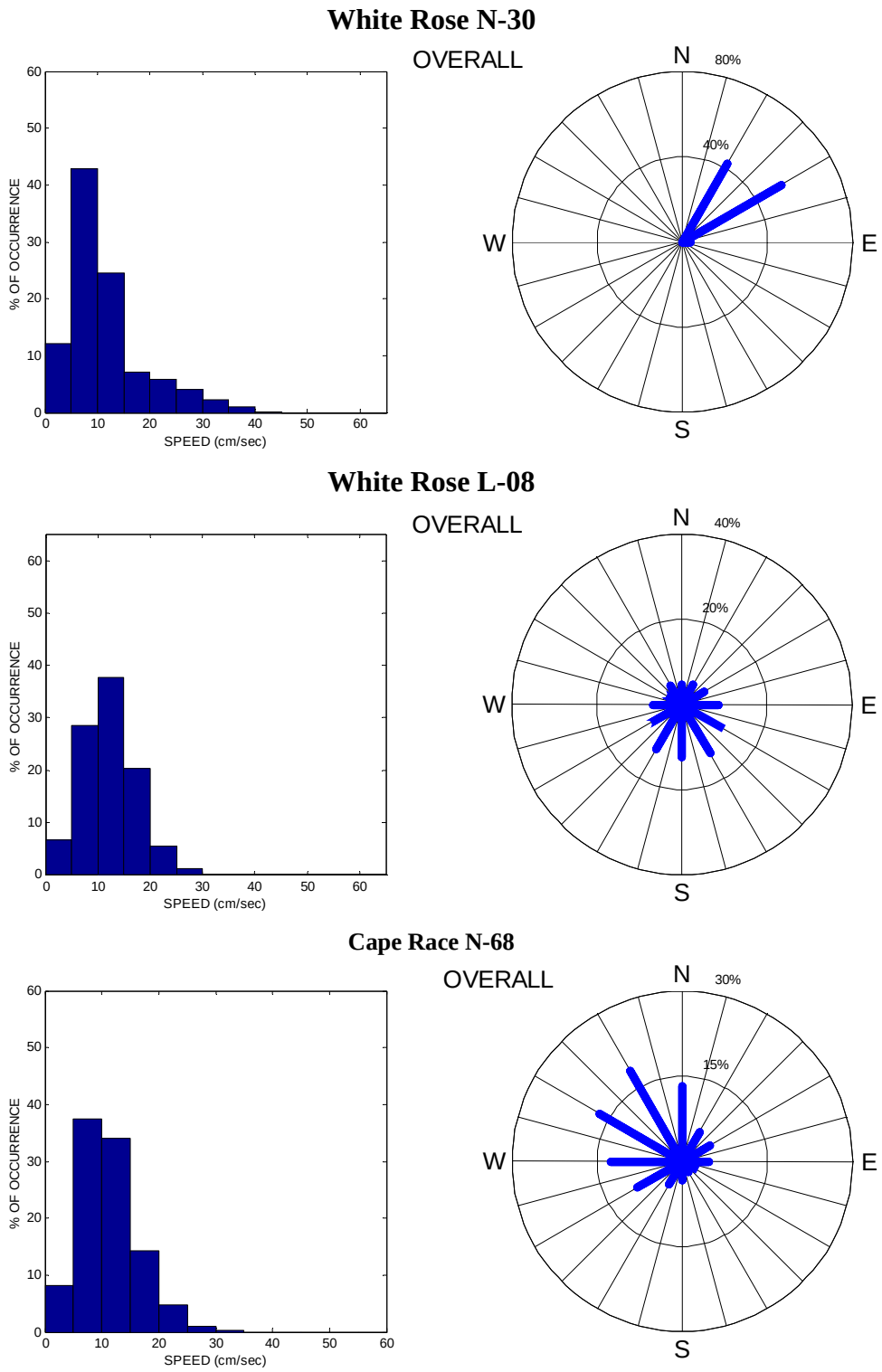

Figure 3.13 Histograms of Speed and Direction for the Mid-Water Depths.

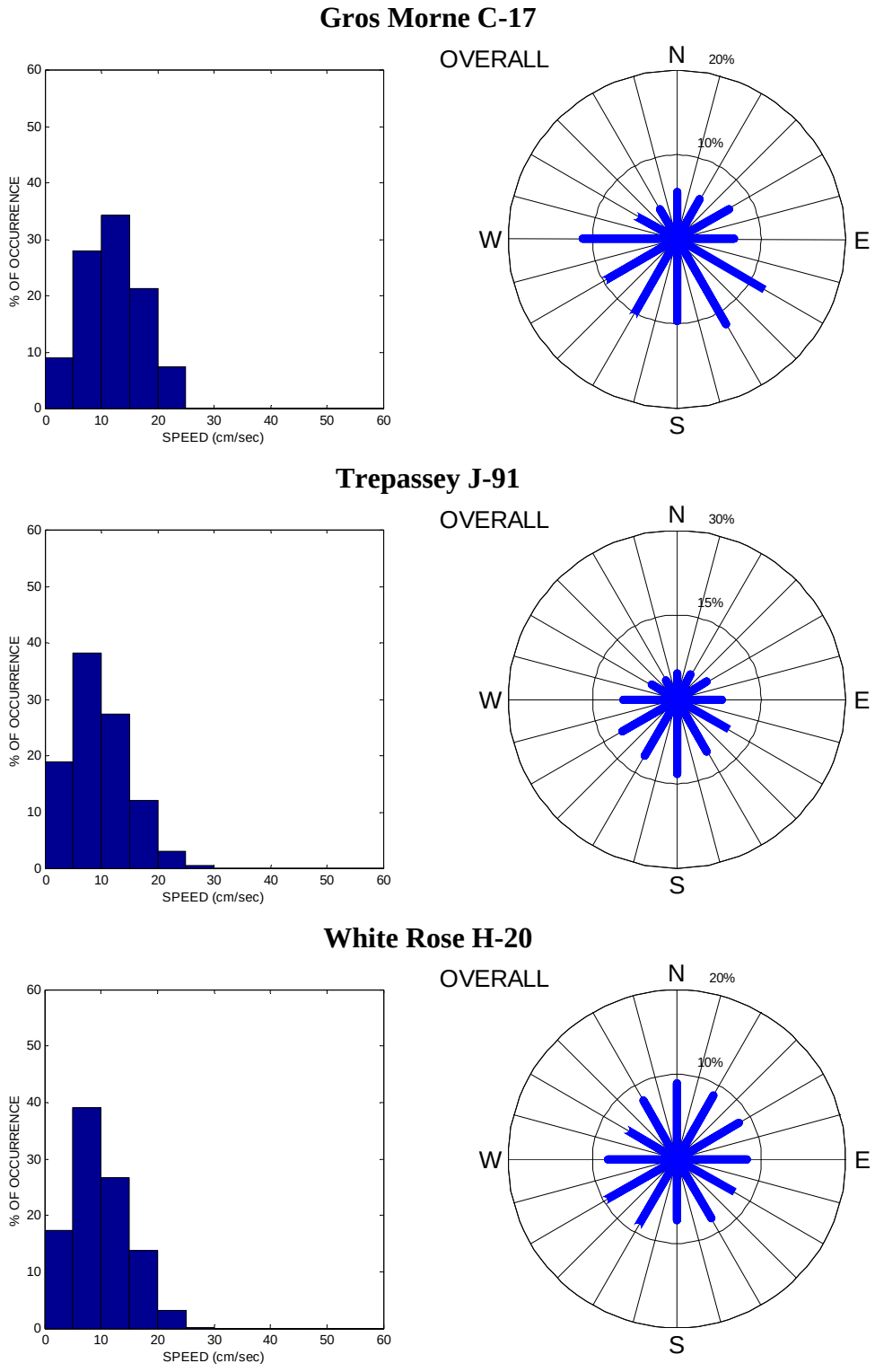

Figure 3.13(cont'd) Histograms of Speed and Direction for the Mid-Water Depths.

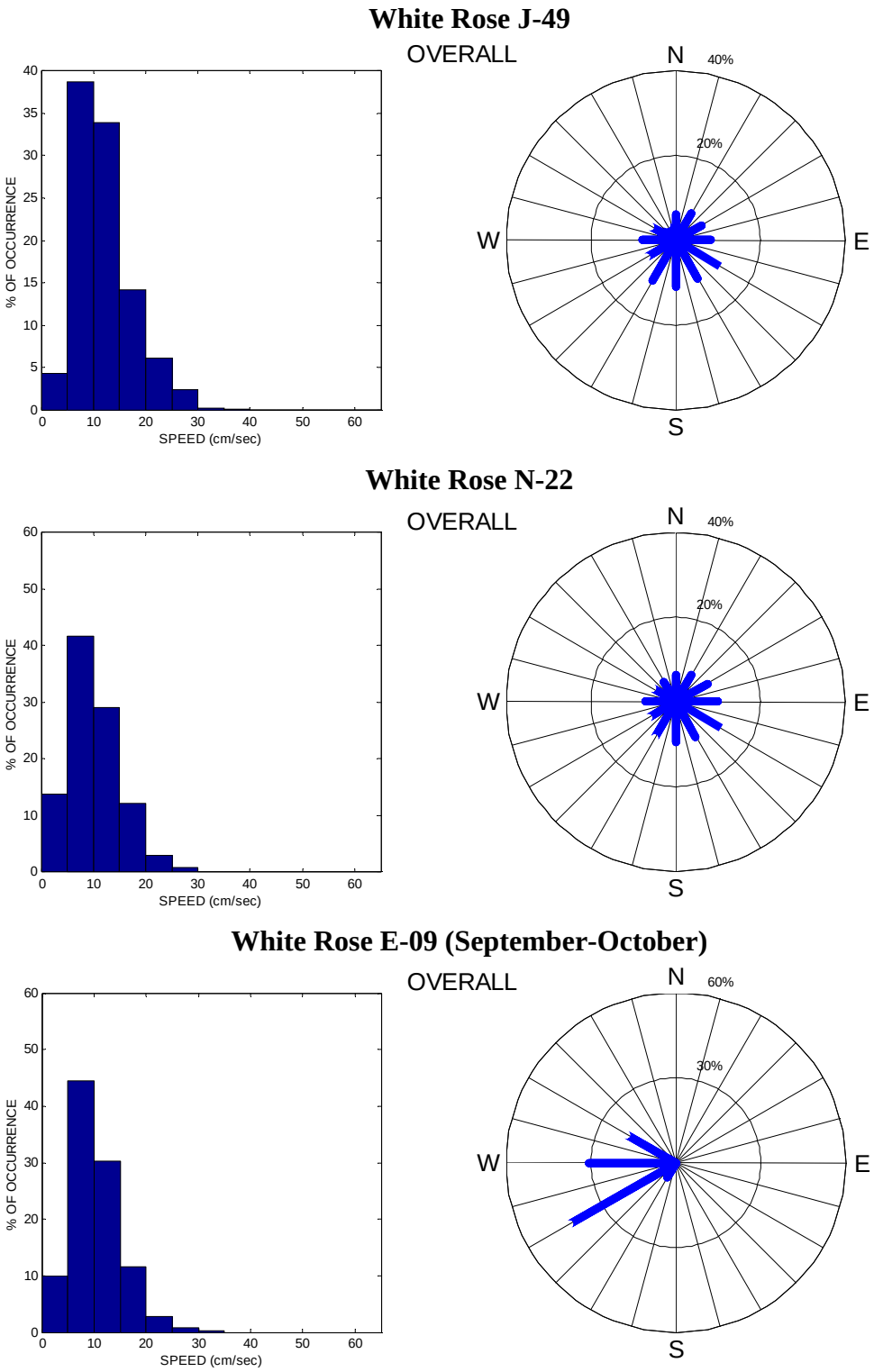

Figure 3.13(cont'd) Histograms of Speed and Direction for the Mid-Water Depths.

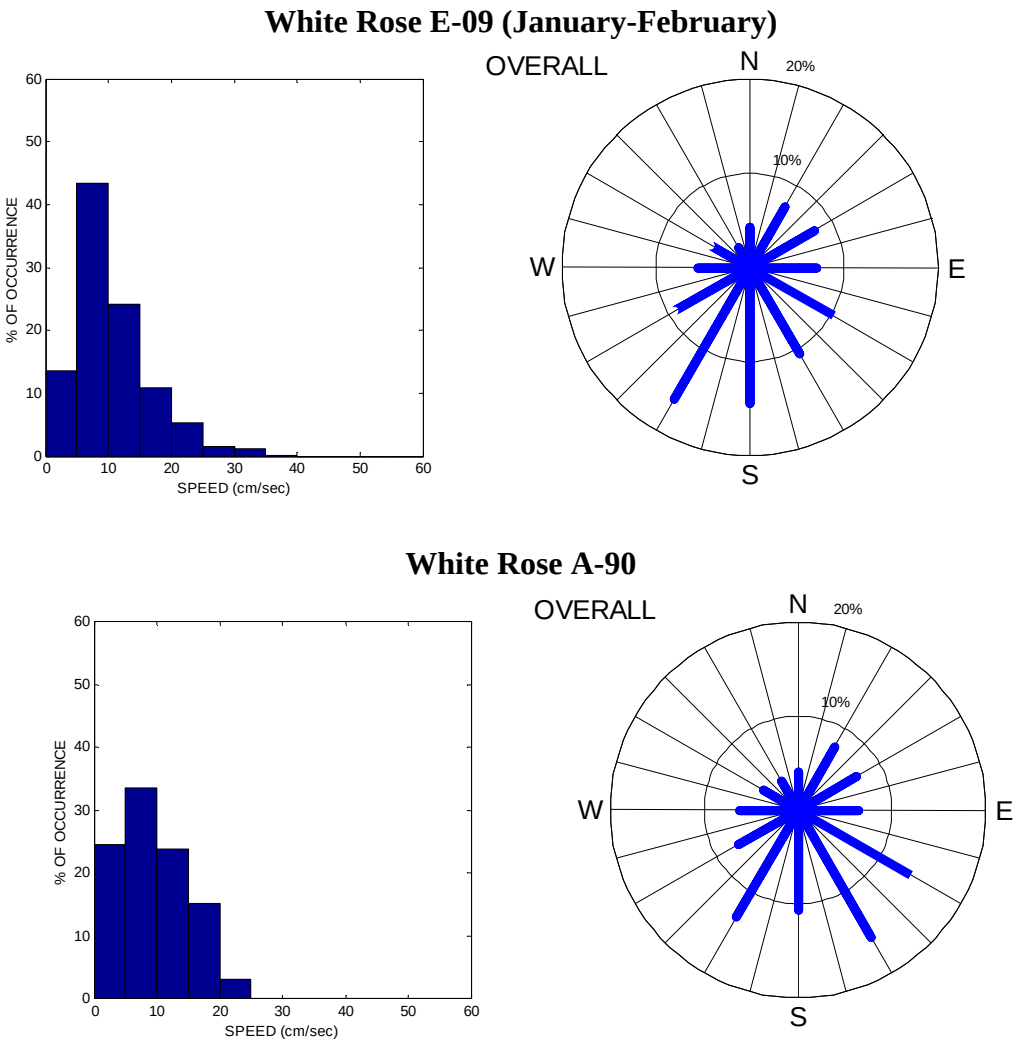

Figure 3.13(cont'd) Histograms of Speed and Direction for the Mid-Water Depths.

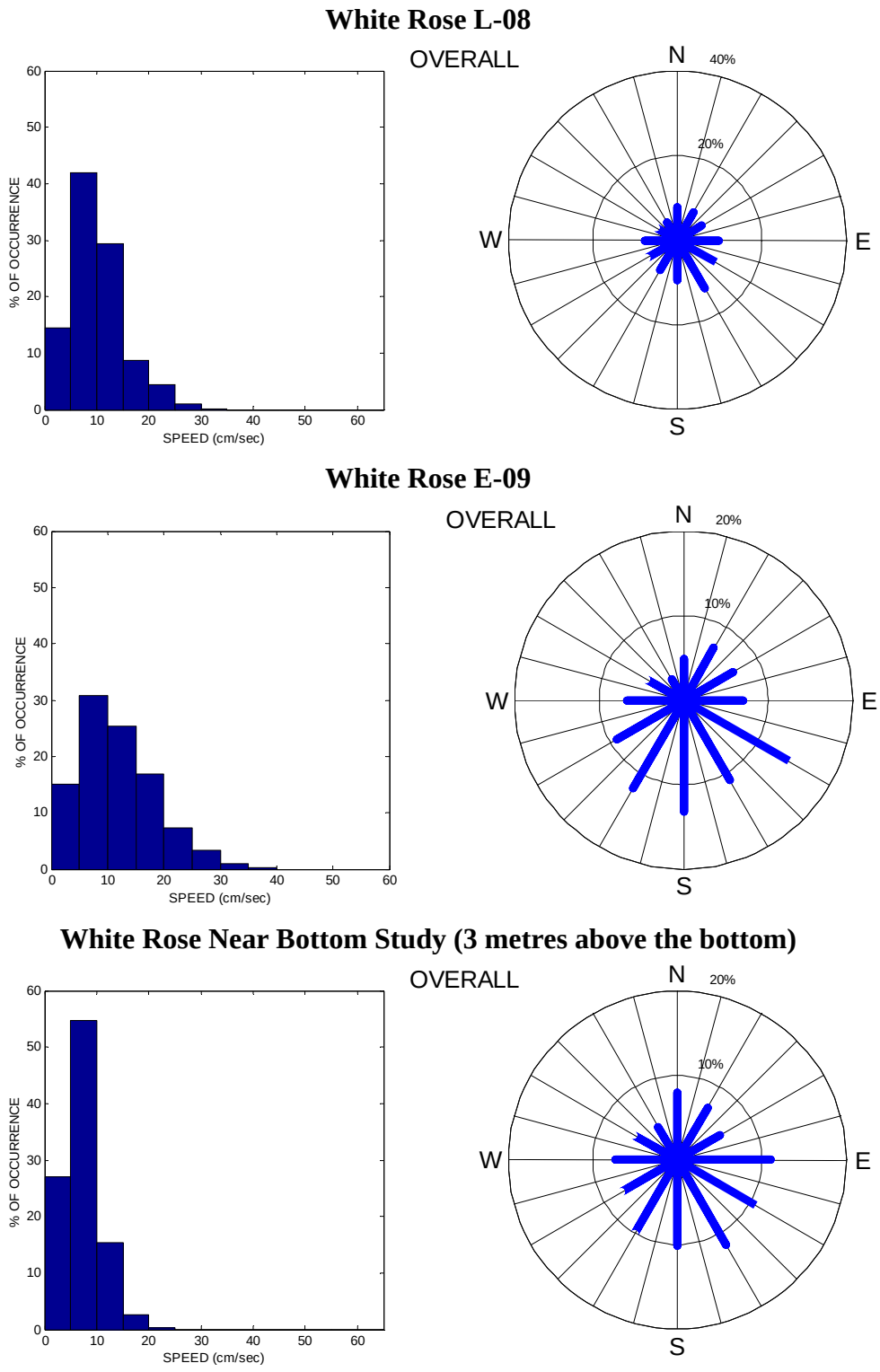

Figure 3.14 Histograms of Speed and Direction for the Near-Bottom Depths.

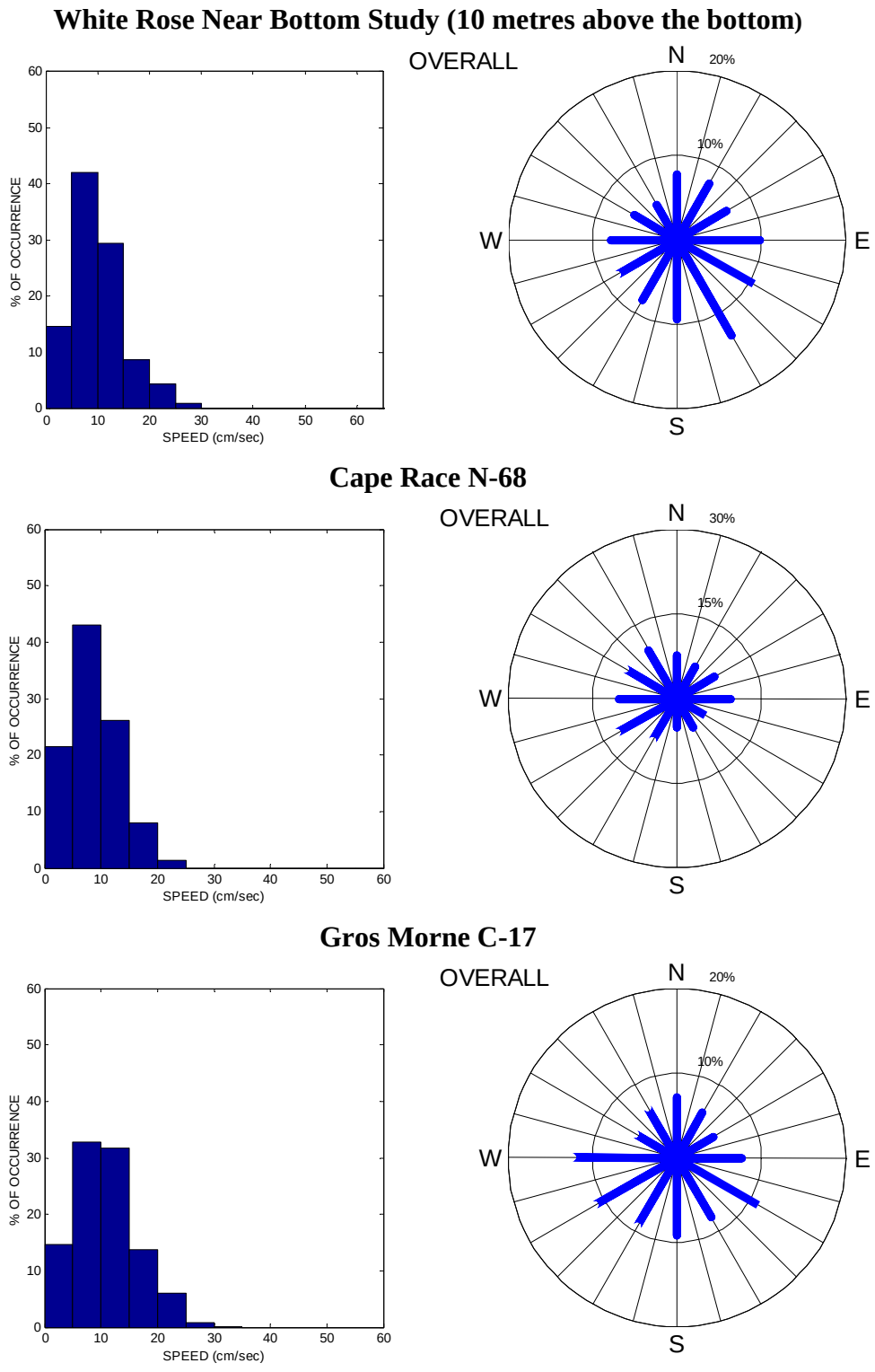

Figure 3.14 (cont'd) Histograms of Speed and Direction for the Near-Bottom Depths.

Trepassey J-91

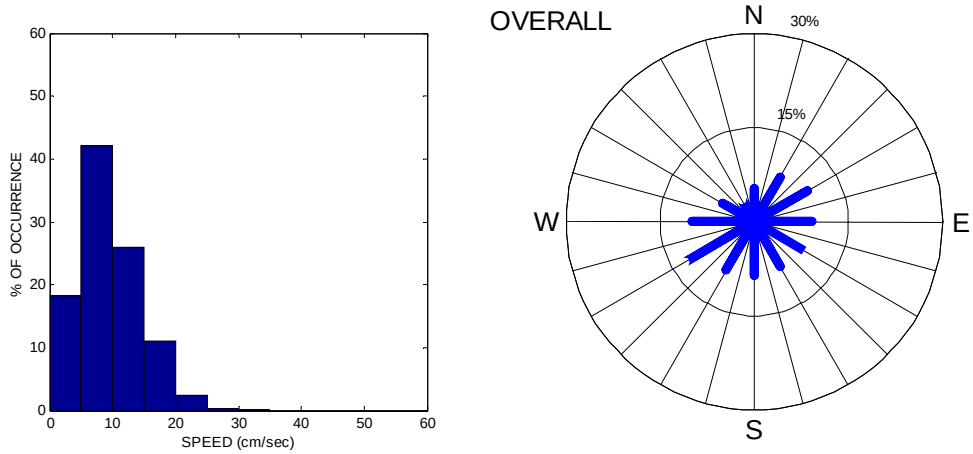

White Rose H-20

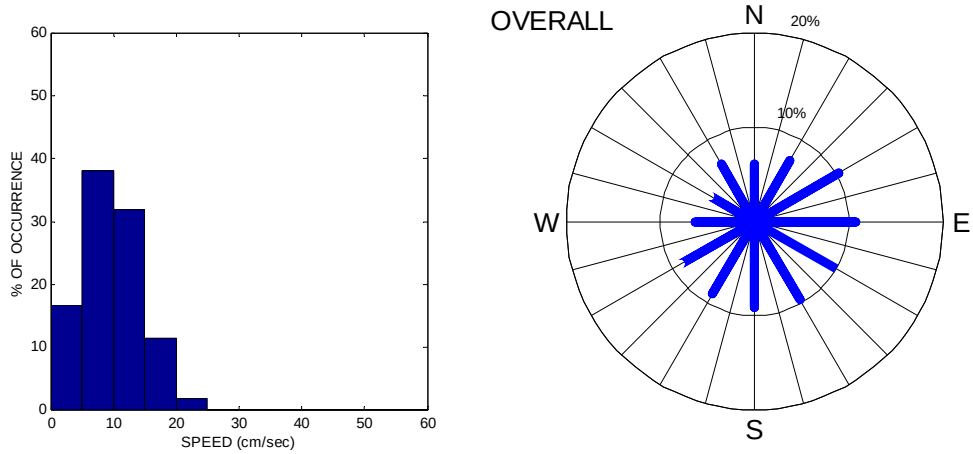

White Rose J-49

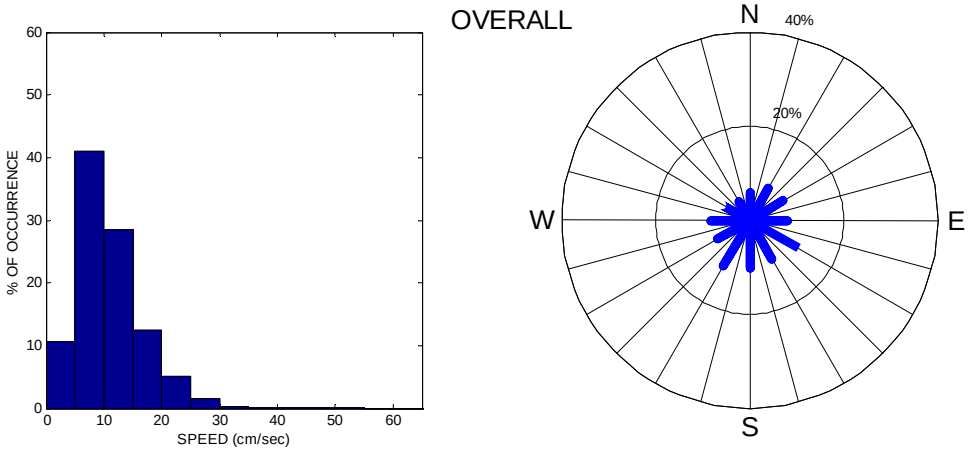

Figure 3.14 (cont'd) Histograms of Speed and Direction for the Near-Bottom Depths.

White Rose E-09 (September-November)

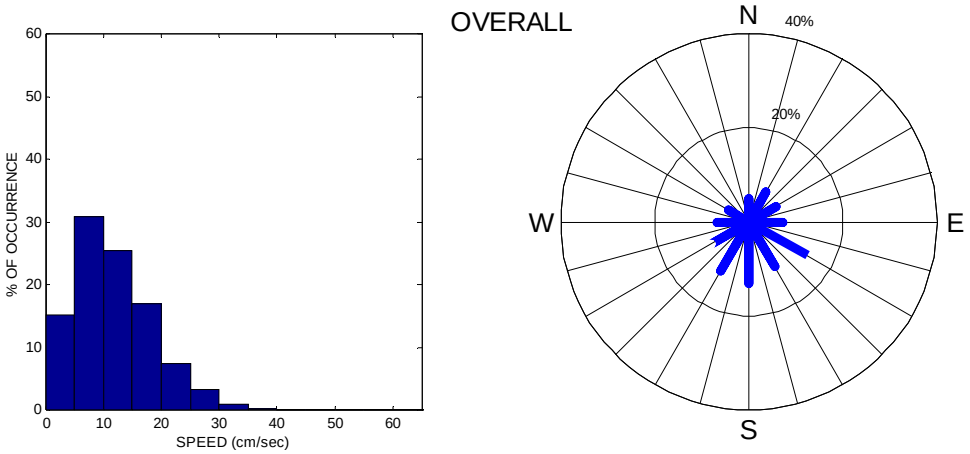

White Rose E-09 (January-February)

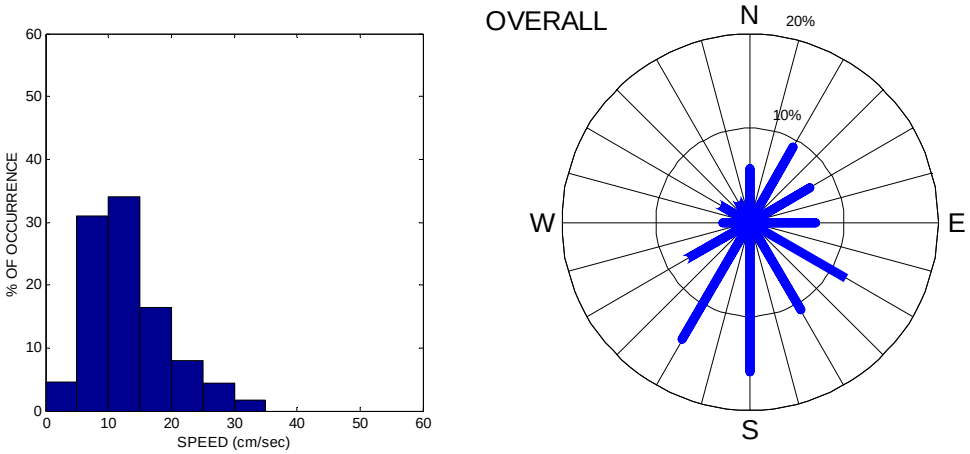

White Rose A-90

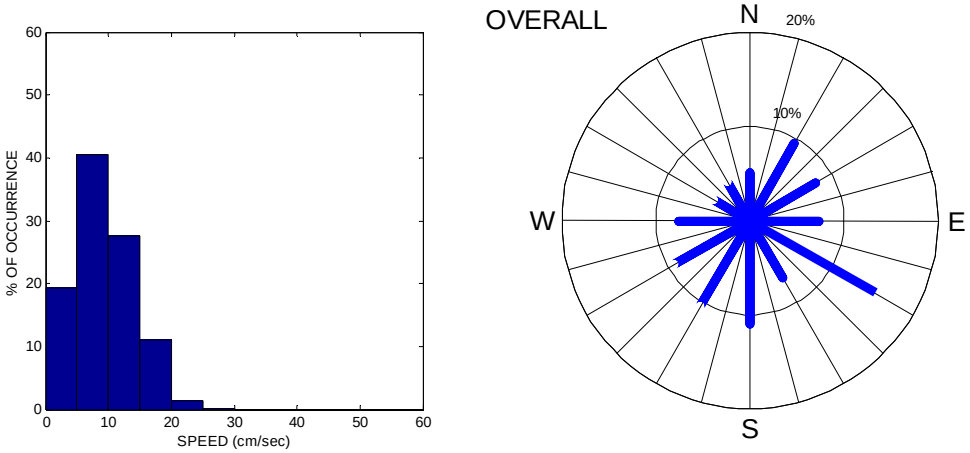

Figure 3.14 (cont'd) Histograms of Speed and Direction for the Near-Bottom Depths.

3.2.4 Harmonic Analysis of the Tidal Currents

With the help of tidal harmonic analysis it is possible to study the variability of the astronomically determined components of the marine currents. Tidal ellipses represent the orientation and magnitude of the major and minor axes of variability of the tidal currents.

Tidal constituent M_2, the semidiurnal lunar constituent, with a frequency of two cycles per lunar day is by far, the most important tidal component in the area in terms of the variability it brings into the current systems.

Figures 3.15 to 3.17 show the elliptical hodographs based on the parameters of M_2. Two important characteristics of the elliptical hodographs are the magnitude of its major axis and its rotation with respect to the geographic coordinate system. The orientation of the ellipse is an indicator of the principal direction of the tidal component and the shape of the ellipse indicates the variability associated with the tidal movements at the given frequency. The length of its major axis describes the magnitude of the tidal flow.

Thus, knowing the orientation and magnitude of the elliptic hodographs for M_2 will show the behavior of the tidal circulation in the area and its relationship with the main flow in which it takes place.

The maximum semi-duirnal tidal component near the surface, mid-depth, and near bottom was 7.2 cm/sec, 6.0 cm/sec, and 6.3 cm/sec, respectively.

According to Figures 3.15 to 3.17, in most of the cases, the orientation of the major axes of the tidal ellipses for M_2 is in the Southeast/Northwest direction. This is the dominant orientation of the tidal flow at the semidiurnal frequencies. This trend is observed at all discussed locations and depth levels, however there were some exceptions. At White Rose L-61 in the subsurface layer and at White Rose H-20 for both the mid-water and near-bottom levels, the tidal ellipses were more oriented along the Southwest/Northeast axis.

The contribution of the tidal motion to the total variability of the flow increased with depth. The tidal contribution was within the range of 10.6% and 29% at the subsurface levels. At mid-water depths the tidal contribution to the current flow was between 20% and 70%, and near the bottom between 29% and 63%.

General remarks

The mean speeds for this area varied in the range of 10 cm/sec to 27 cm/sec in the subsurface layer, between 9 cm/sec and 12 cm/sec for the mid-water layer, and between 6 cm/sec and 11 cm/sec near the bottom. Maximum speeds reached 90 cm/sec in the upper layer, 44 cm/sec in the middle layer and 50 cm/sec near the bottom. In all cases, the higher speeds occurred during the fall season during the passage of low pressure systems.

According to the data, currents in the study area were generally in the southeast direction, but exceptions to this general rule applied. In some instances, currents to the northwest or the northeast developed for an extended period of time. The duration of the anomalies indicates that the current in the area are complex. In order to understand the nature of the dynamics involved, water mass properties would need to be measured as the same time as current measurements. In general the mean velocities of the anomalies were higher than the mean velocities associated with the presence of the offshore branch of the Labrador Current.

The currents at White Rose are comprised of semi-diurnal and diurnal tidal currents, direct wind driven currents, inertial currents, geostrophic currents, and low frequency mesoscale currents resulting from such potential features as meteorological disturbances, meanders and eddies, and propagation of continental shelf waves.

White Rose N-30

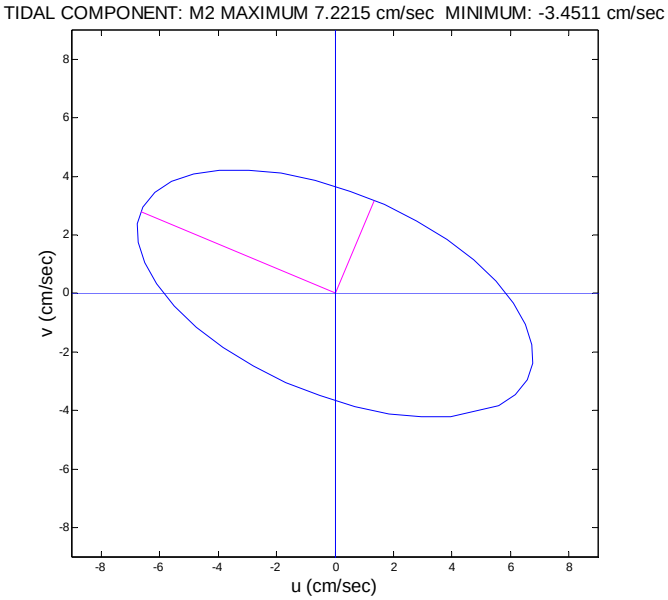

White Rose A-17

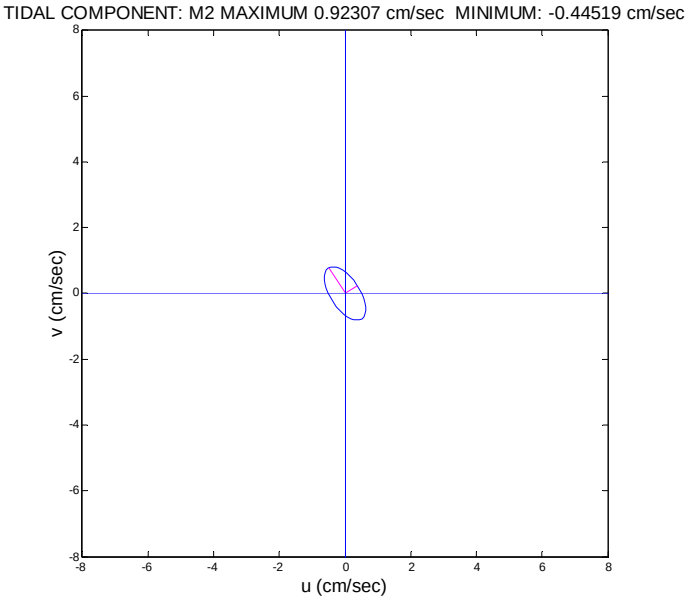

White Rose J-49

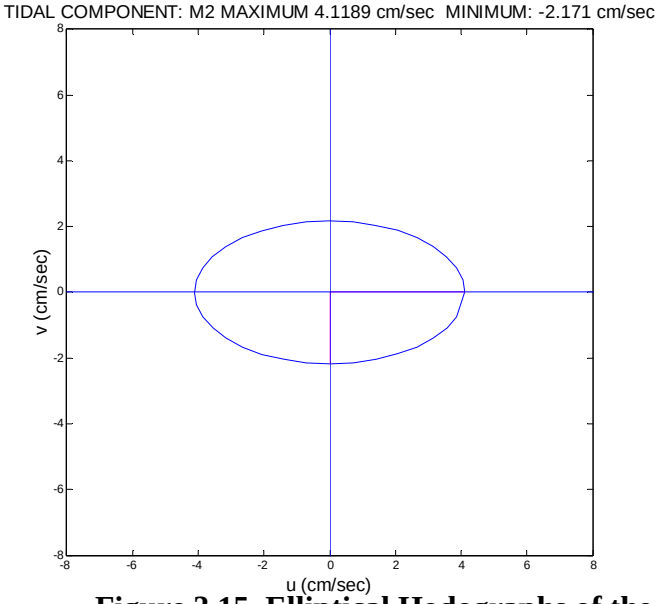

White Rose L-08

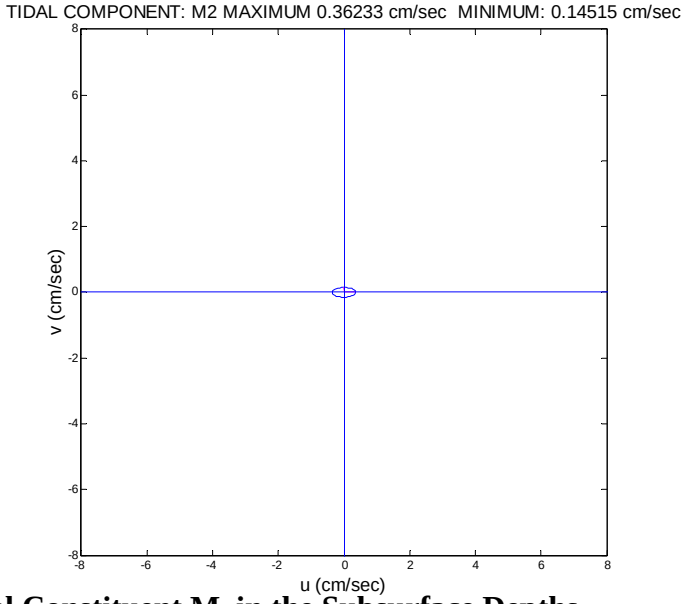

Figure 3.15 Elliptical Hodographs of the Tidal Constituent M_2 in the Subsurface Depths.

(Note: The ADCP data at this level did not have the quality required for harmonic analysis)

White Rose A-90 **White Rose L-61**

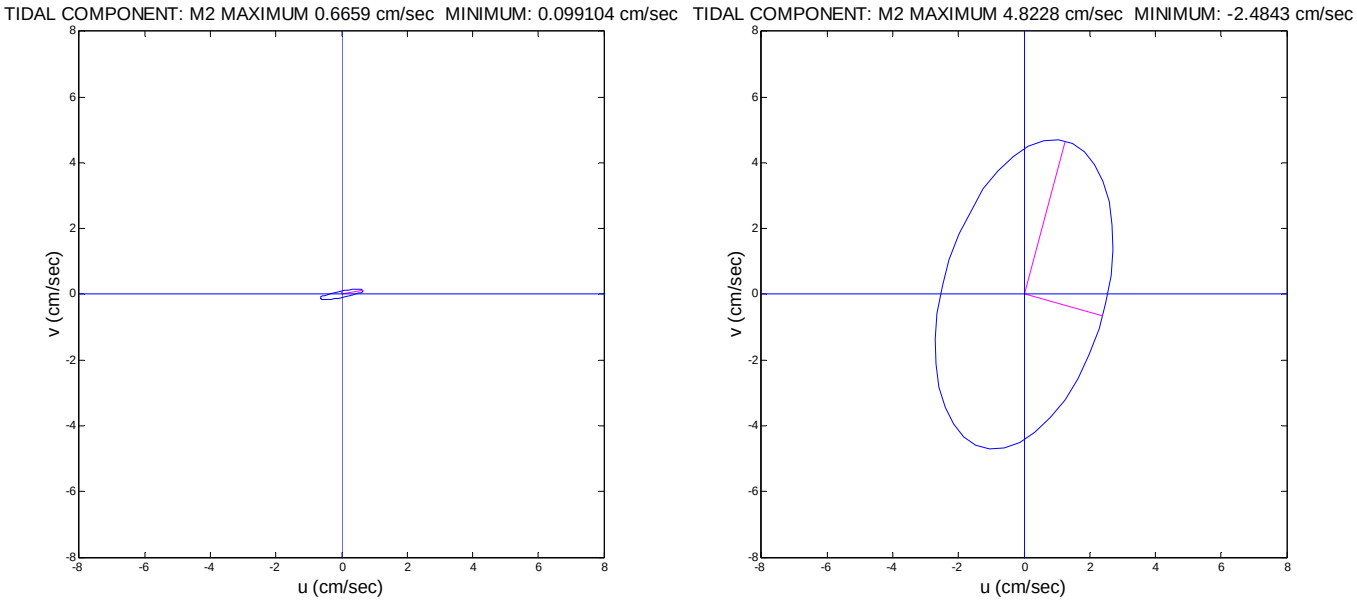

Figure 3.15 (cont'd) Elliptical Hodographs of the Tidal Constituent M_2 in the Subsurface Depths.

White Rose N-30

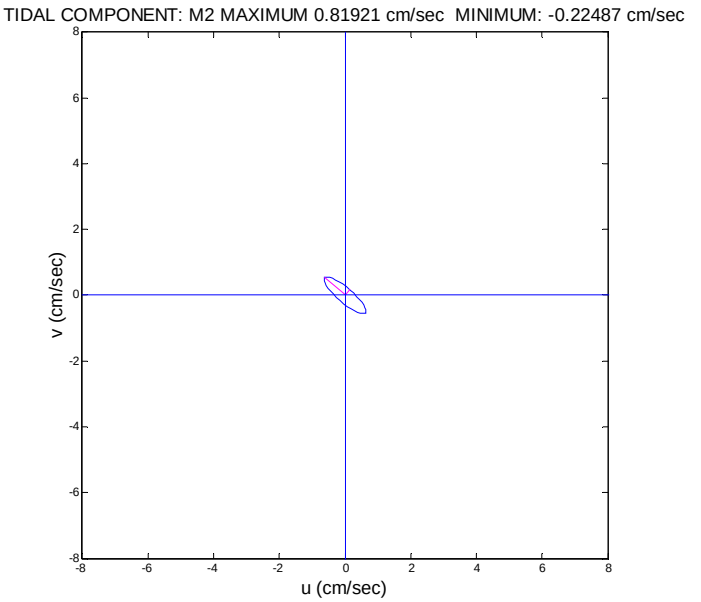

White Rose L-08

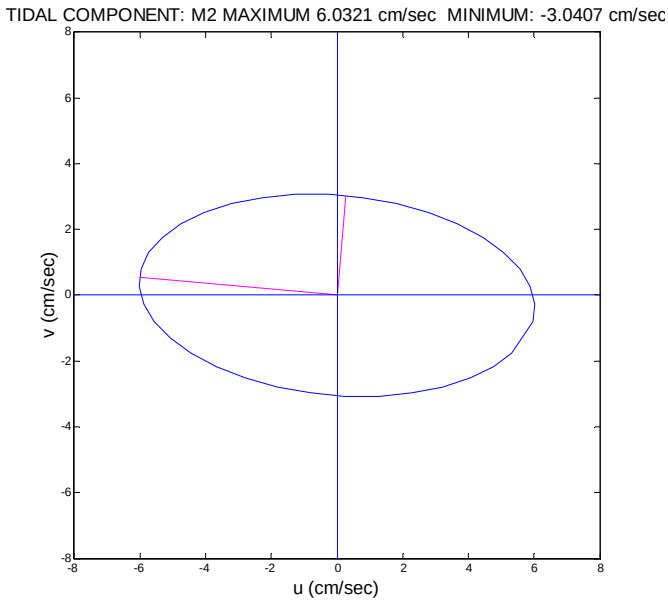

White Rose H-20

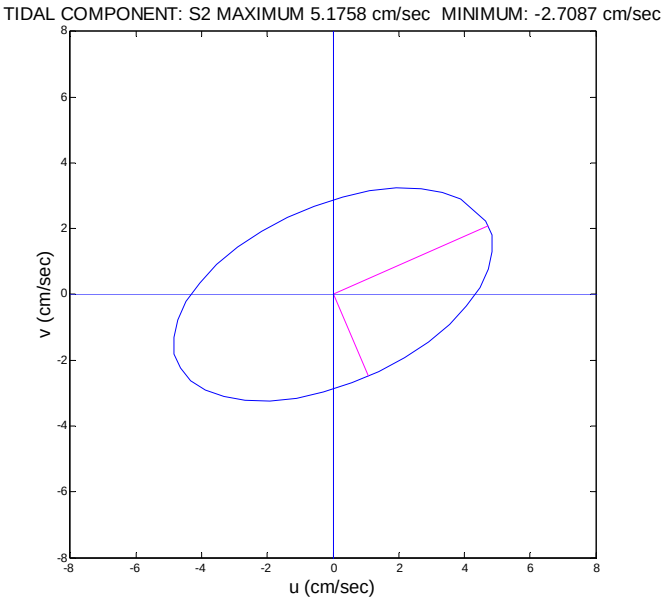

White Rose J-49

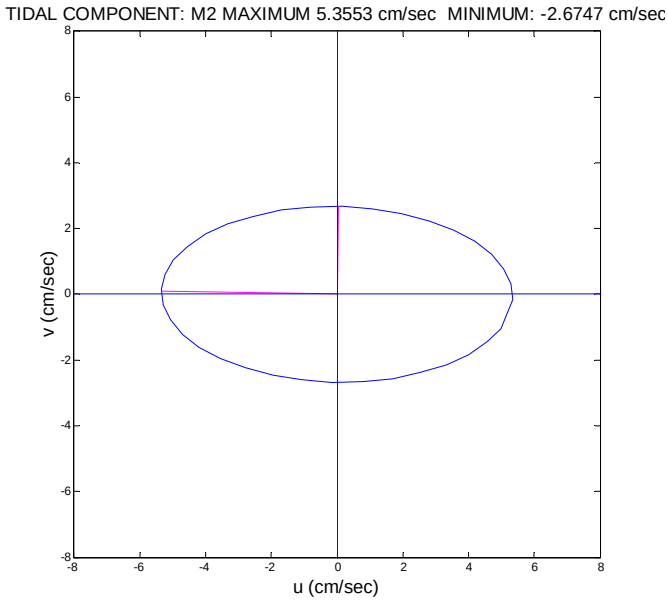

Figure 3.16 Elliptical Hodographs of the Tidal Constituent M_2 in the Mid-Water Depths.

White Rose N-22 80m

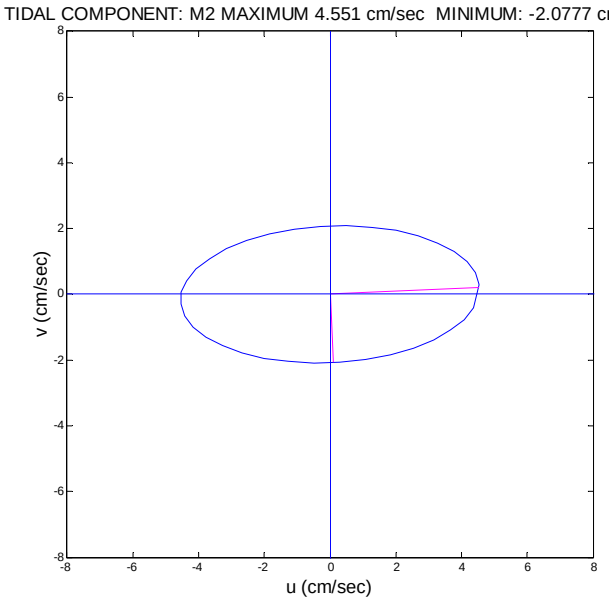

White Rose E-09 (Sep-Nov)

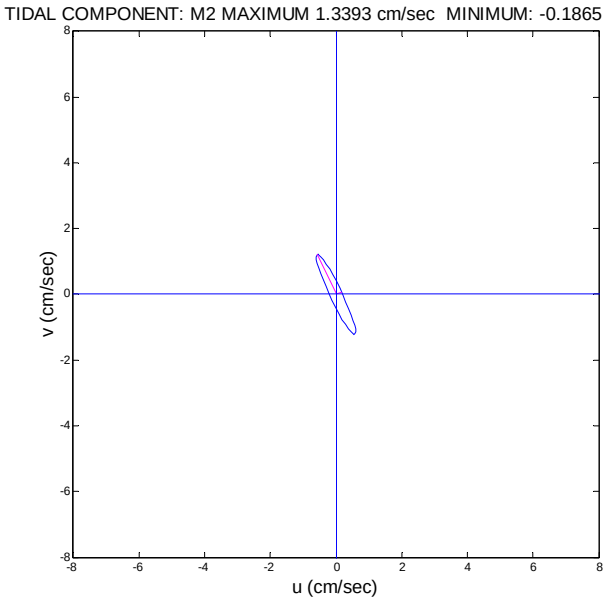

White Rose E-09 (Jan-Feb)

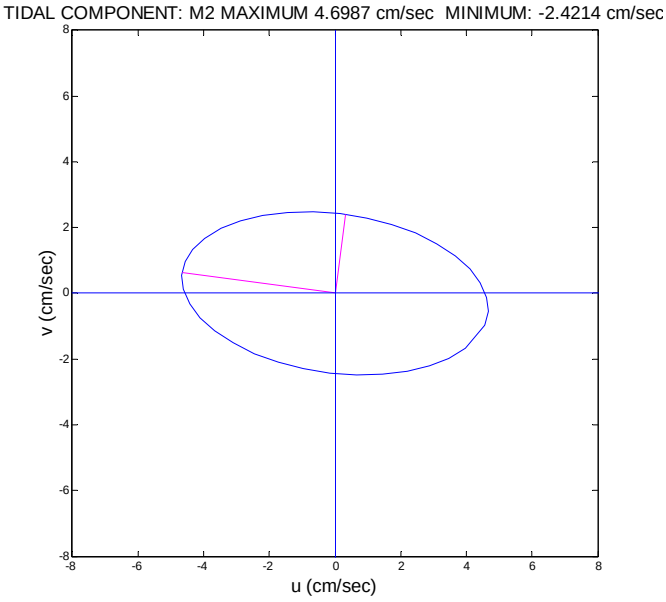

White Rose A-90

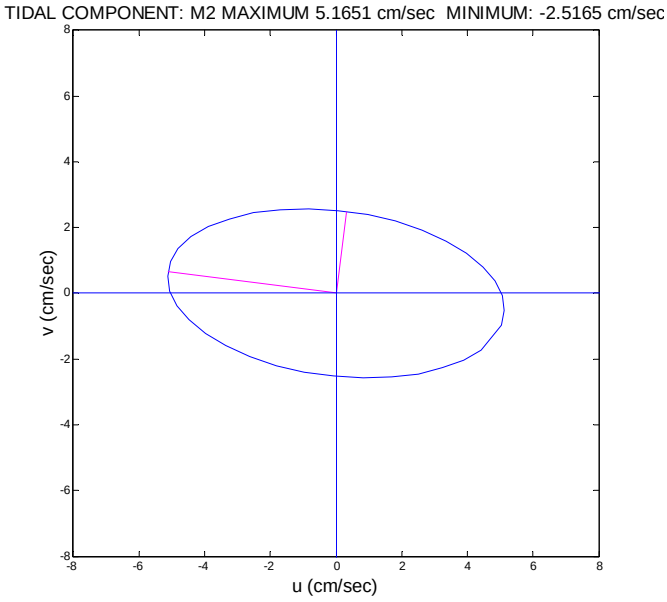

Figure 3.16 (cont'd) Elliptical Hodographs of the Tidal Constituent M_2 in the Mid-Water Depths.

White Rose L-08

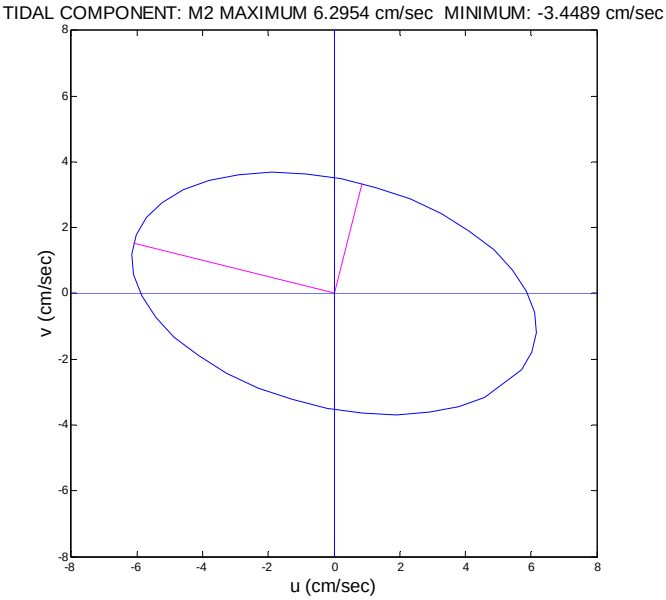

White Rose E-09

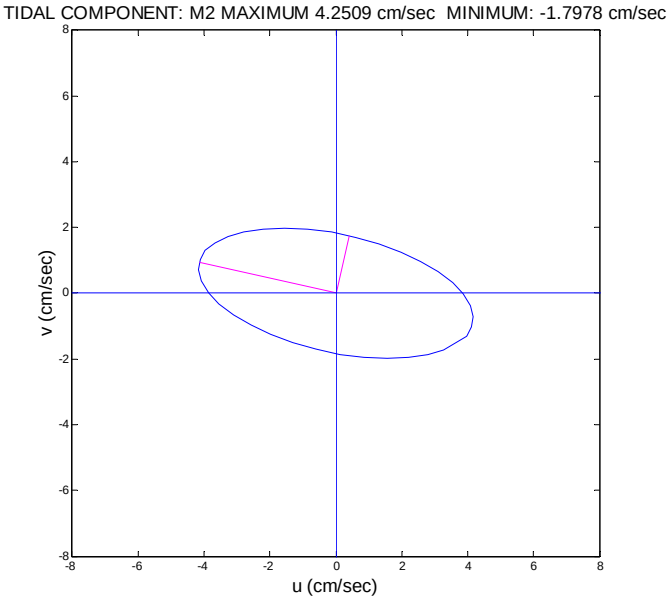

White Rose Near-Bottom Study (3 m above)

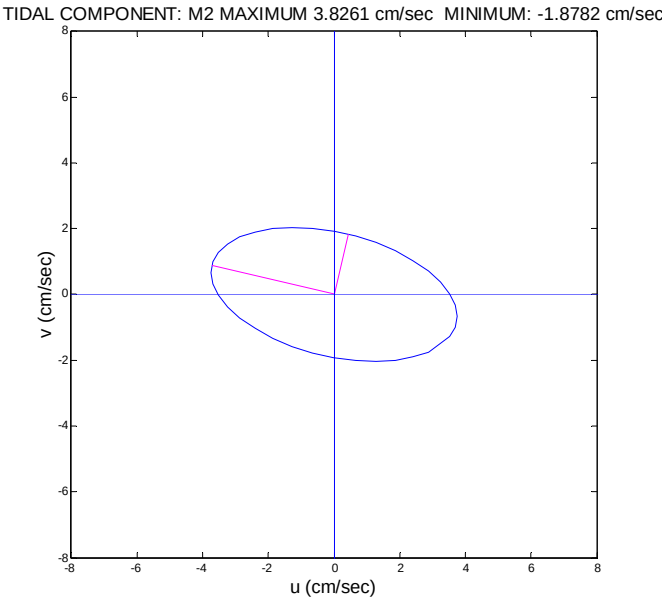

White Rose Near-Bottom Study (10 m above)

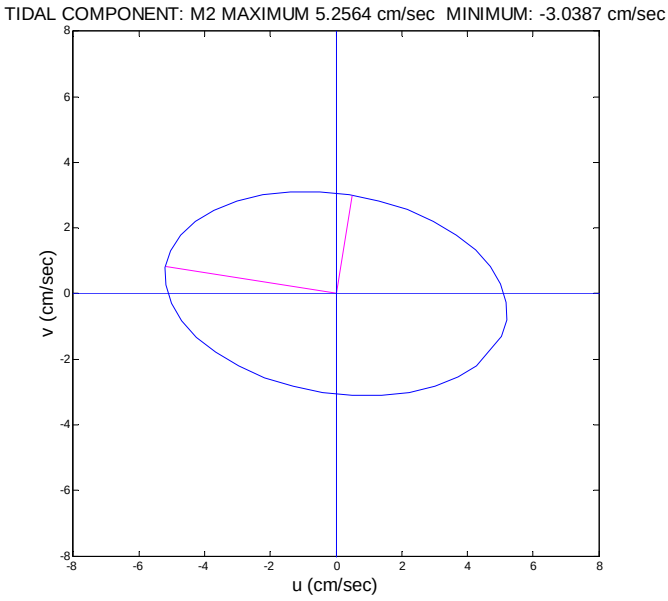

Figure 3.17 Elliptical Hodographs of the Tidal Constituent M_2 near the Bottom.

White Rose H-20

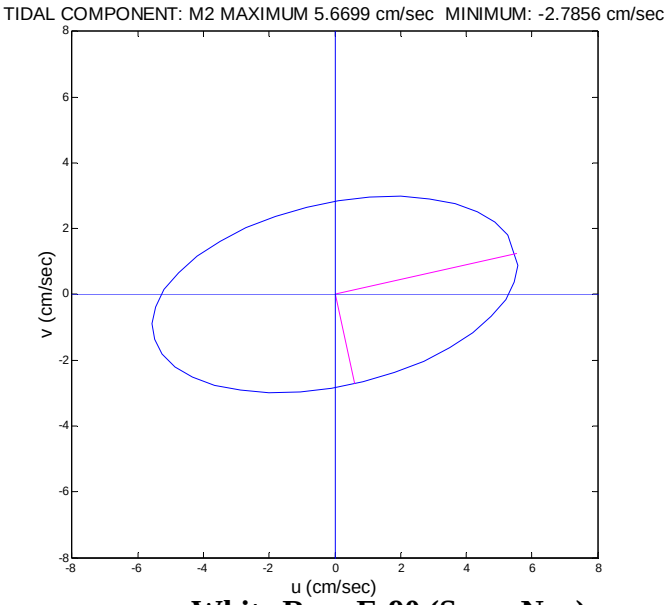

White Rose J-49

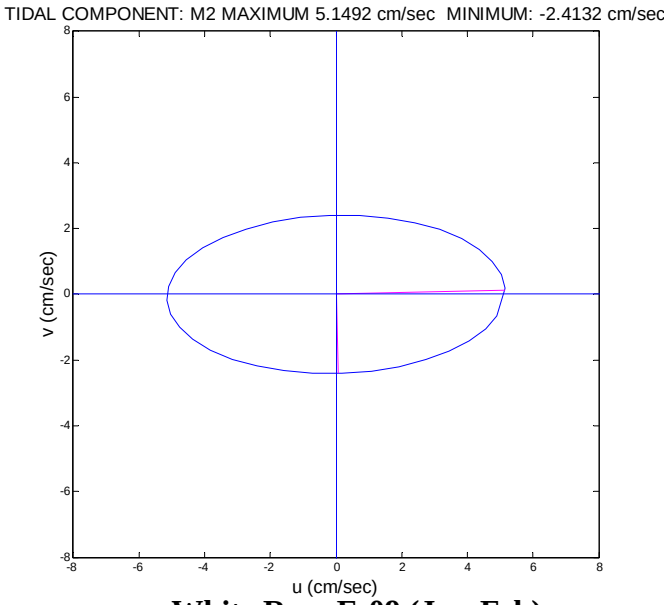

White Rose E-90 (Sep – Nov)

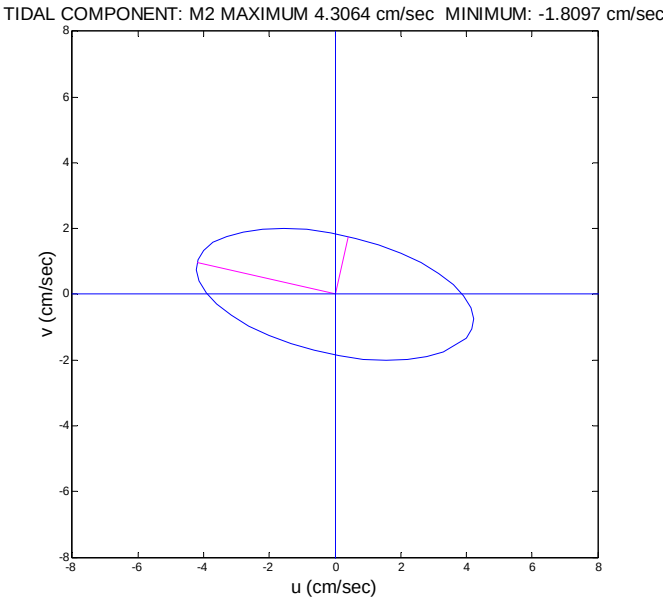

White Rose E-09 (Jan-Feb)

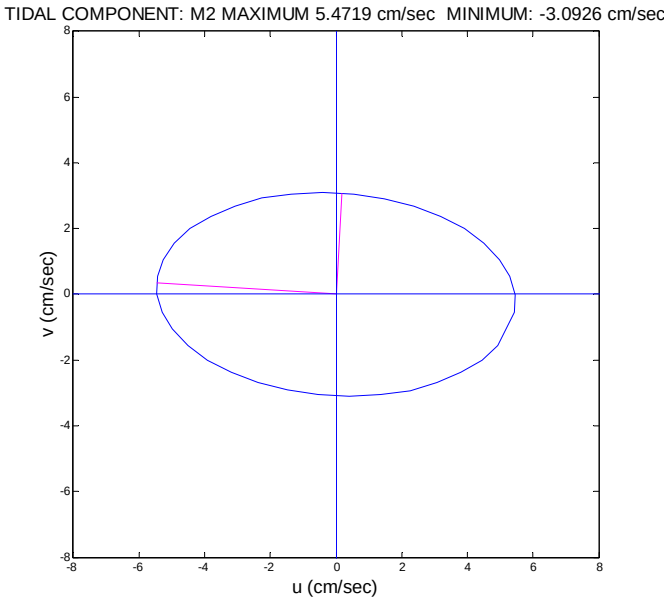

Figure 3.17 (cont'd) Elliptical Hodographs of the Tidal Constituent M_2 near the Bottom.

White Rose A-90

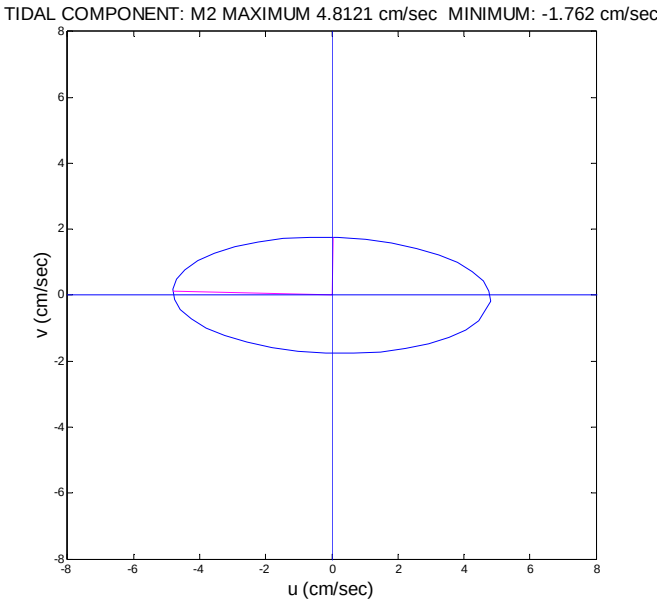

Figure 3.17 (cont'd) Elliptical Hodographs of the Tidal Constituent M_2 near the Bottom.

References

Colbourne E., B. deYoung, S. Narayanan, and J. Helbig (1997). Comparison of hydrography and circulation on the Newfoundland Shelf during 1990–1993 with the long-term mean. *Can. J. Fish. Aquat. Sci*. Vol. 54(Suppl. 1), 1997

Colbourne E., and C. Fitzpatrick, 2002. Physical oceanographic conditions in NAFO subareas 2 and 3 on the Newfoundland and Labrador Shelves during 2001. NAFO SCR Doc. 02/41, 23p.

Colbourne E., (2000). Interannual variations in the stratification and transport of the Labrador Current on the Newfoundland Shelf. *International Council for the Explorations of the Sea*. CM 2000/L:2.

Colbourne E., 2004. Decadal Changes in the Ocean Climate in Newfoundland. e. J. Northwest Atlantic Fishery Science, V34, No. 4.

DeTracey B. M., C. L. Tang, P. C. Smith, (1996). Low-frequency currents at the northern shelf edge of the Grand Banks. *Journal of Geophysical Research*, Volume 101, Issue C6, p. 14223-14236.

Hayes R. M., D. G. Mountain, and T. C. Wolford, 1977. Physical oceanography and the abiotic influence on cod recruitment in the Flemish Cap region. ICNAF Res. Doc., No. 54, Serial No. 5107, 33 p.

Hendry R. M., R. A. Clarke, J. R. N. Lazier, and I.M. Yashayaev,1998. Changes in Labrador Sea properties from 1998 to 1999. Annex H – Area 2b (Labrador Sea) Canadian Report, 6p.

Hinrichsen H. H., and M. Tomczak, 1993. Optimum multiparameter analysis of the water mass structure in the western North Atlantic Ocean. J. Geophys. Res. 98: 10,155-10,169.

Lazier J. R. N., 1982. Seasonal variability of temperature and salinity in the Labrador Current. J. Mar. Res. 40: 341-356.

Lazier J.R.N., and D.G. Wright, 1993. Annual Velocity variations in the Labrador Current, J. Phys. Oceanogr., 23, 659-678.

Mamayev O.I., 1975. Temperature - Salinity Analysis of the World Ocean Waters. Elsevier Scientific, Amsterdam, 374 p.

Petrie B., S. Akenhead, J. Lazier, and J. Loder, 1988. The cold intermediate layer on the Labrador and Northeast Newfoundland Shelves, 1978–1986. NAFO Sci. Counc. Stud. 12: 57–69.

Winterstein S.R., T. Ude, C.A. Cornell, P. Jarager, and S. Haver, 1993. Environmental Parameters for Extreme Response: Inverse FORM with Omission Factors. ICOSSar-3, Paper No 509/11/3, Innsbruck, 3-12 August 1993.

Appendix A

Monthly Wind Roses for AES-40 Grid Point 5622

Latitude 46.875 N, Longitude 48.333 W

Table A.1 Percentage Occurrence of Wind Speed by Direction for January.

January									
Wind Speed Range (m/s)	**Center of 45 Degree Direction Bins**								
	045	**090**	**135**	**180**	**225**	**270**	**315**	**360**	**Totals**
0.0 - < 5.0	1.10	0.97	1.22	1.45	1.88	1.73	1.15	1.18	10.68
5.0 - < 10.0	2.30	2.07	2.63	3.82	6.39	8.21	6.55	2.95	34.92
10.0 - < 15.0	0.87	1.25	2.34	4.03	5.97	13.20	7.04	2.21	36.92
15.0 - < 20.0	0.36	0.38	1.07	2.14	2.98	4.58	2.39	0.63	14.52
20.0 - < 25.0	0.02	0.05	0.12	0.38	0.46	1.04	0.56	0.18	2.80
25.0 - < 30.0	0.00	0.00	0.00	0.02	0.03	0.10	0.02	0.00	0.16
30.0 - < 35.0	0.00	0.00	0.00	0.00	0.00	0.00	0.00	0.00	0.00
Totals	4.66	4.72	7.37	11.83	17.71	28.85	17.71	7.14	100.00

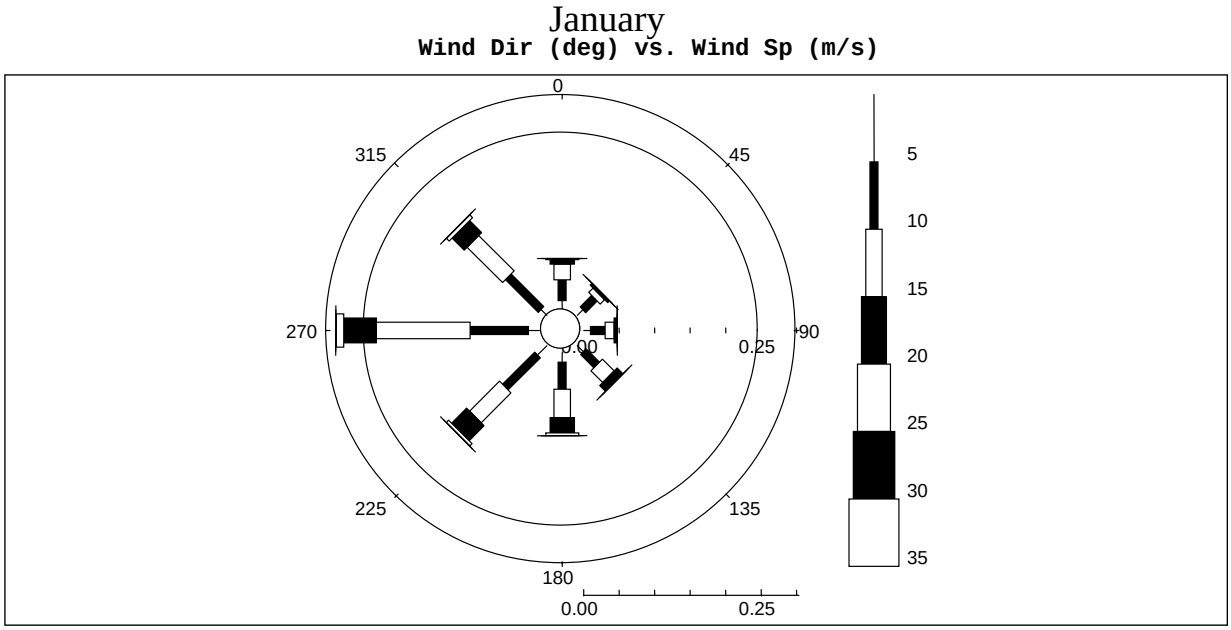

Figure A.1 Wind Rose for January.

Table A.2 Percentage Occurrence of Wind Speed by Direction for February.

February									
Wind Speed Range (m/s)	**Center of 45 Degree Direction Bins**								
	045	**090**	**135**	**180**	**225**	**270**	**315**	**360**	**Totals**
0.0 - < 5.0	0.94	1.23	0.92	1.39	1.55	1.45	1.52	1.03	10.03
5.0 - < 10.0	2.53	2.33	3.27	4.05	5.74	7.97	6.11	3.72	35.71
10.0 - < 15.0	1.45	1.68	2.93	3.76	5.87	11.42	7.44	2.24	36.78
15.0 - < 20.0	0.33	0.38	0.96	2.01	2.13	4.93	2.98	0.69	14.40
20.0 - < 25.0	0.11	0.05	0.13	0.36	0.45	0.92	0.58	0.13	2.73
25.0 - < 30.0	0.02	0.00	0.02	0.02	0.05	0.11	0.07	0.05	0.34
30.0 - < 35.0	0.00	0.00	0.00	0.00	0.02	0.00	0.00	0.00	0.02
Totals	5.36	5.67	8.22	11.58	15.82	26.79	18.70	7.86	100.00

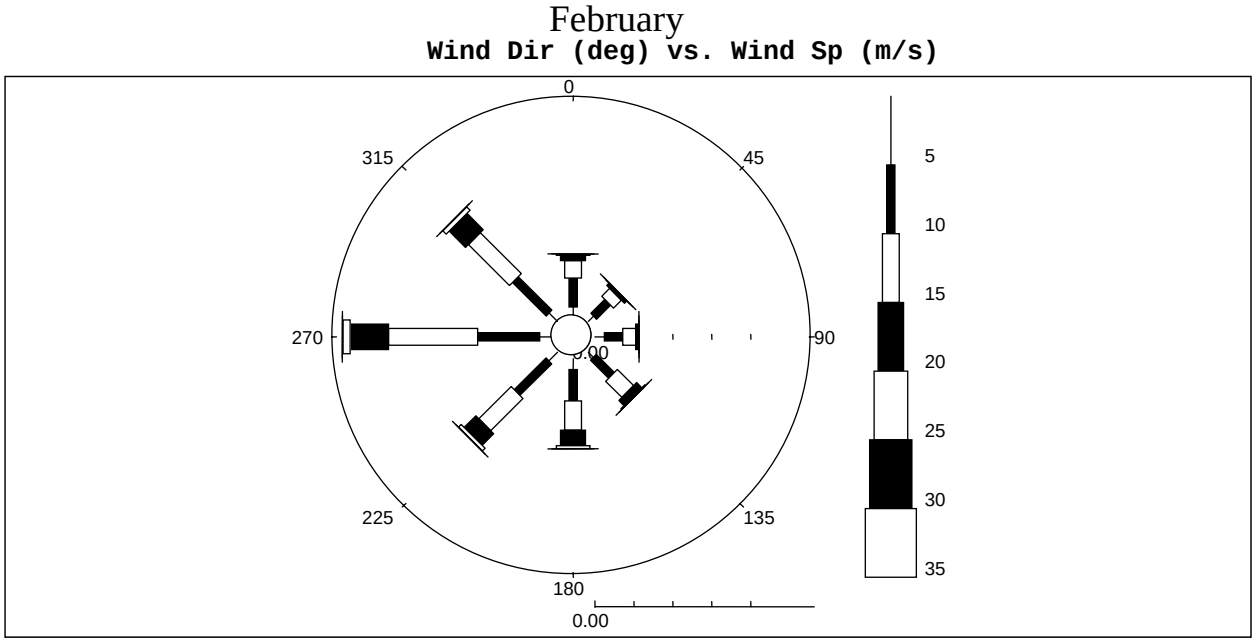

Figure A.2 Wind Rose for February.

Table A.3 Percentage Occurrence of Wind Speed by Direction for March.

March									
Wind Speed Range (m/s)	**Center of 45 Degree Direction Bins**								
	045	**090**	**135**	**180**	**225**	**270**	**315**	**360**	**Totals**
0.0 - < 5.0	1.40	1.71	1.40	2.12	2.24	1.97	1.93	1.74	14.52
5.0 - < 10.0	3.37	2.72	3.24	4.20	7.13	8.06	6.17	4.64	39.53
10.0 - < 15.0	2.11	1.66	2.27	4.38	5.45	8.94	6.35	3.37	34.53
15.0 - < 20.0	0.61	0.46	0.66	1.58	1.78	3.01	1.50	0.87	10.47
20.0 - < 25.0	0.12	0.02	0.03	0.10	0.15	0.25	0.15	0.10	0.91
25.0 - < 30.0	0.00	0.00	0.00	0.00	0.00	0.00	0.02	0.03	0.05
30.0 - < 35.0	0.00	0.00	0.00	0.00	0.00	0.00	0.00	0.00	0.00
Totals	7.60	6.57	7.60	12.38	16.74	22.24	16.11	10.76	100.00

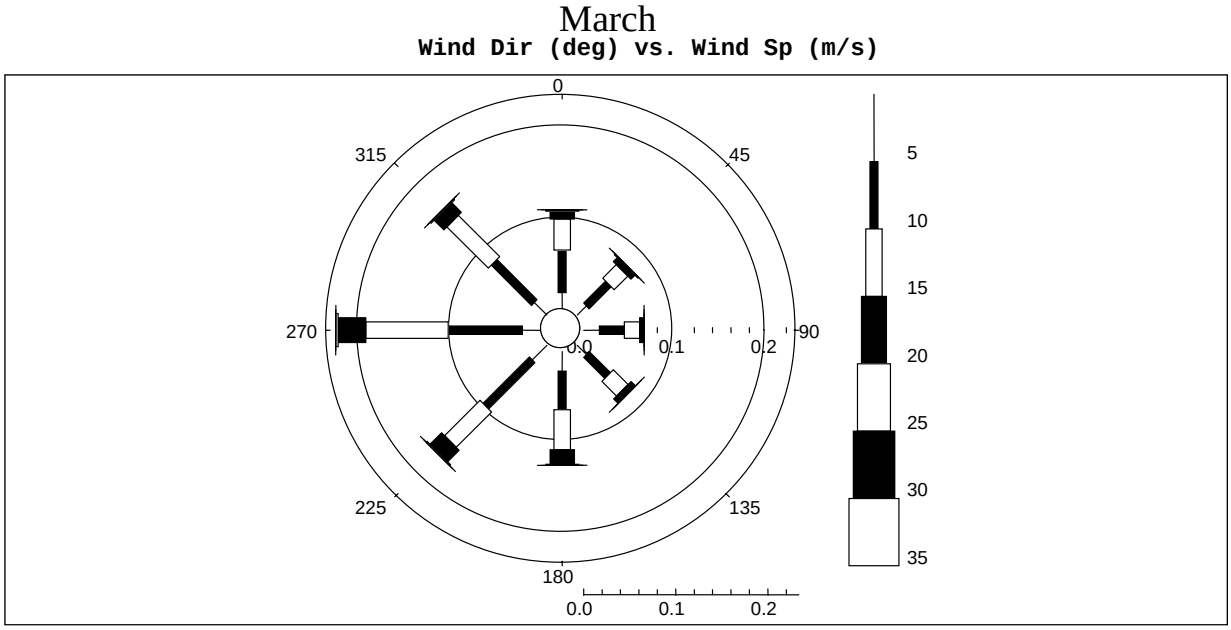

Figure A.3 Wind Rose for March.

Table A.4 Percentage Occurrence of Wind Speed by Direction for April.

April									
Wind Speed Range (m/s)	**Center of 45 Degree Direction Bins**								
	045	**090**	**135**	**180**	**225**	**270**	**315**	**360**	**Totals**
0.0 - < 5.0	2.23	2.47	2.94	2.70	3.86	3.21	2.35	2.33	22.09
5.0 - < 10.0	3.35	4.13	5.00	5.80	9.37	9.13	6.24	4.17	47.19
10.0 - < 15.0	1.63	1.33	2.06	3.28	5.53	4.61	4.49	2.50	25.43
15.0 - < 20.0	0.29	0.27	0.27	0.77	0.70	0.95	1.00	0.58	4.83
20.0 - < 25.0	0.09	0.02	0.02	0.02	0.02	0.09	0.09	0.12	0.44
25.0 - < 30.0	0.00	0.00	0.00	0.02	0.00	0.00	0.00	0.00	0.02
30.0 - < 35.0	0.00	0.00	0.00	0.00	0.00	0.00	0.00	0.00	0.00
Totals	7.59	8.21	10.29	12.59	19.47	17.99	14.17	9.69	100.00

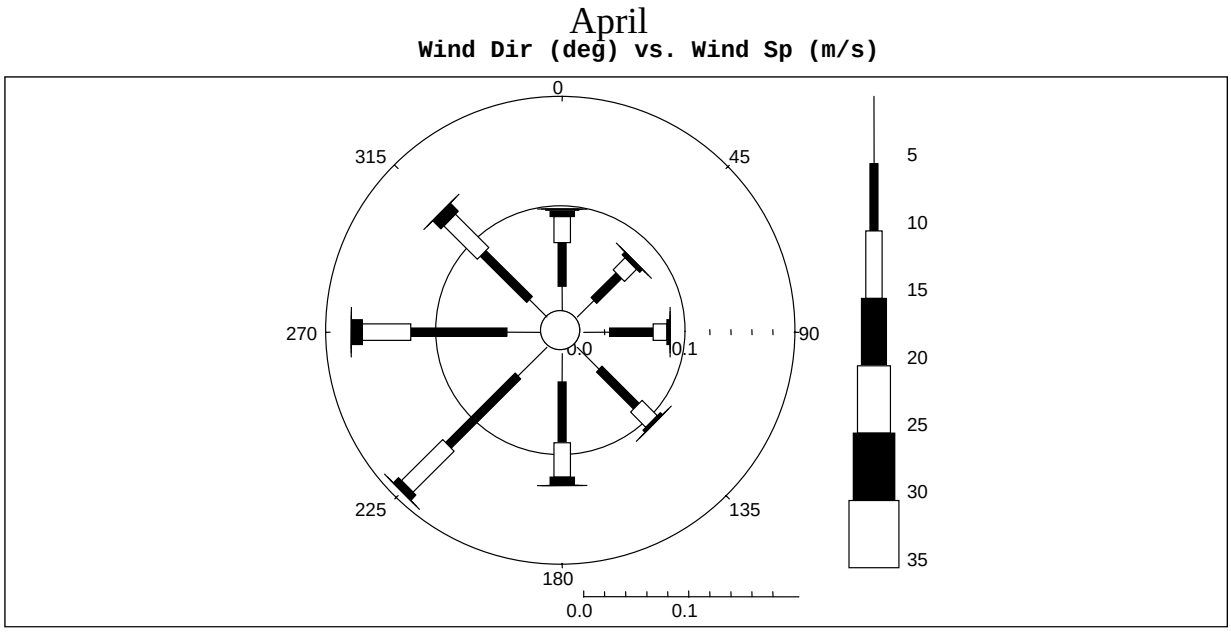

Figure A.4 Wind Rose for April.

Table A.5 Percentage Occurrence of Wind Speed by Direction for May.

May									
Wind Speed Range (m/s)	**Center of 45 Degree Direction Bins**								
	045	**090**	**135**	**180**	**225**	**270**	**315**	**360**	**Totals**
0.0 - < 5.0	3.41	2.95	3.46	4.71	5.83	4.33	3.28	2.70	30.65
5.0 - < 10.0	3.39	3.09	3.87	8.41	11.36	9.28	6.25	4.36	50.02
10.0 - < 15.0	1.04	0.76	0.94	2.50	4.34	3.28	2.37	2.06	17.28
15.0 - < 20.0	0.03	0.10	0.07	0.41	0.51	0.30	0.36	0.18	1.96
20.0 - < 25.0	0.00	0.00	0.00	0.00	0.02	0.00	0.07	0.02	0.10
25.0 - < 30.0	0.00	0.00	0.00	0.00	0.00	0.00	0.00	0.00	0.00
30.0 - < 35.0	0.00	0.00	0.00	0.00	0.00	0.00	0.00	0.00	0.00
Totals	7.87	6.90	8.33	16.03	22.05	17.18	12.33	9.32	100.00

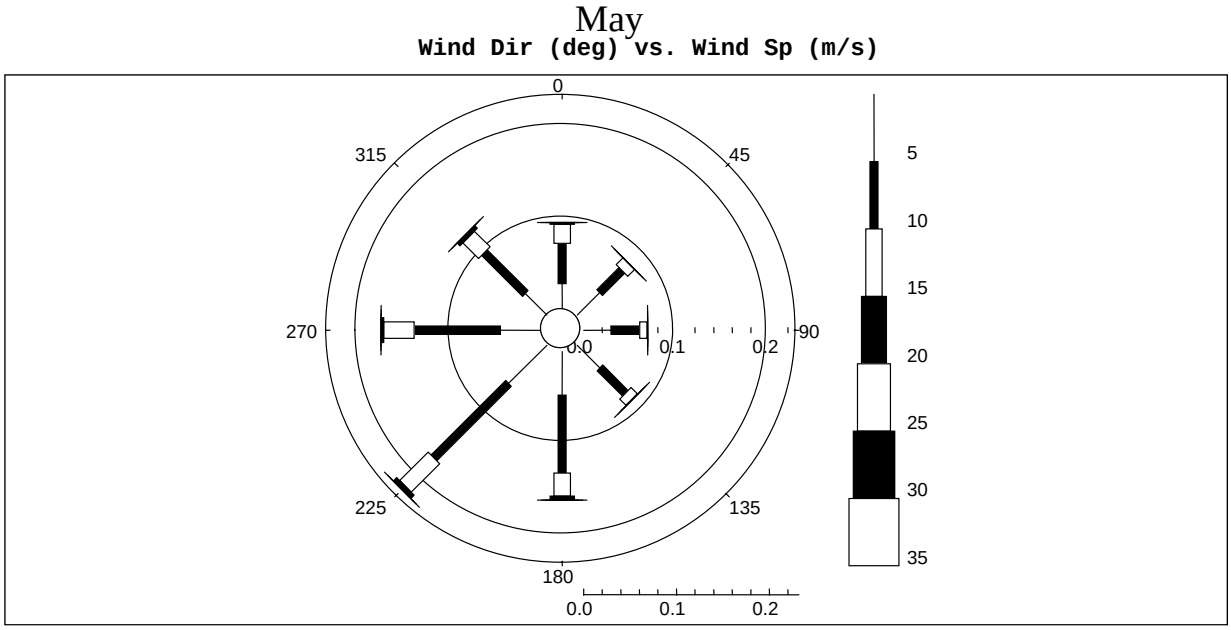

Figure A.5 Wind Rose for May.

Table A.6 Percentage Occurrence of Wind Speed by Direction for June.

June									
Wind Speed Range (m/s)	**Center of 45 Degree Direction Bins**								
	045	**090**	**135**	**180**	**225**	**270**	**315**	**360**	**Totals**
0.0 - < 5.0	2.24	2.28	3.84	5.37	7.74	5.90	3.30	2.98	33.66
5.0 - < 10.0	1.90	2.11	2.60	8.67	19.40	8.91	4.74	3.42	51.77
10.0 - < 15.0	0.48	0.29	0.63	2.69	6.00	2.02	0.90	0.73	13.74
15.0 - < 20.0	0.02	0.05	0.09	0.20	0.22	0.12	0.10	0.00	0.80
20.0 - < 25.0	0.00	0.00	0.00	0.00	0.00	0.02	0.02	0.00	0.03
25.0 - < 30.0	0.00	0.00	0.00	0.00	0.00	0.00	0.00	0.00	0.00
30.0 - < 35.0	0.00	0.00	0.00	0.00	0.00	0.00	0.00	0.00	0.00
Totals	4.64	4.73	7.16	16.94	33.37	16.97	9.06	7.13	100.00

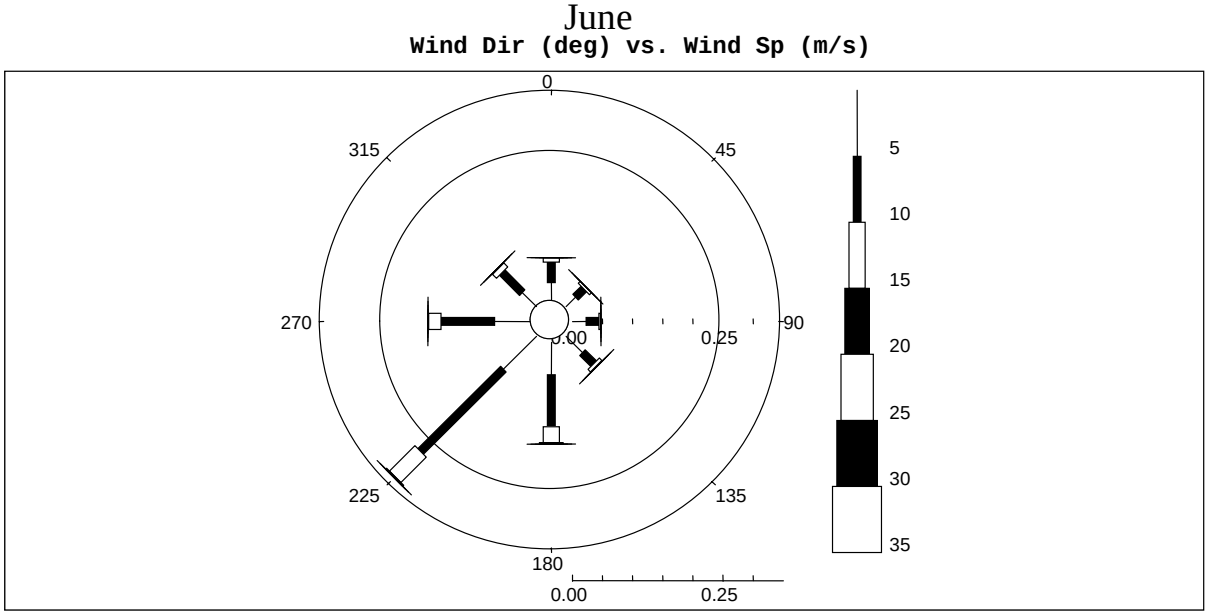

Figure A.6 Wind Rose for June.

Table A.7 Percentage Occurrence of Wind Speed by Direction for July.

July									
Wind Speed Range (m/s)	**Center of 45 Degree Direction Bins**								
	045	**090**	**135**	**180**	**225**	**270**	**315**	**360**	**Totals**
0.0 - < 5.0	1.66	1.89	3.08	7.31	10.43	6.44	3.13	1.91	35.85
5.0 - < 10.0	1.14	1.05	2.88	11.32	26.18	8.36	2.32	1.63	54.89
10.0 - < 15.0	0.12	0.10	0.38	2.25	3.79	1.25	0.66	0.21	8.76
15.0 - < 20.0	0.03	0.02	0.03	0.25	0.08	0.02	0.07	0.00	0.49
20.0 - < 25.0	0.00	0.00	0.00	0.00	0.02	0.00	0.00	0.00	0.02
25.0 - < 30.0	0.00	0.00	0.00	0.00	0.00	0.00	0.00	0.00	0.00
30.0 - < 35.0	0.00	0.00	0.00	0.00	0.00	0.00	0.00	0.00	0.00
Totals	2.95	3.06	6.37	21.13	40.50	16.06	6.17	3.75	100.00

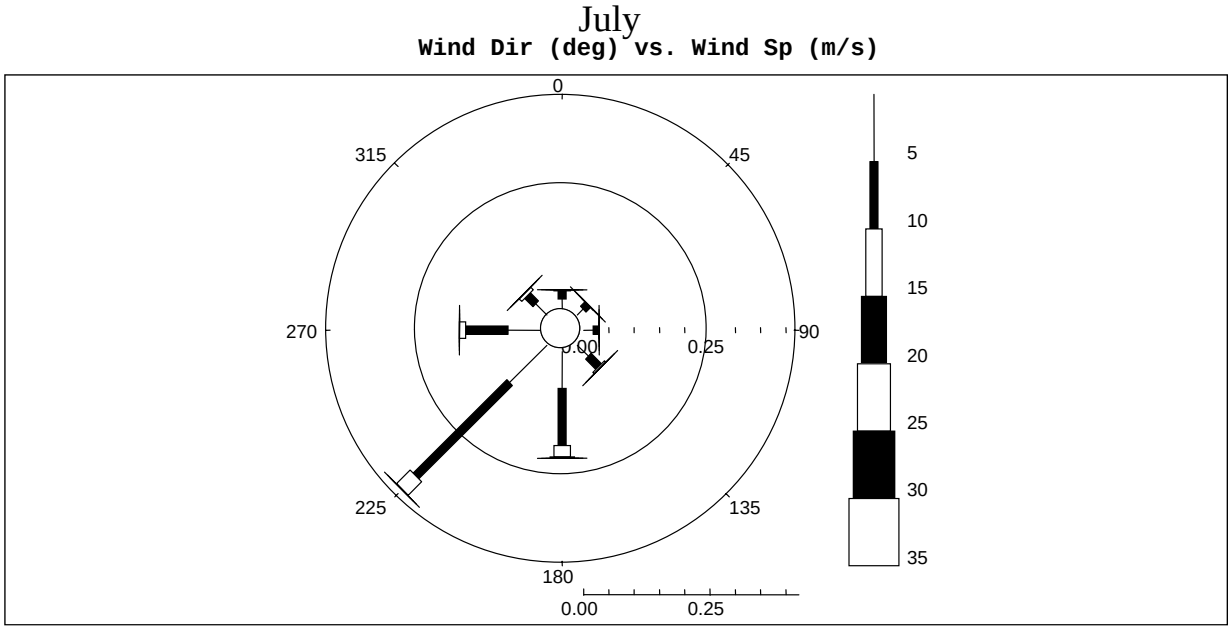

Figure A.7 Wind Rose for July.

Table A.8 Percentage Occurrence of Wind Speed by Direction for August.

August									
Wind Speed Range (m/s)	**Center of 45 Degree Direction Bins**								
	045	**090**	**135**	**180**	**225**	**270**	**315**	**360**	**Totals**
0.0 - < 5.0	1.70	2.11	3.97	6.20	8.20	6.27	3.31	2.45	34.20
5.0 - < 10.0	2.07	1.18	3.01	9.96	19.95	10.09	3.72	3.04	53.03
10.0 - < 15.0	0.56	0.25	0.54	2.25	4.23	2.02	1.15	0.61	11.62
15.0 - < 20.0	0.10	0.05	0.08	0.13	0.26	0.20	0.15	0.13	1.10
20.0 - < 25.0	0.00	0.00	0.00	0.02	0.00	0.00	0.00	0.03	0.05
25.0 - < 30.0	0.00	0.00	0.00	0.00	0.00	0.00	0.00	0.00	0.00
30.0 - < 35.0	0.00	0.00	0.00	0.00	0.00	0.00	0.00	0.00	0.00
Totals	4.43	3.59	7.60	18.56	32.64	18.58	8.33	6.27	100.00

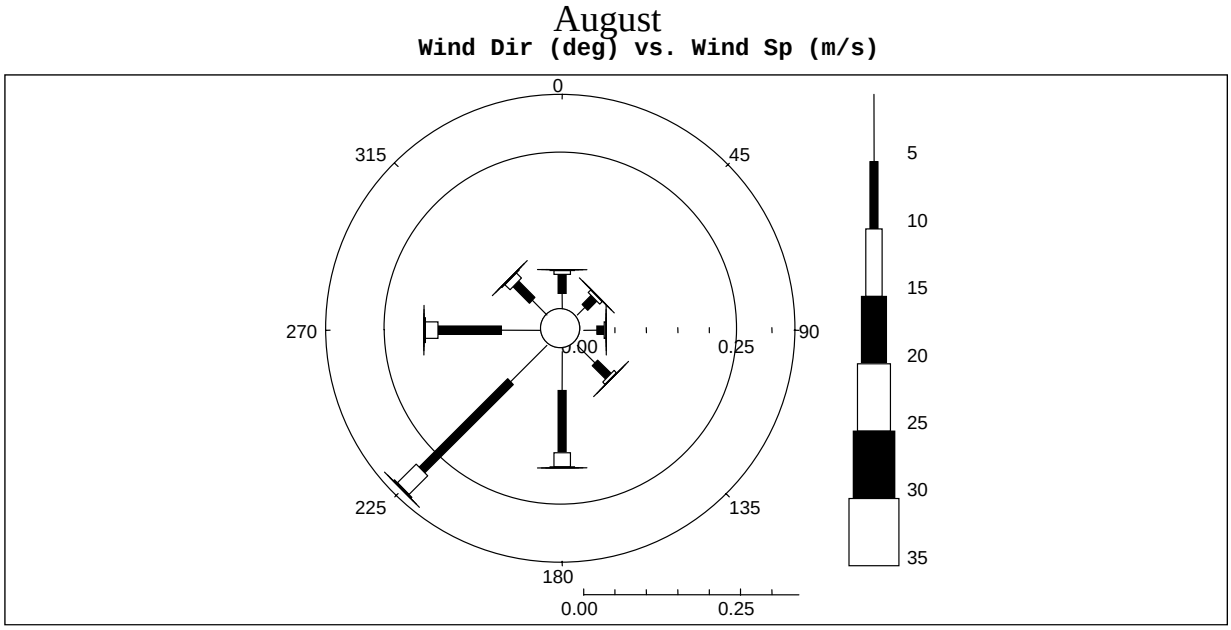

Figure A.8 Wind Rose for August.

Table A.9 Percentage Occurrence of Wind Speed by Direction for September.

September									
Wind Speed Range	**Center of 45 Degree Direction Bins**								
(m/s)	**045**	**090**	**135**	**180**	**225**	**270**	**315**	**360**	**Totals**
0.0 - < 5.0	1.92	1.96	2.48	3.86	5.26	5.26	3.55	2.57	26.85
5.0 - < 10.0	3.28	1.94	2.84	7.52	12.86	11.38	7.35	4.06	51.22
10.0 - < 15.0	0.78	0.53	0.83	2.89	4.47	4.22	3.47	1.75	18.95
15.0 - < 20.0	0.19	0.12	0.15	0.49	0.49	0.48	0.56	0.15	2.64
20.0 - < 25.0	0.02	0.02	0.00	0.07	0.07	0.12	0.03	0.02	0.34
25.0 - < 30.0	0.00	0.00	0.00	0.00	0.00	0.00	0.00	0.00	0.00
30.0 - < 35.0	0.00	0.00	0.00	0.00	0.00	0.00	0.00	0.00	0.00
Totals	6.19	4.56	6.31	14.83	23.15	21.45	14.97	8.55	100.00

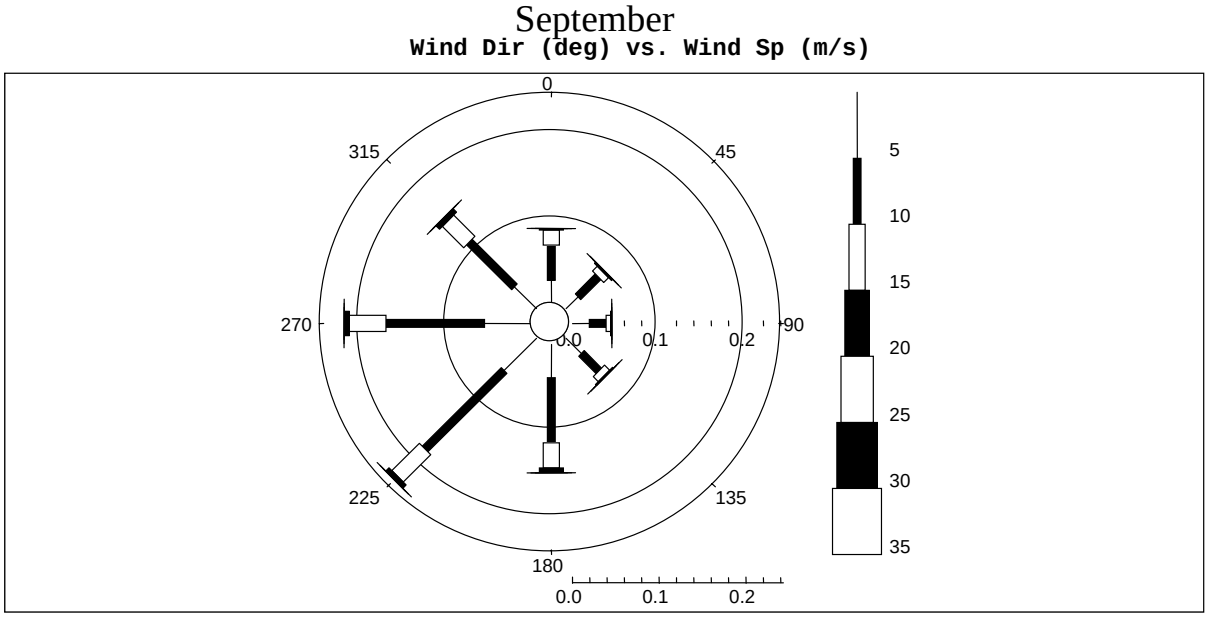

Figure A.9 Wind Rose for September.

Table A.10 Percentage Occurrence of Wind Speed by Direction for October.

October									
Wind Speed Range (m/s)	**Center of 45 Degree Direction Bins**								
	045	**090**	**135**	**180**	**225**	**270**	**315**	**360**	**Totals**
0.0 - < 5.0	1.37	1.50	1.91	2.90	3.72	3.37	2.22	1.58	18.56
5.0 - < 10.0	1.99	2.16	3.08	6.30	9.51	11.37	7.95	4.28	46.64
10.0 - < 15.0	1.07	0.61	1.45	3.75	5.60	6.96	6.81	2.32	28.57
15.0 - < 20.0	0.30	0.13	0.33	0.86	0.72	1.15	1.50	0.66	5.65
20.0 - < 25.0	0.07	0.00	0.02	0.05	0.05	0.07	0.16	0.13	0.54
25.0 - < 30.0	0.00	0.00	0.00	0.00	0.02	0.02	0.00	0.00	0.03
30.0 - < 35.0	0.00	0.00	0.00	0.00	0.00	0.00	0.00	0.00	0.00
Totals	4.79	4.39	6.78	13.86	19.62	22.94	18.65	8.97	100.00

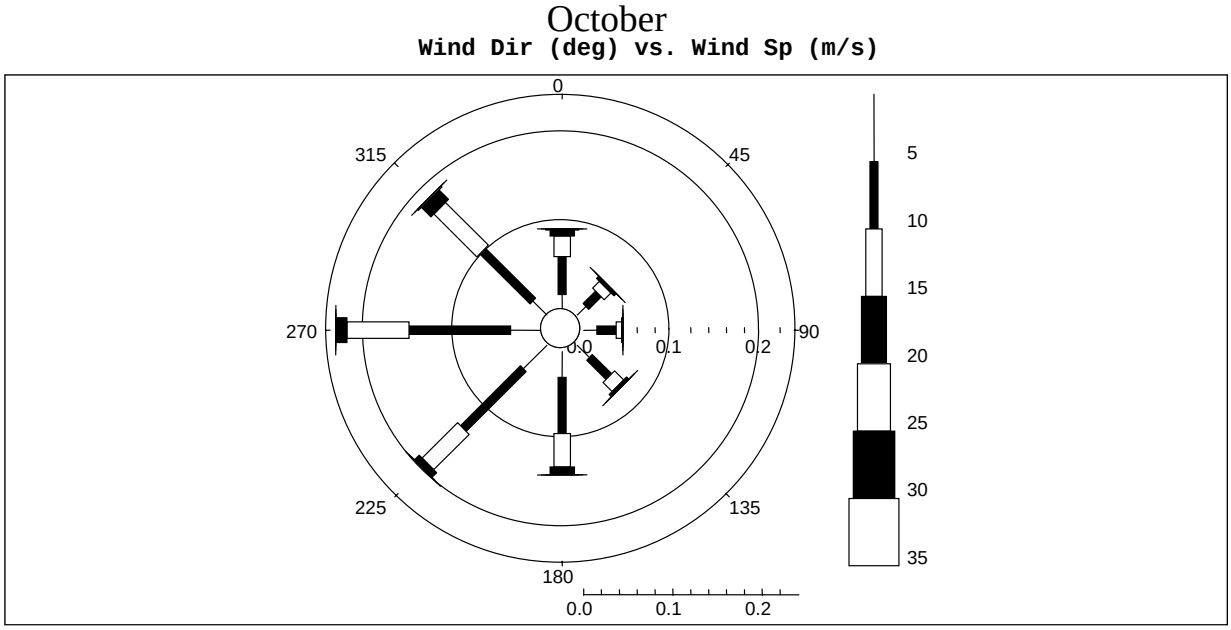

AE Gpt 5622, Lat 46.875n, Long 48.3333w, Depth 1000m
Defined Period: Operational

Figure A.10 Wind Rose for October.

Table A.11 Percentage Occurrence of Wind Speed by Direction for November.

November									
Wind Speed Range (m/s)	**Center of 45 Degree Direction Bins**								
	045	**090**	**135**	**180**	**225**	**270**	**315**	**360**	**Totals**
0.0 - < 5.0	1.07	1.21	1.92	2.50	2.52	2.30	2.02	1.38	14.91
5.0 - < 10.0	2.62	2.55	3.71	5.65	8.55	8.98	7.74	3.49	43.28
10.0 - < 15.0	1.21	1.19	2.23	4.63	5.65	7.98	6.63	2.06	31.56
15.0 - < 20.0	0.37	0.20	0.66	1.46	1.33	2.41	2.06	0.70	9.20
20.0 - < 25.0	0.09	0.02	0.05	0.10	0.10	0.19	0.39	0.07	1.00
25.0 - < 30.0	0.00	0.00	0.00	0.02	0.00	0.00	0.00	0.02	0.03
30.0 - < 35.0	0.00	0.00	0.00	0.00	0.00	0.00	0.00	0.00	0.00
Totals	5.36	5.17	8.57	14.35	18.15	21.85	18.84	7.70	100.00

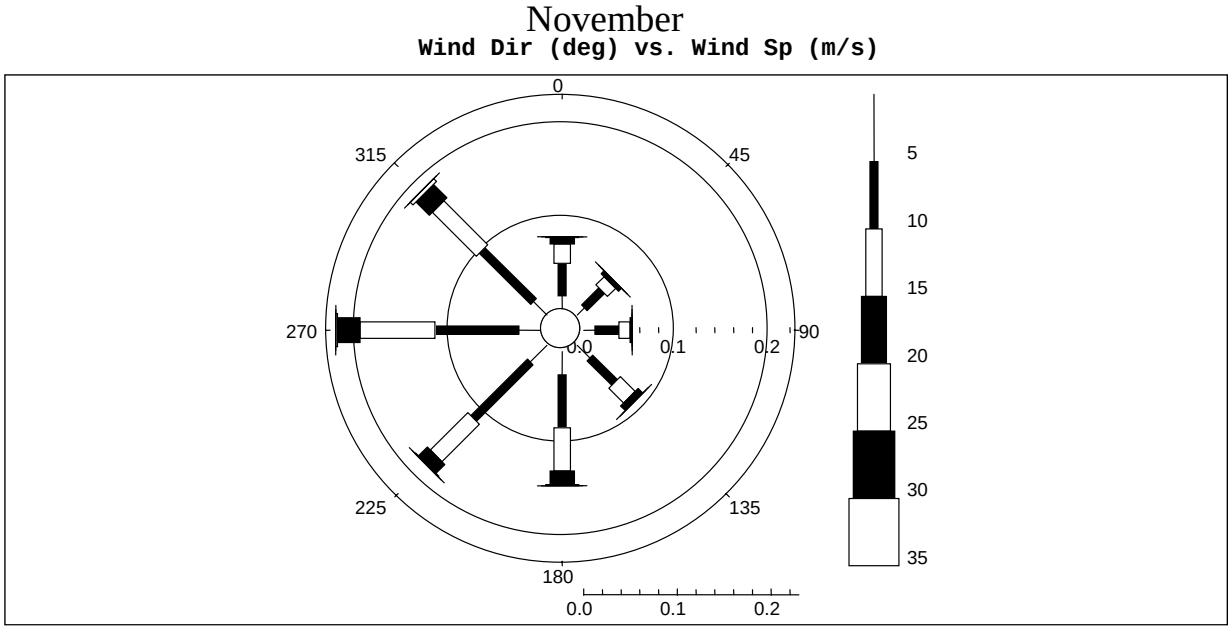

Figure A.11 Wind Rose for November.

Table A.12 Percentage Occurrence of Wind Speed by Direction for December.

December									
Wind Speed Range (m/s)	**Center of 45 Degree Direction Bins**								
	045	**090**	**135**	**180**	**225**	**270**	**315**	**360**	**Totals**
0.0 - < 5.0	0.95	1.22	1.33	1.73	1.71	2.01	1.55	0.95	11.45
5.0 - < 10.0	1.86	2.04	2.96	5.00	6.55	8.84	6.48	3.36	37.10
10.0 - < 15.0	1.18	0.92	2.24	4.49	5.50	10.35	7.19	2.96	34.84
15.0 - < 20.0	0.36	0.30	1.07	2.09	2.30	5.02	2.65	0.91	14.70
20.0 - < 25.0	0.03	0.03	0.10	0.18	0.20	0.79	0.25	0.16	1.74
25.0 - < 30.0	0.00	0.00	0.00	0.00	0.02	0.05	0.07	0.03	0.16
30.0 - < 35.0	0.00	0.00	0.00	0.00	0.00	0.00	0.00	0.00	0.00
Totals	4.39	4.51	7.70	13.50	16.28	27.06	18.19	8.38	100.00

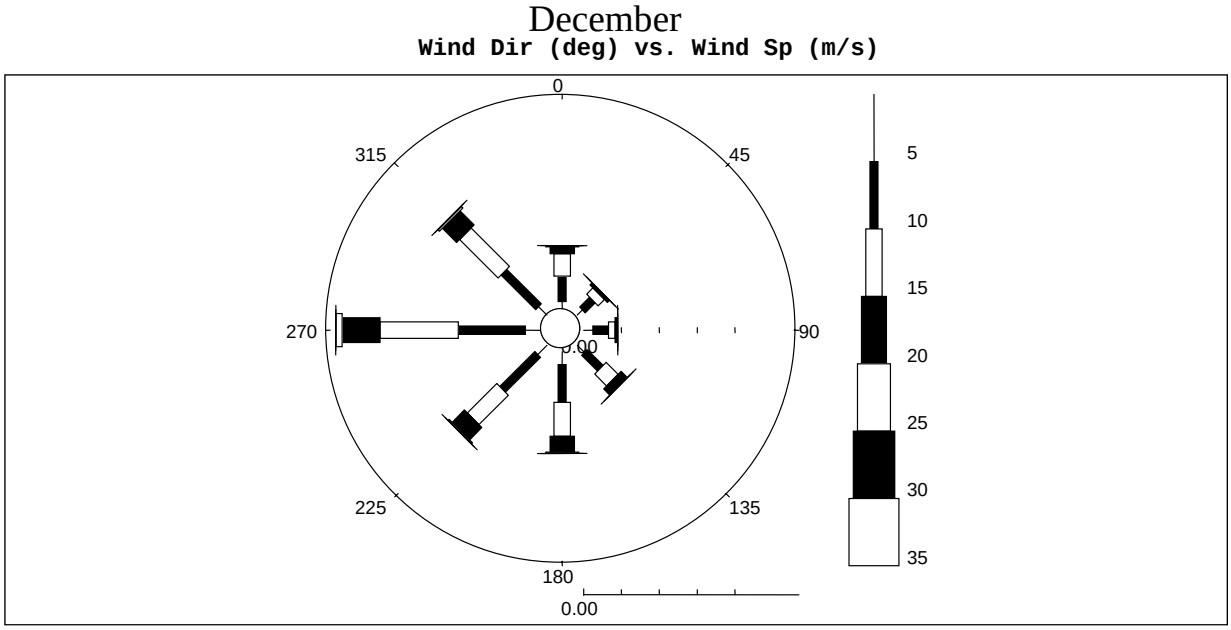

Figure A.12 Wind Rose for December.

Appendix B

Environmental Contour Plots for Each Month

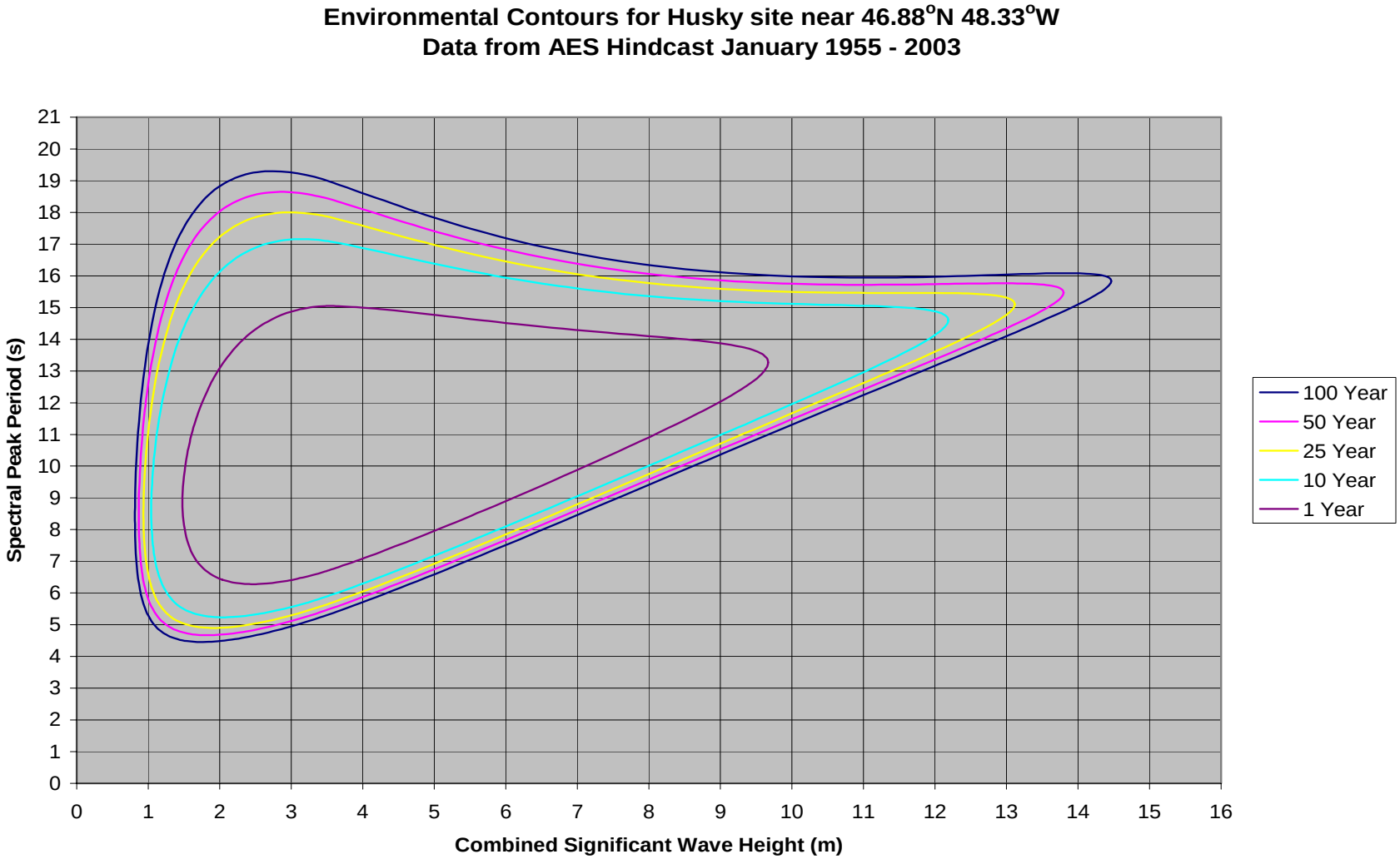

Figure B.1 Environmental Contour Plot for January.

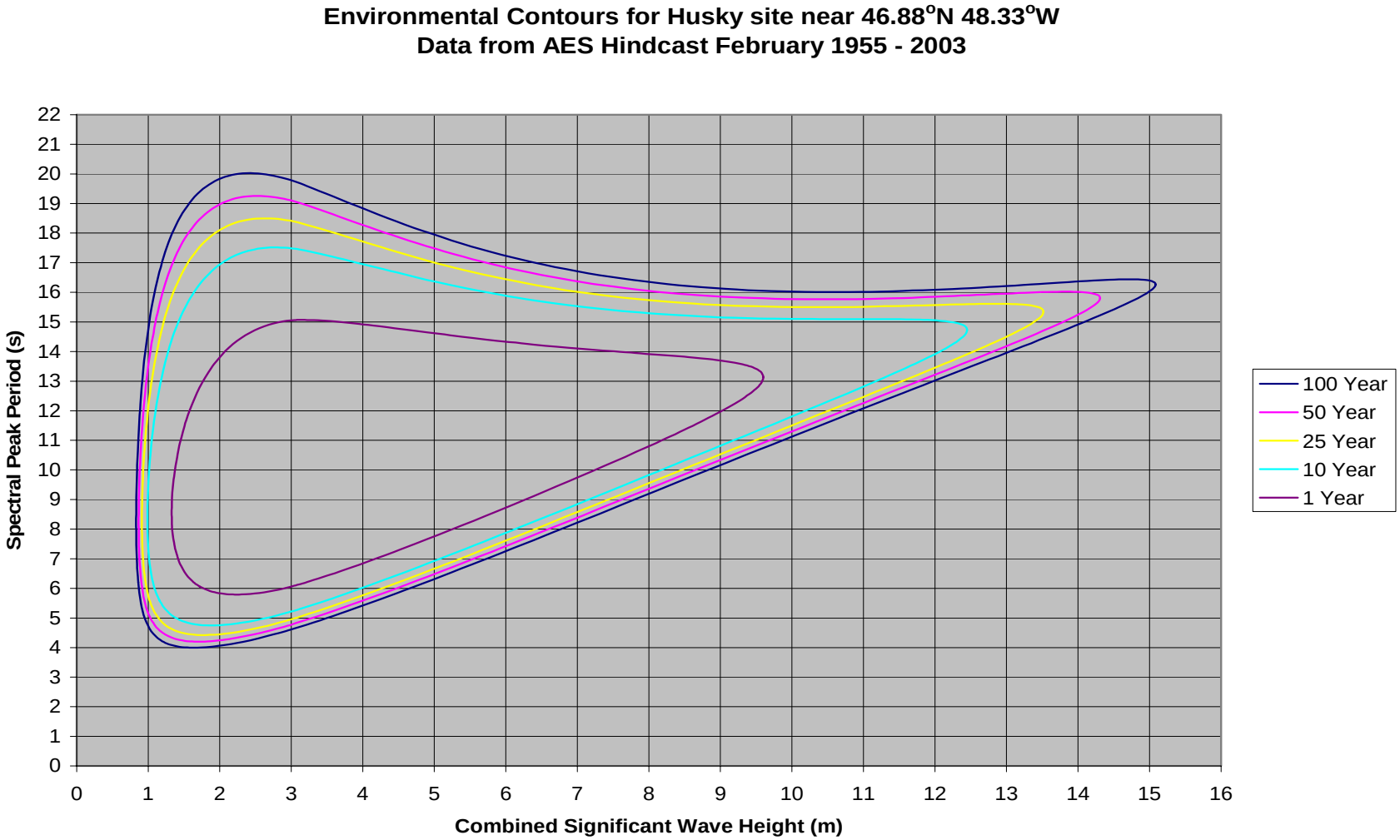

Figure B.2 Environmental Contour Plot for February.

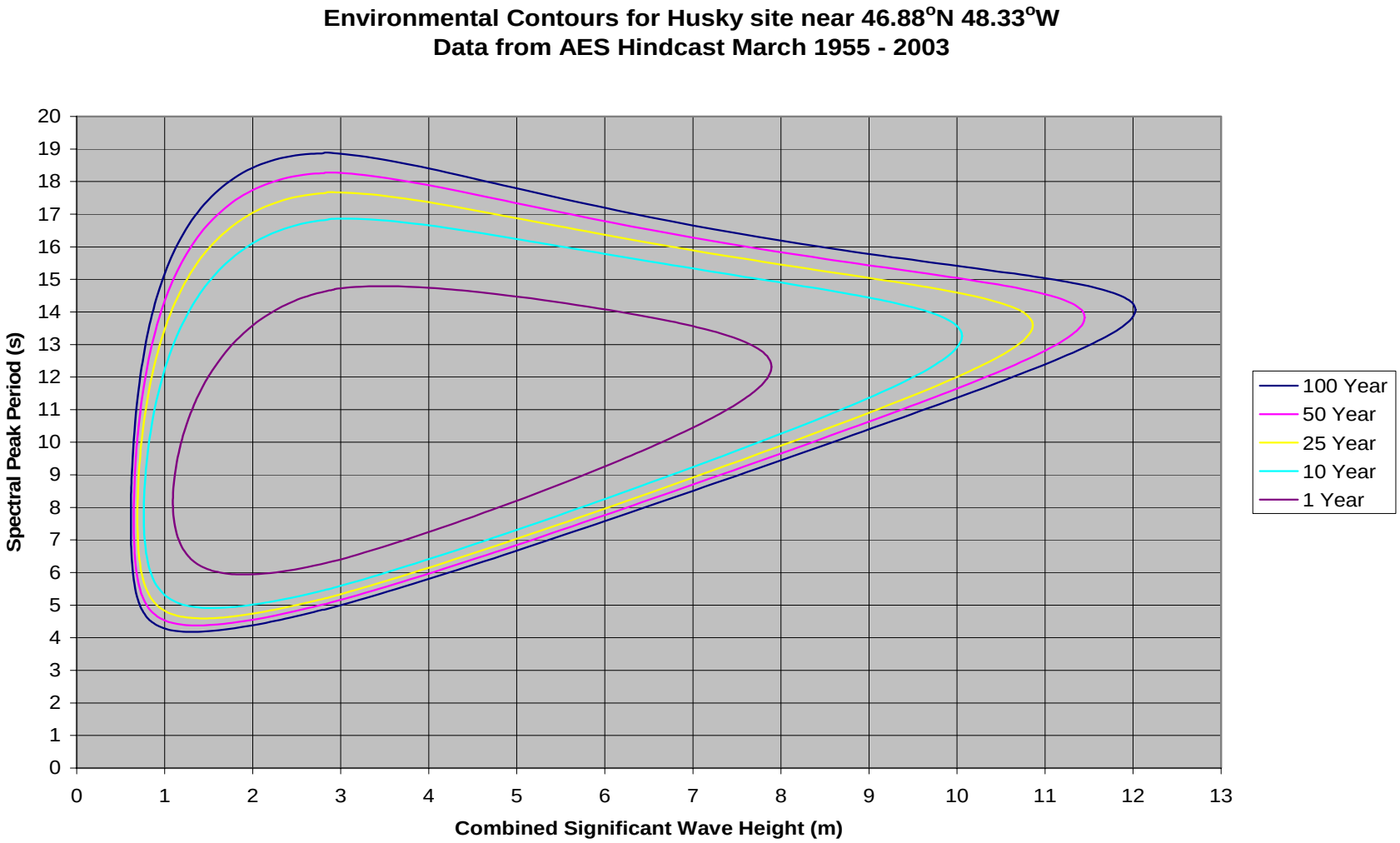

Figure B.3 Environmental Contour Plot for March.

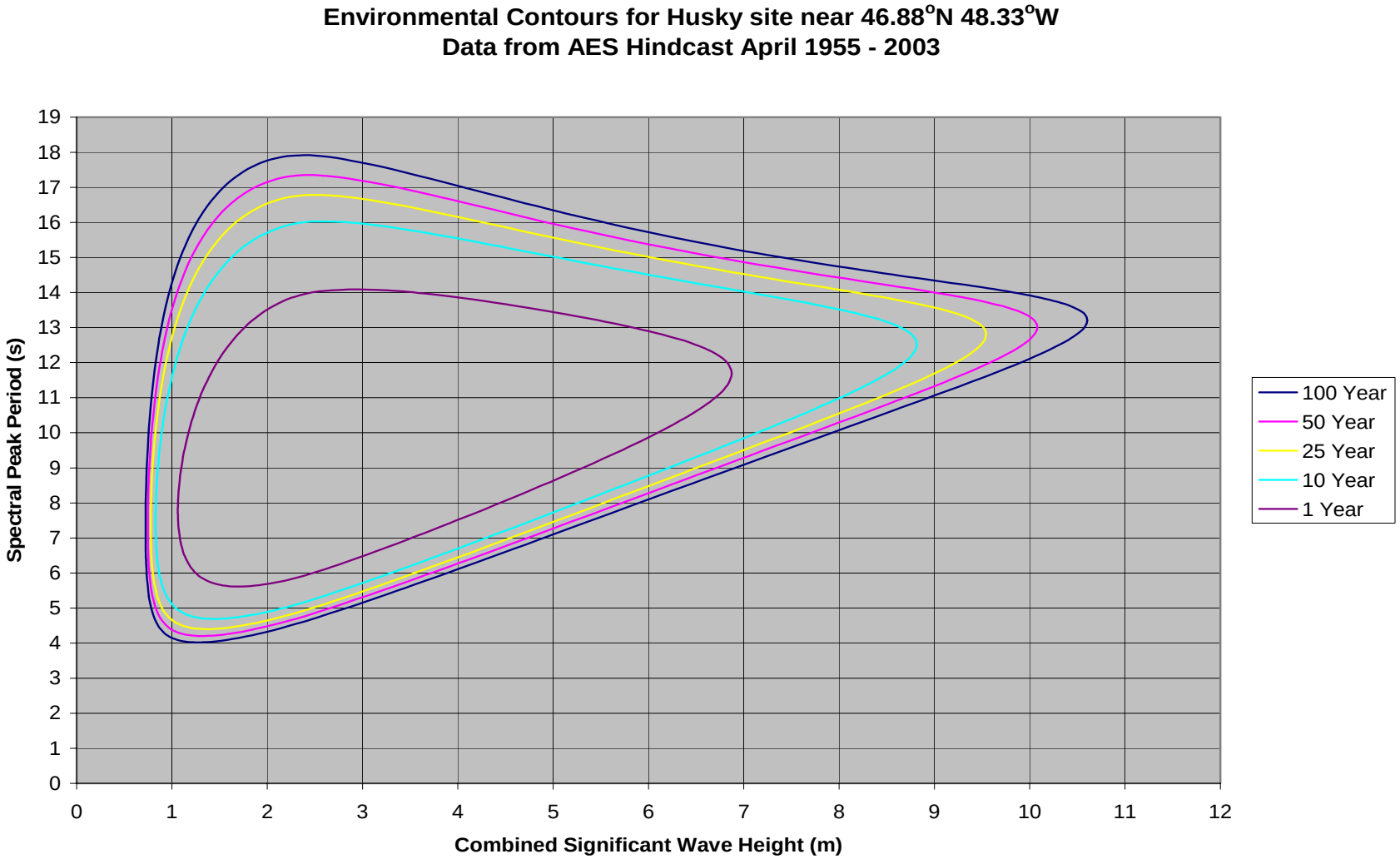

Figure B.4 Environmental Contour Plot for April.

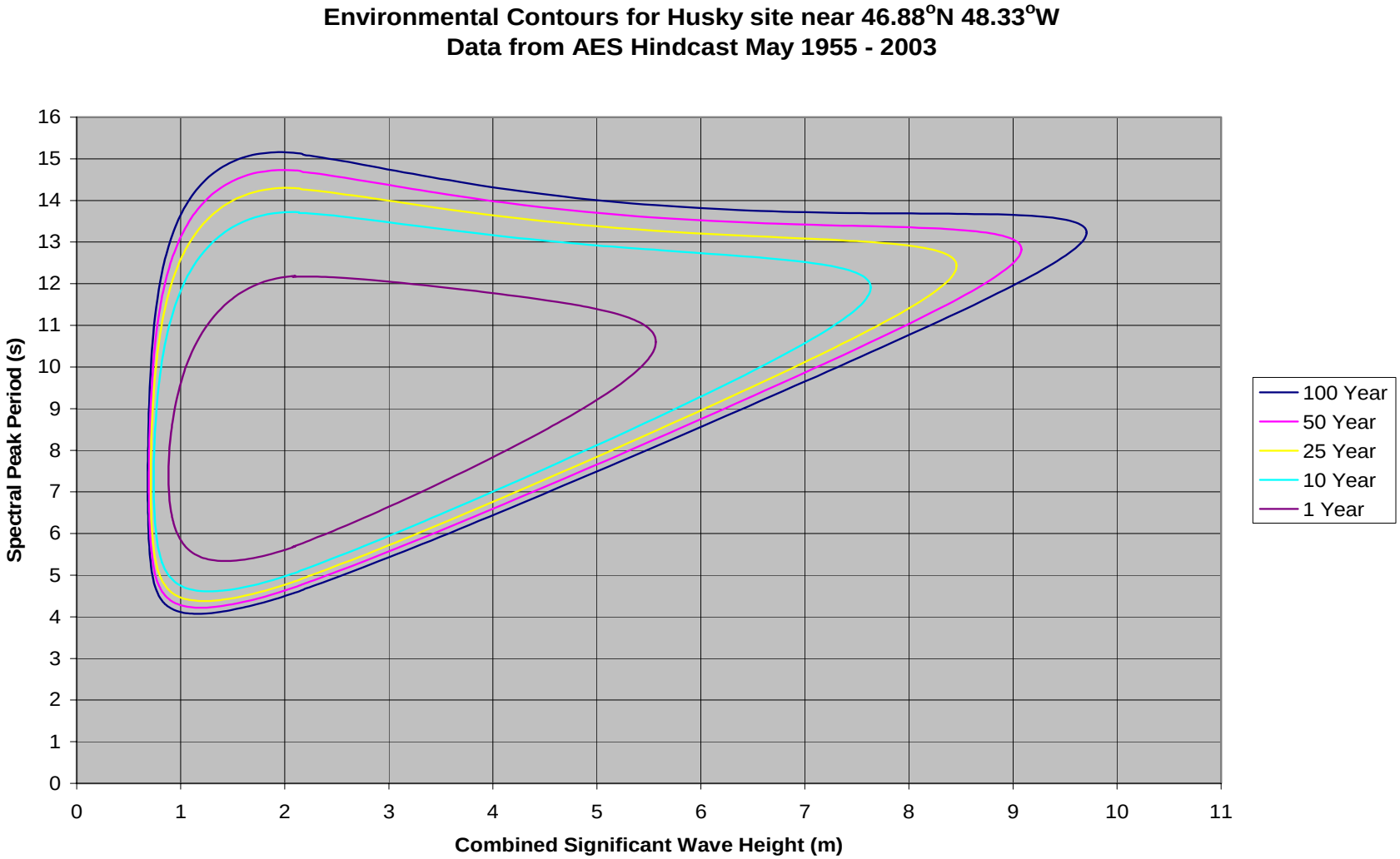

Figure B.5 Environmental Contour Plot for May.

Figure B.6 Environmental Contour Plot for June.

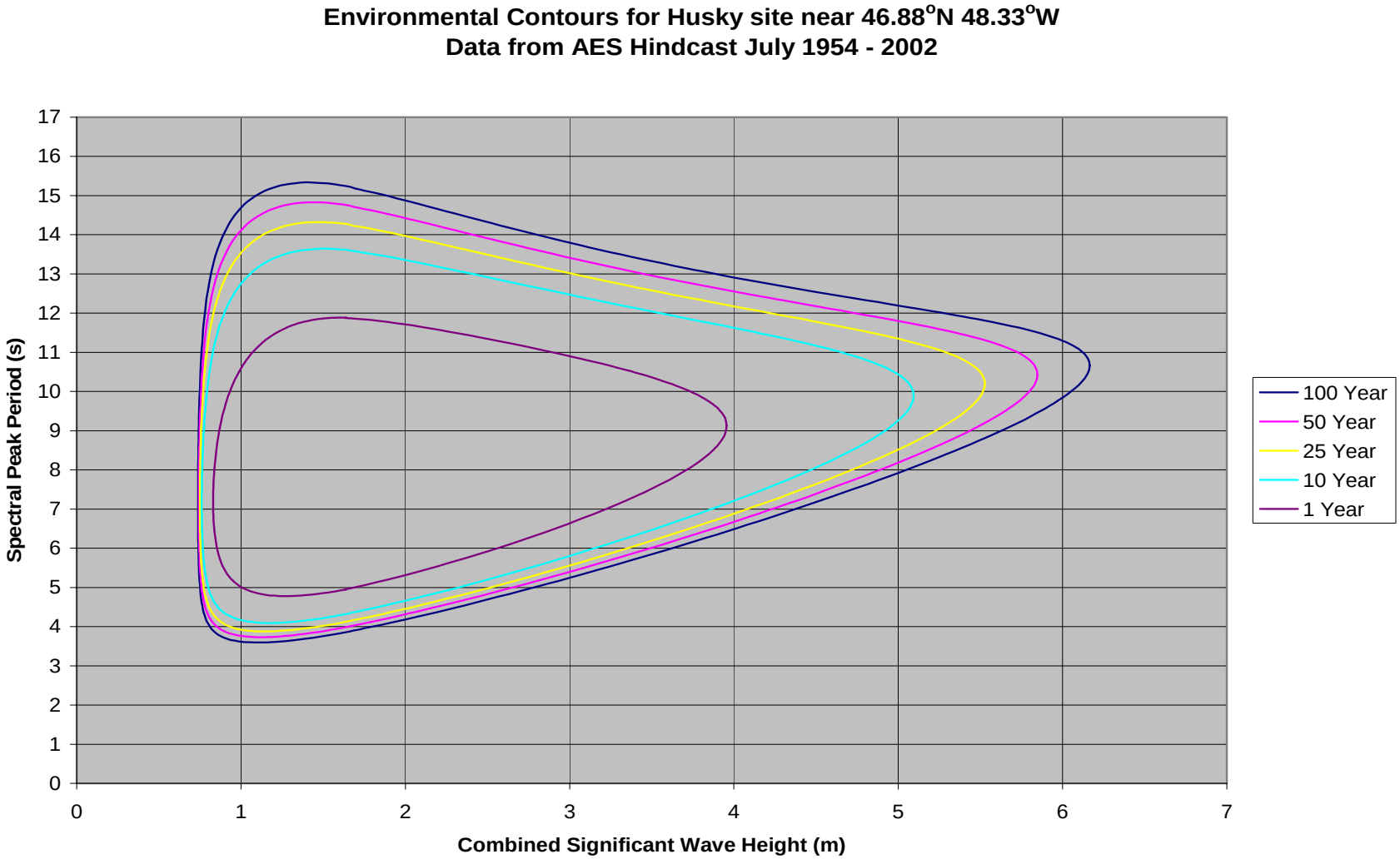

Figure B.7 Environmental Contour Plot for July.

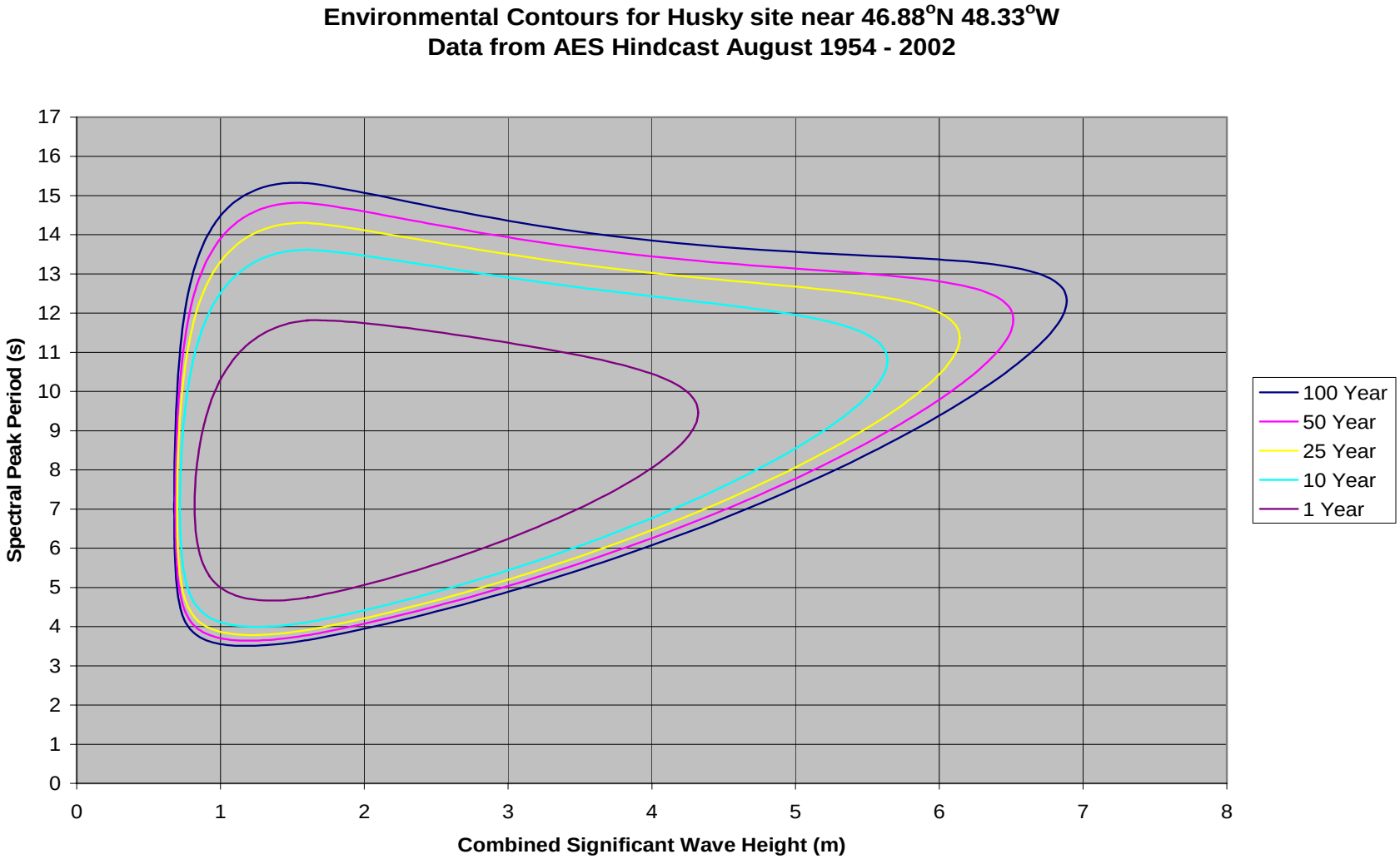

Figure B.8 Environmental Contour Plot for August.

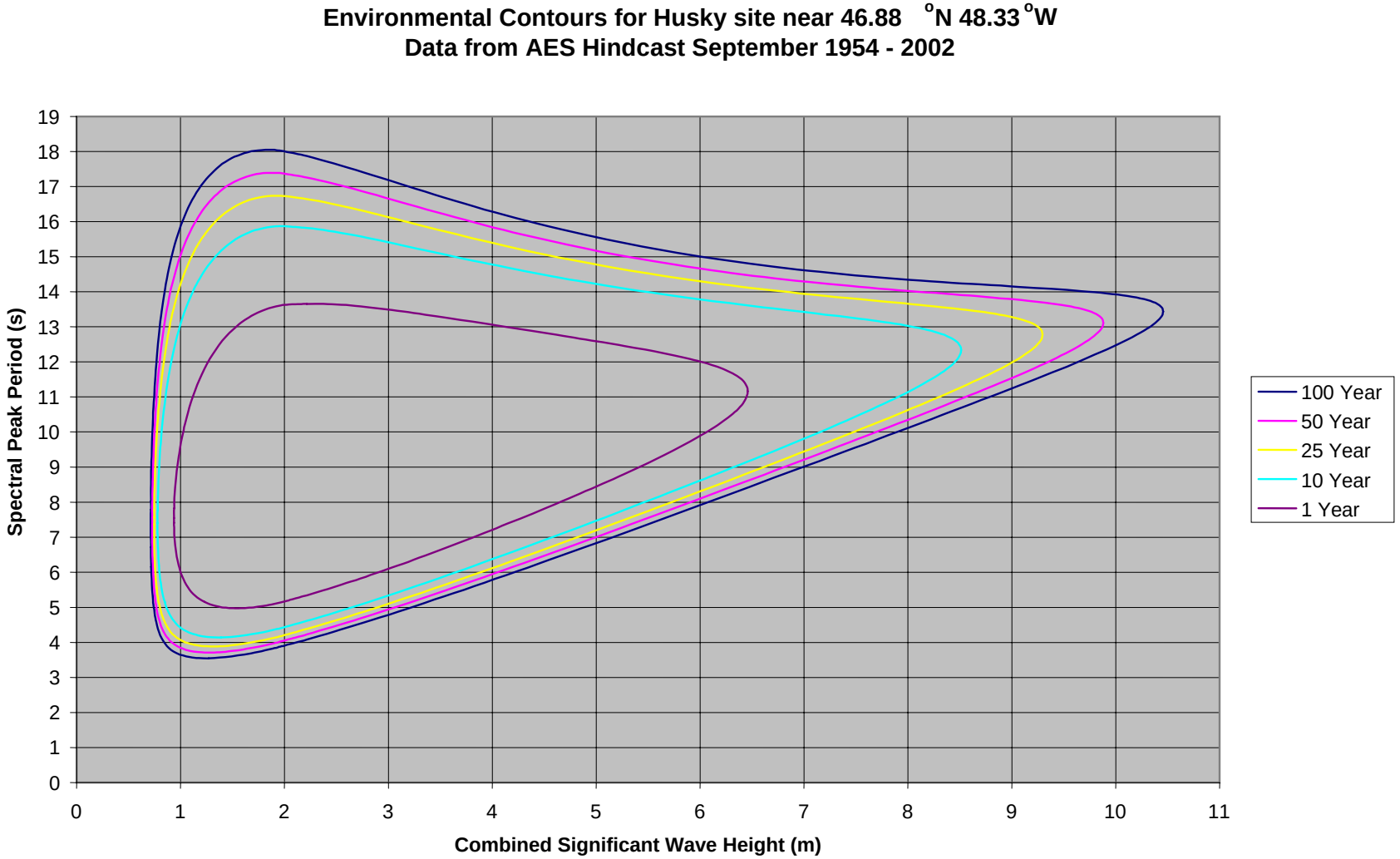

Figure B.9 Environmental Contour Plot for September.

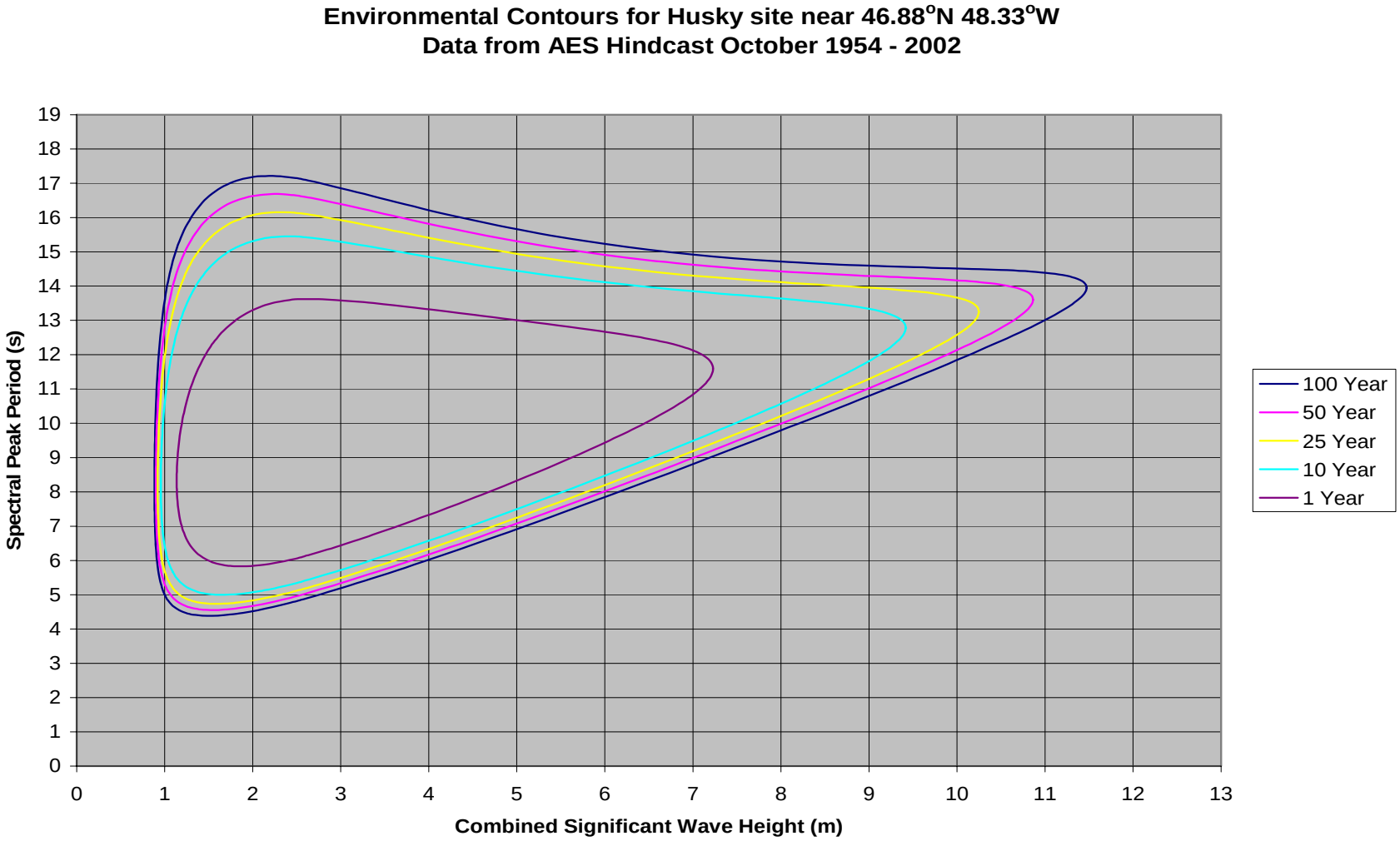

Figure B.10 Environmental Contour Plot for October.

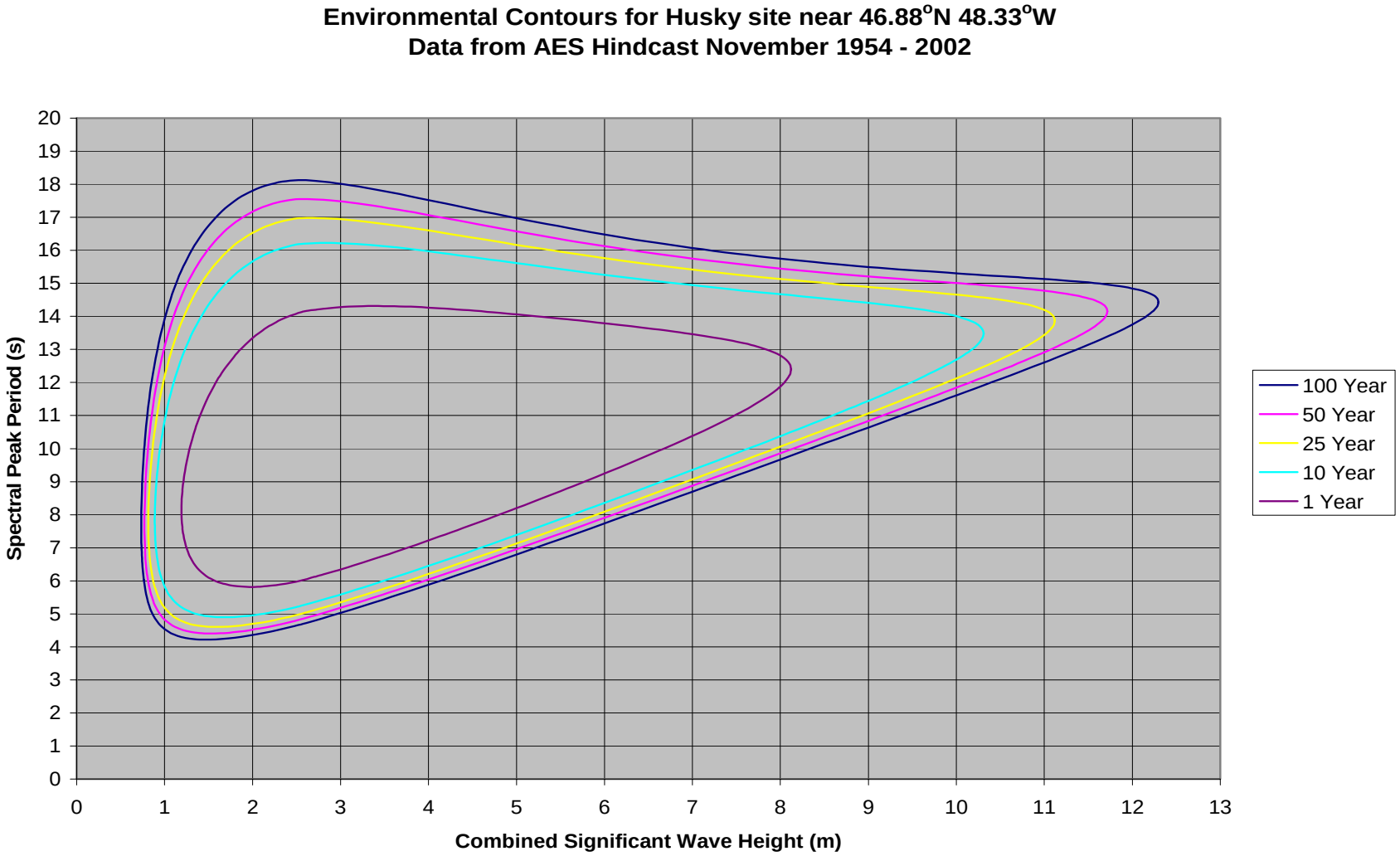

Figure B.11 Environmental Contour Plot for November.

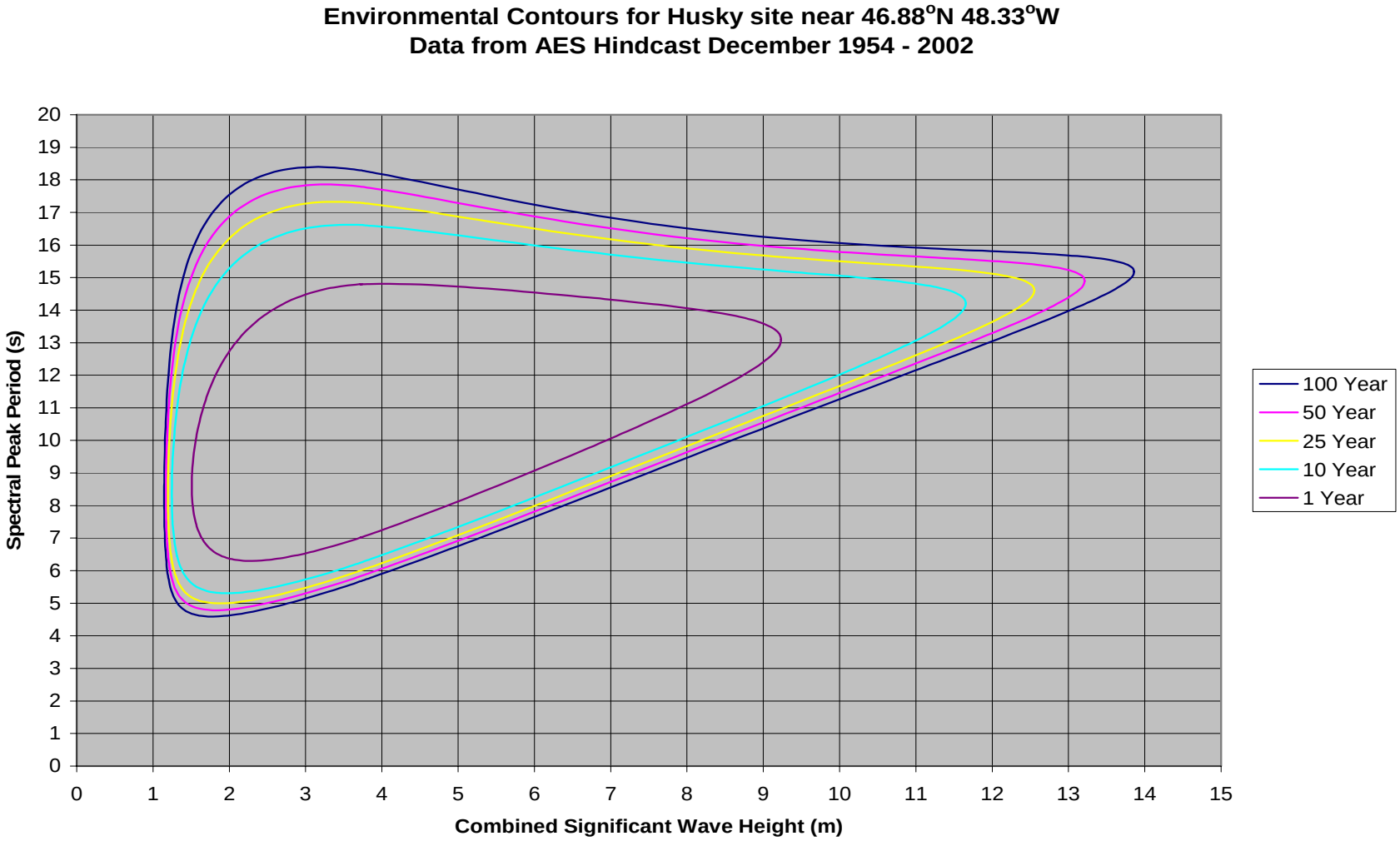

Figure B.12 Environmental Contour Plot for December.

Appendix C

PROGRESSIVE VECTOR DIAGRAMS

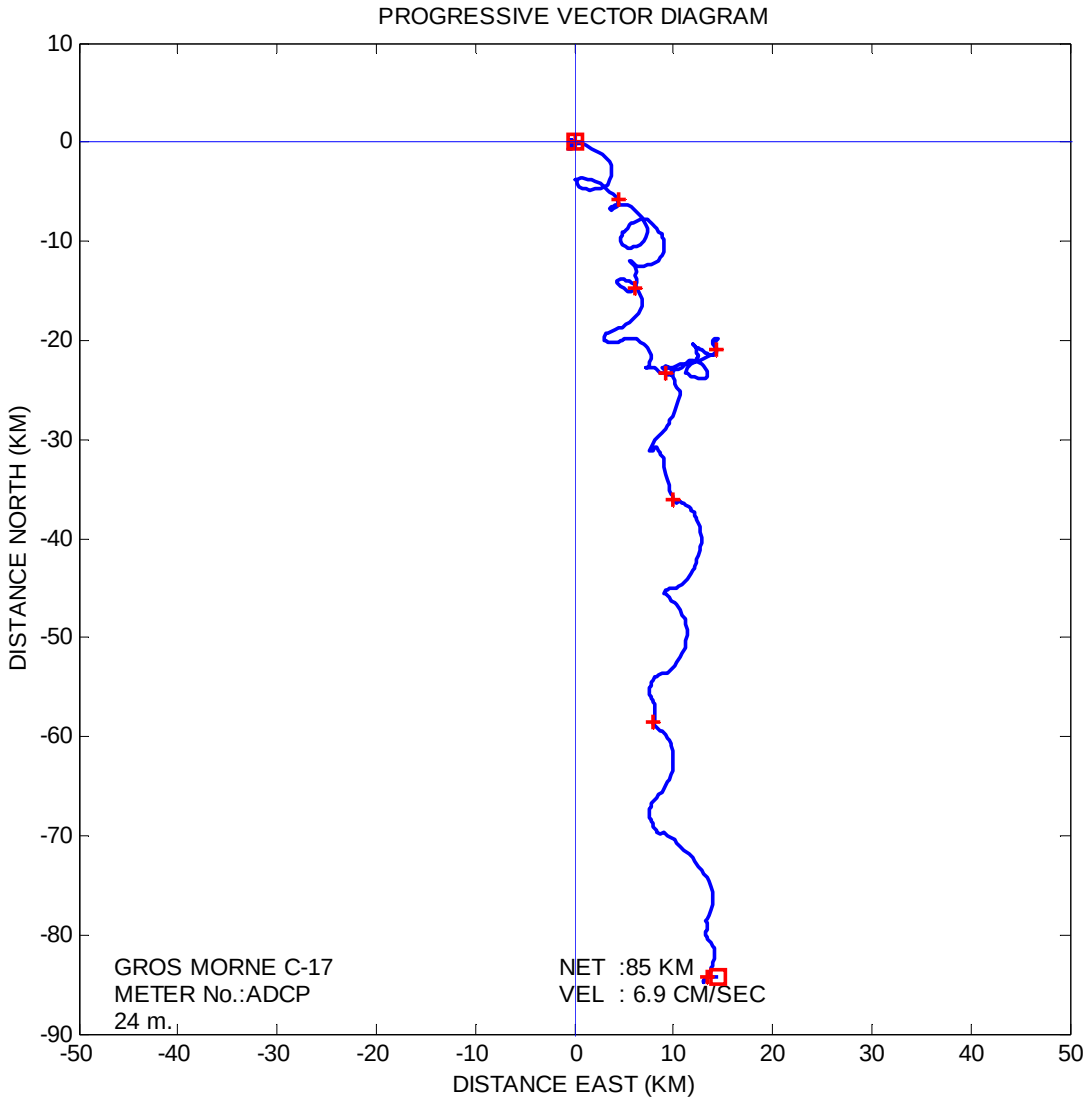

Figure C.1 Currents Near-surface during September, 2002 at Gros Morne C-17.

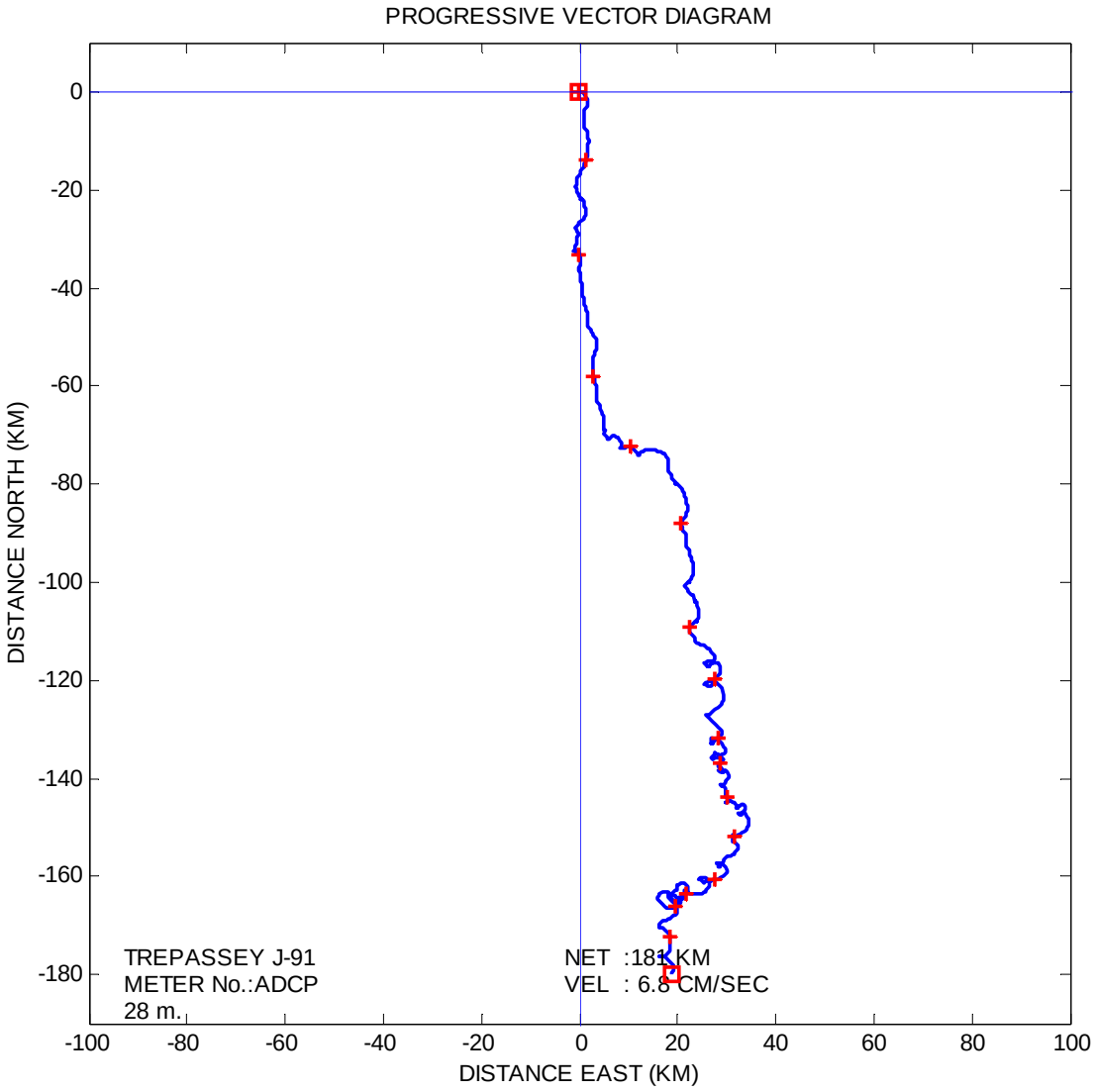

Figure C.2 Currents Near-surface during July and August, 2002 at Trepassey J-91.

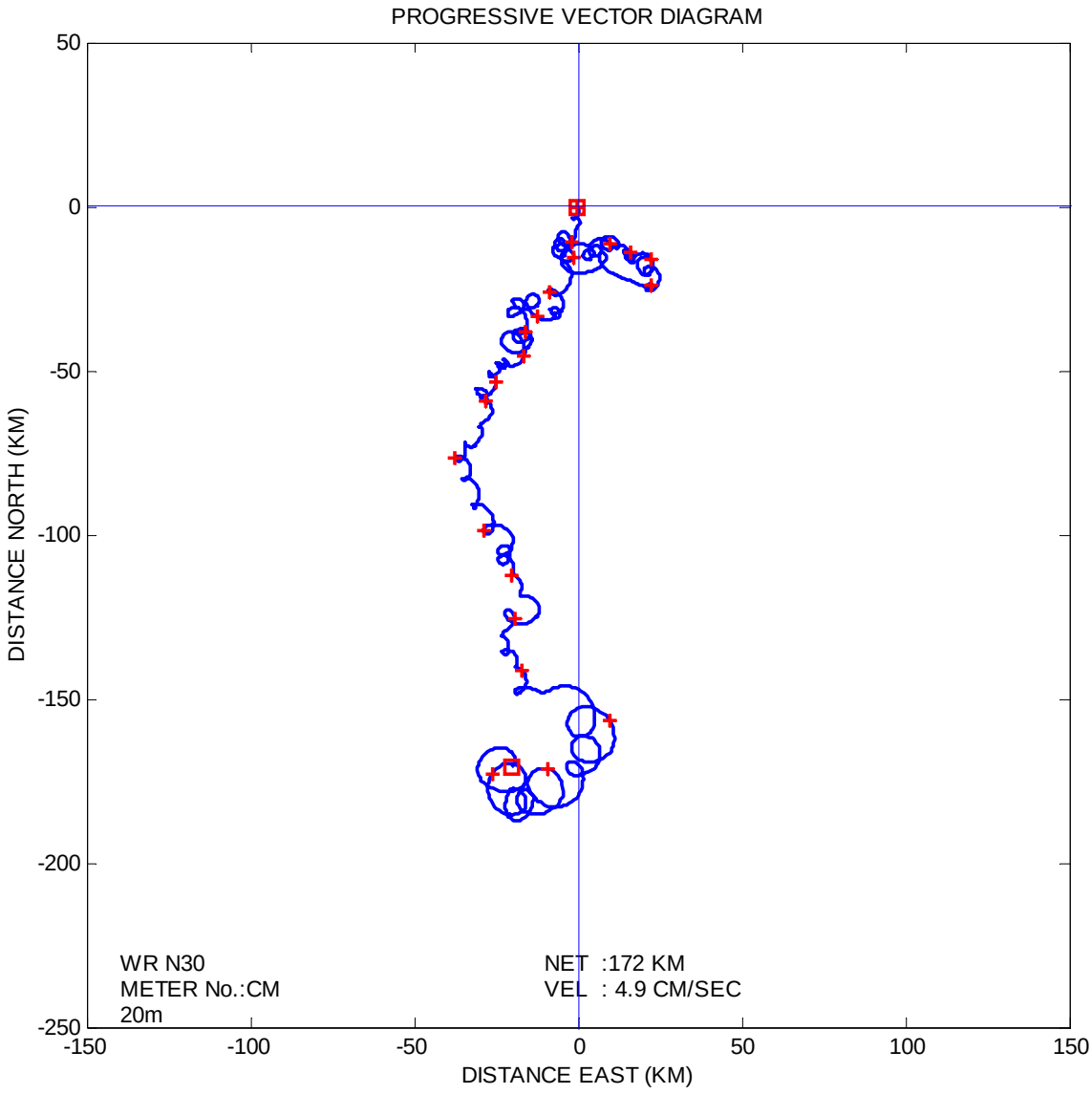

Figure C.3 Currents Near-surface during August and September, 1999 at White Rose N-30.

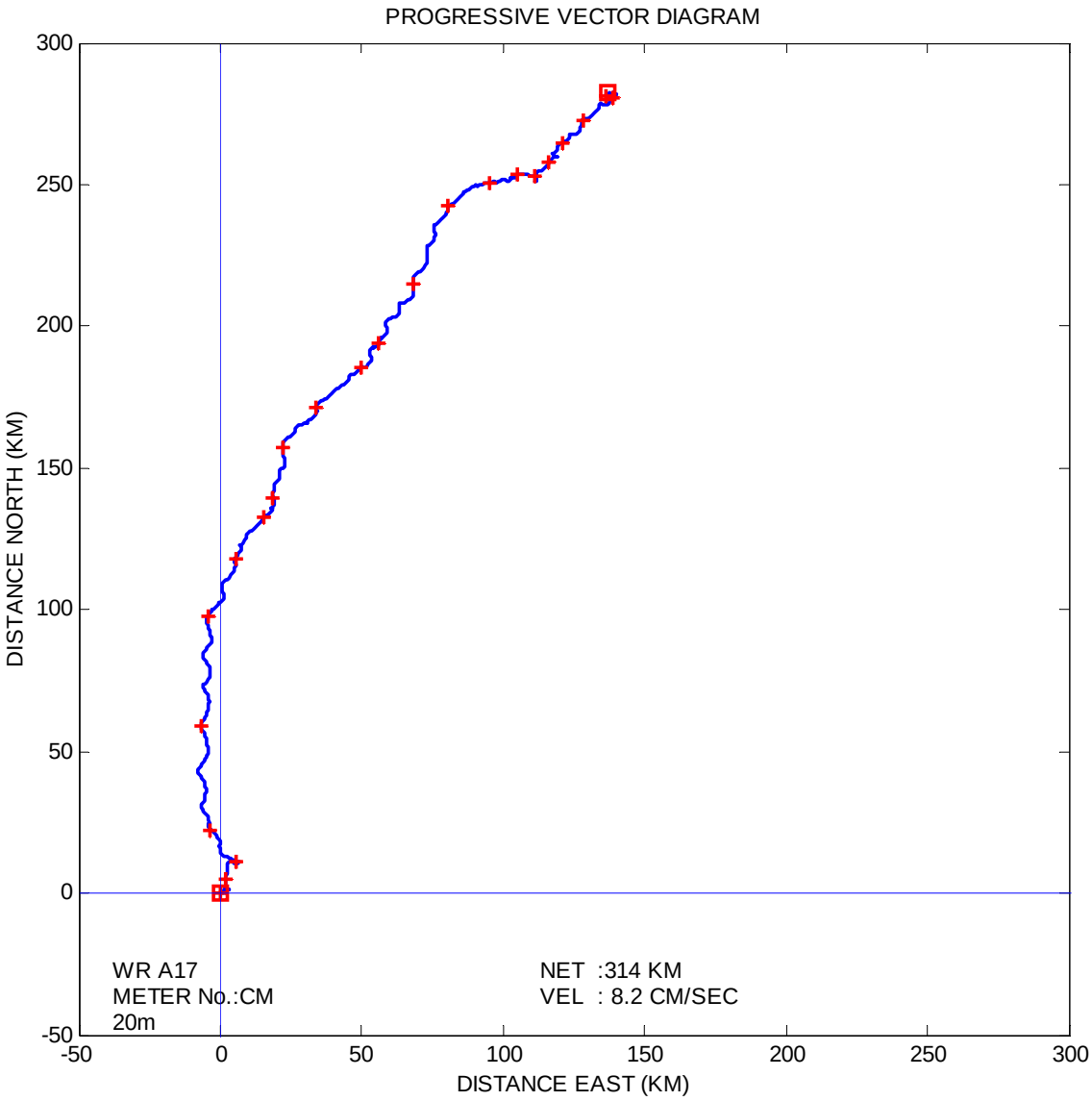

Figure C.4 Currents Near-surface from June to August, 1999 at White Rose A-17.

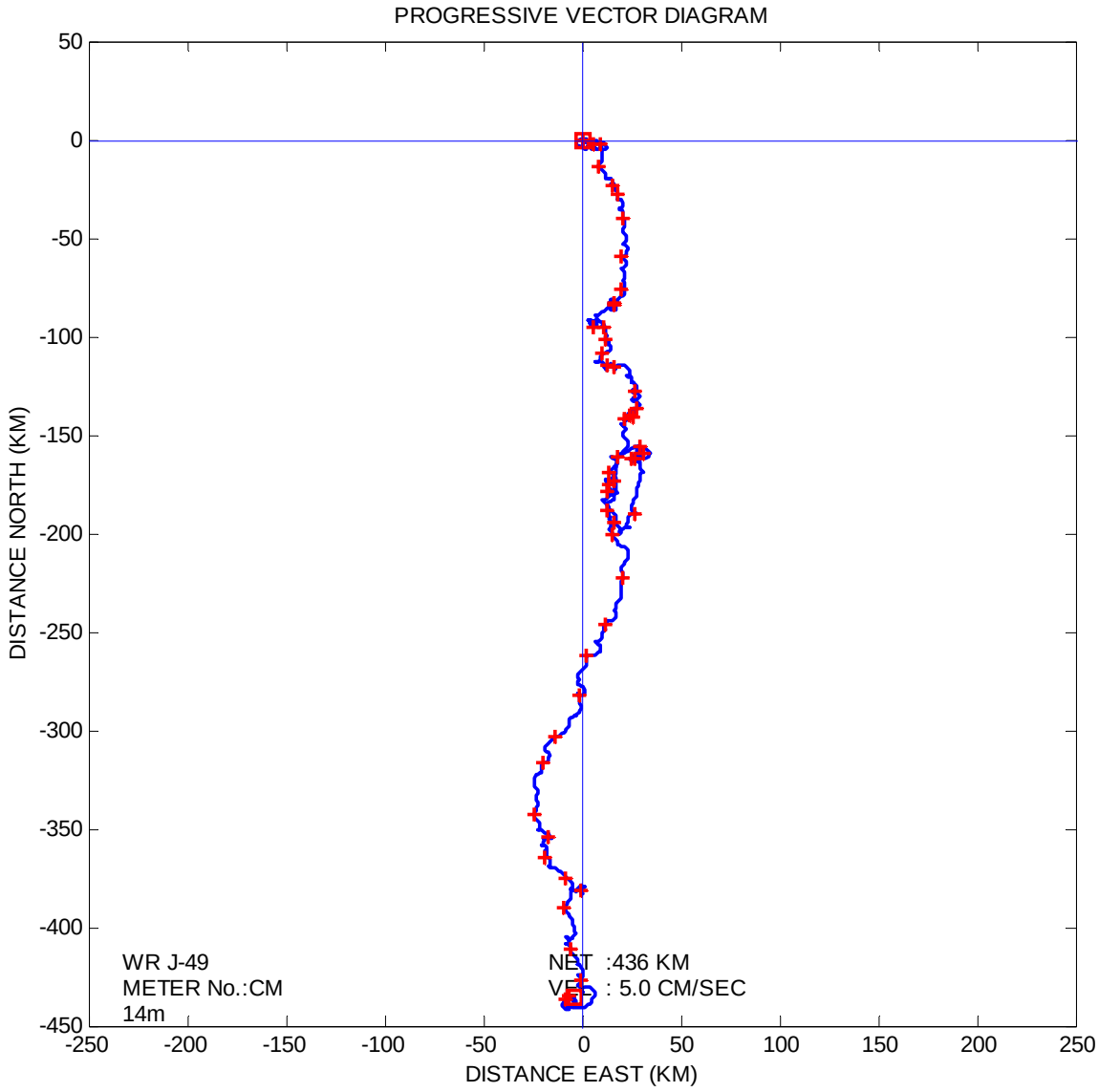

Figure C.5 Currents Near-surface during August to November, 1985 at White Rose J-49.

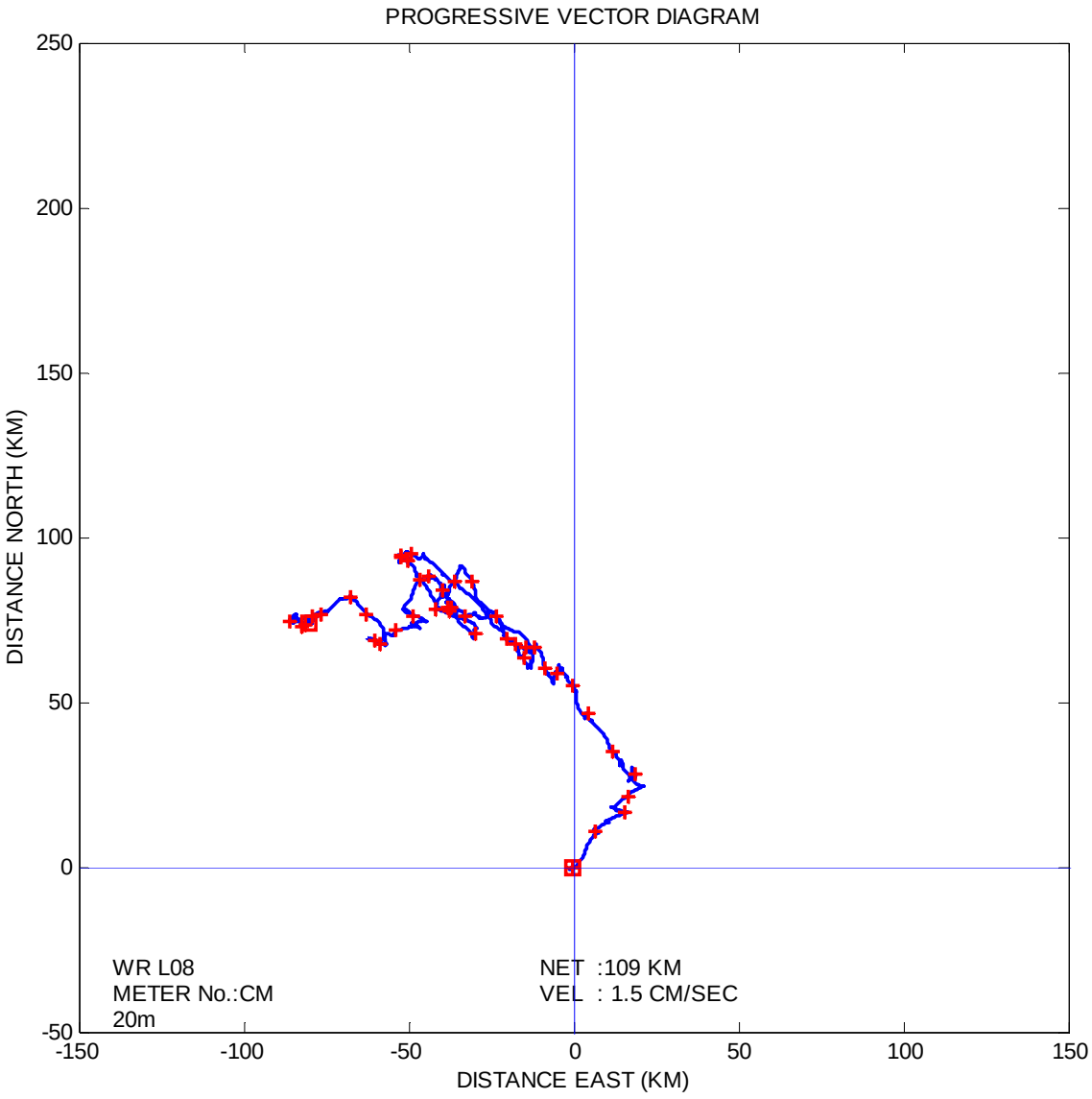

Figure C.6 Currents Near-surface form March to June, 1999 at White Rose L-08.

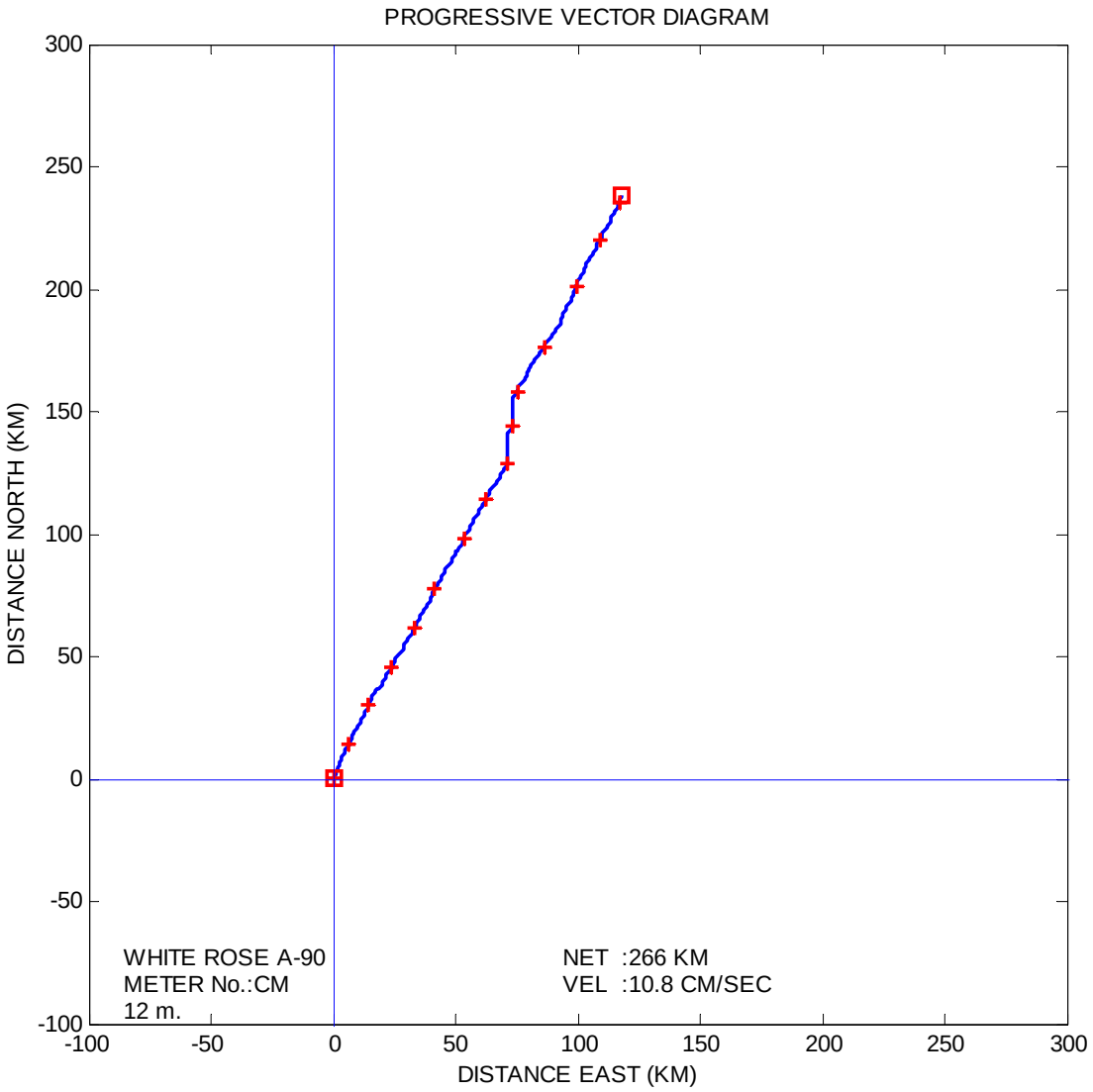

Figure C.7 Currents Near-surface during July and August, 1988 at White Rose A-90.

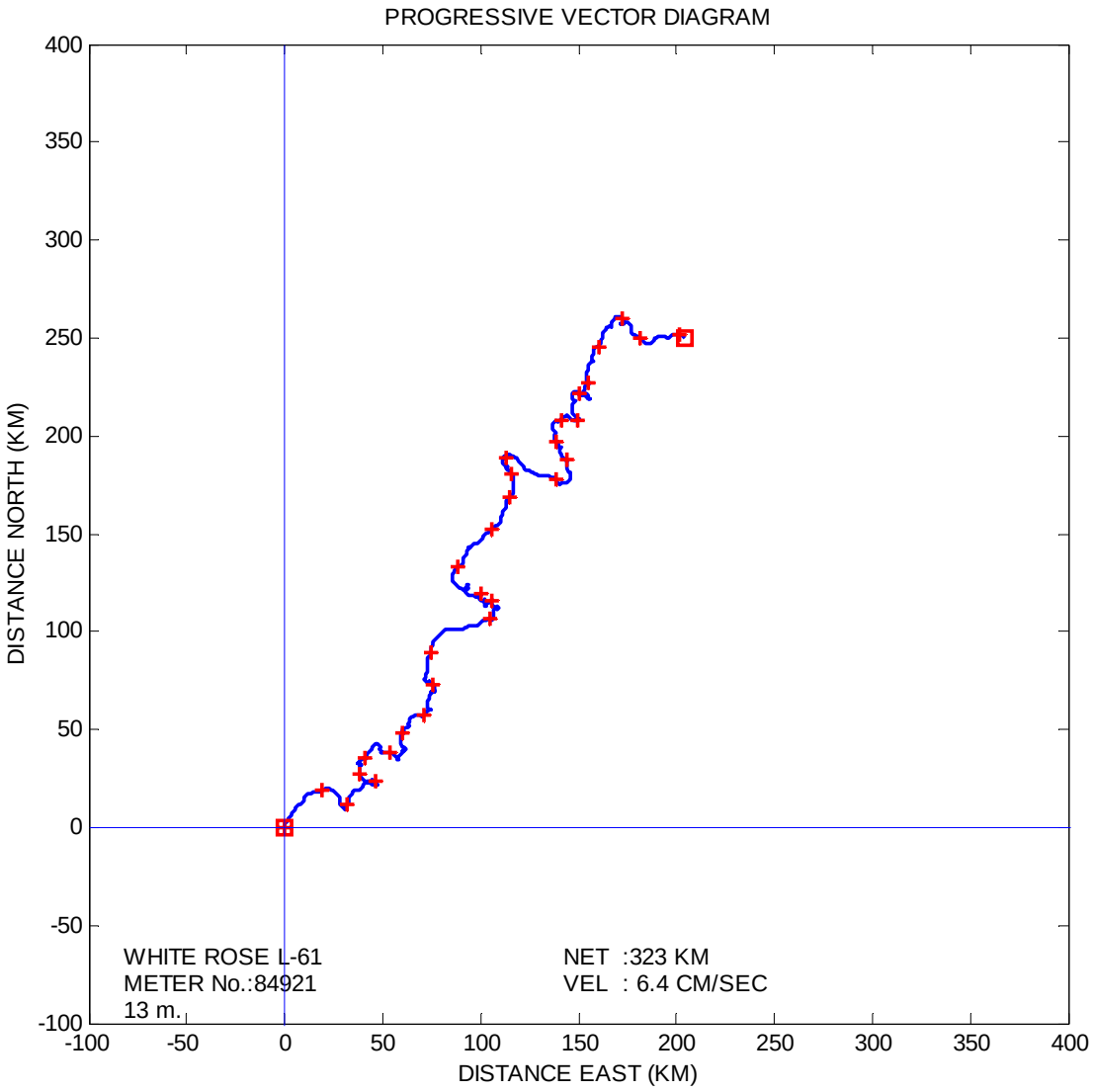

Figure C.8 Currents Near-surface from December to February, 1985 at White Rose L-61.

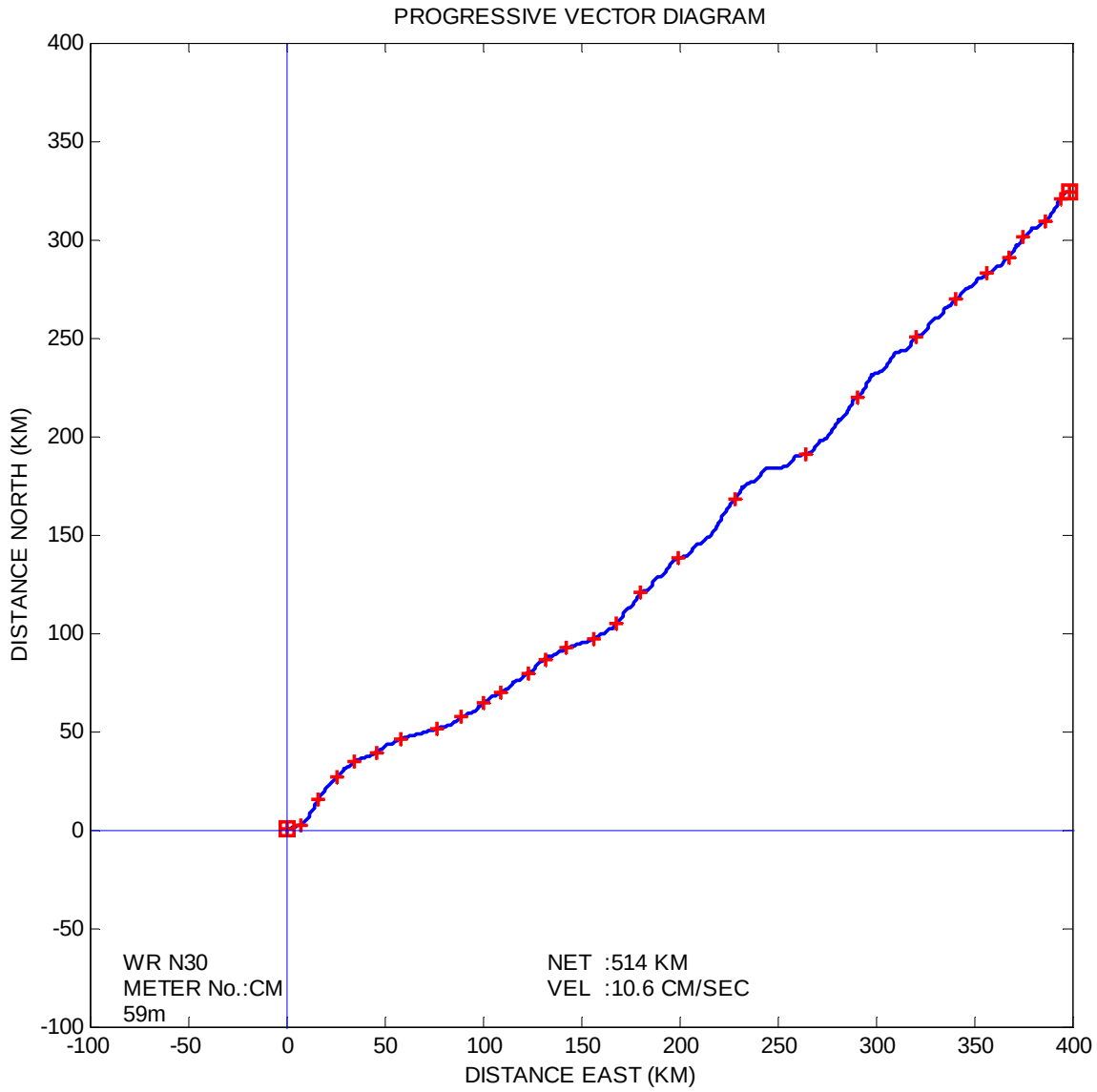

Figure C. 9 Mid-depth Currents from August to October, 1999 at White Rose N-30.

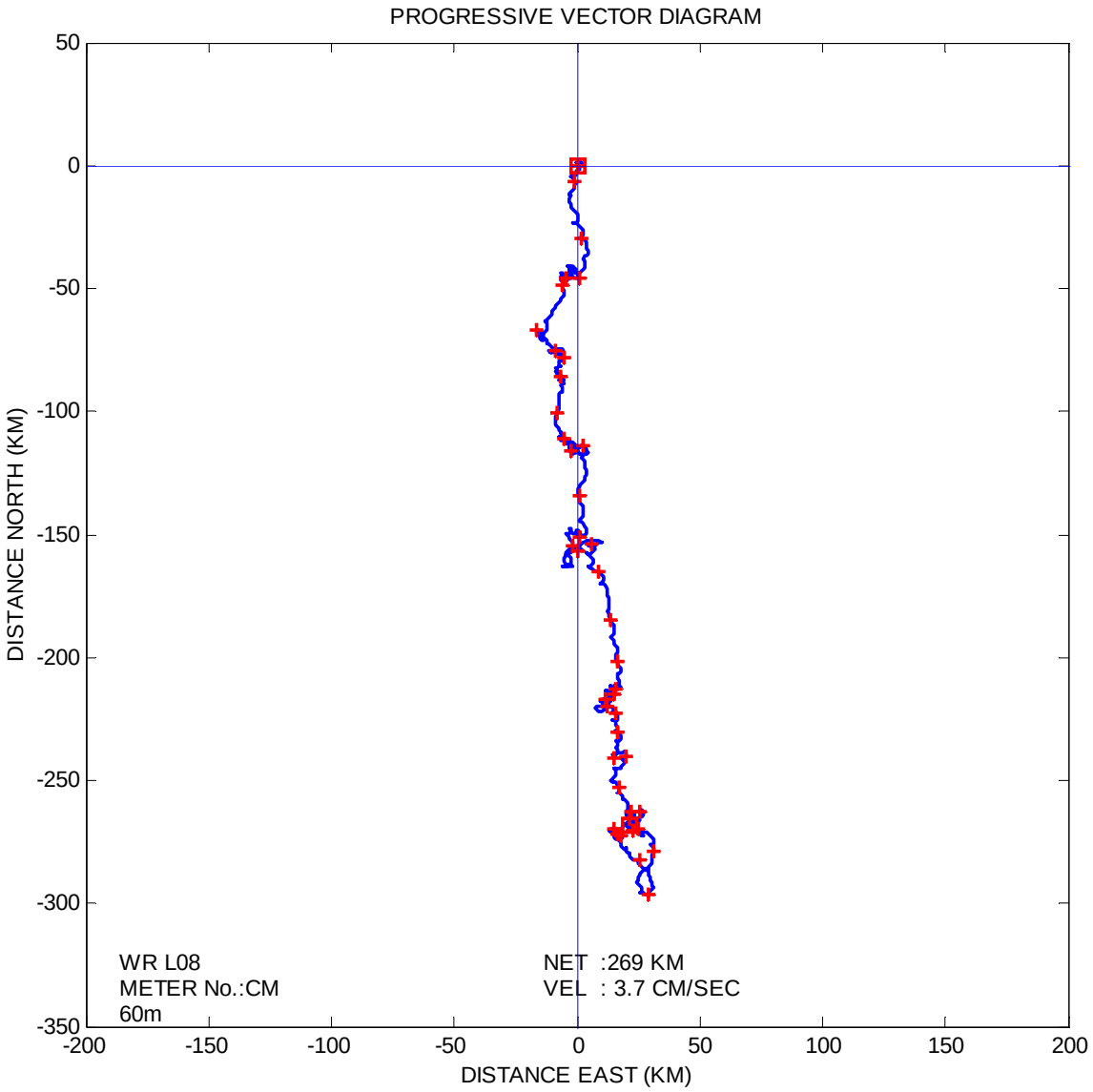

Figure C.10 Mid-depth Currents from March to June, 1999 at White Rose L-08.

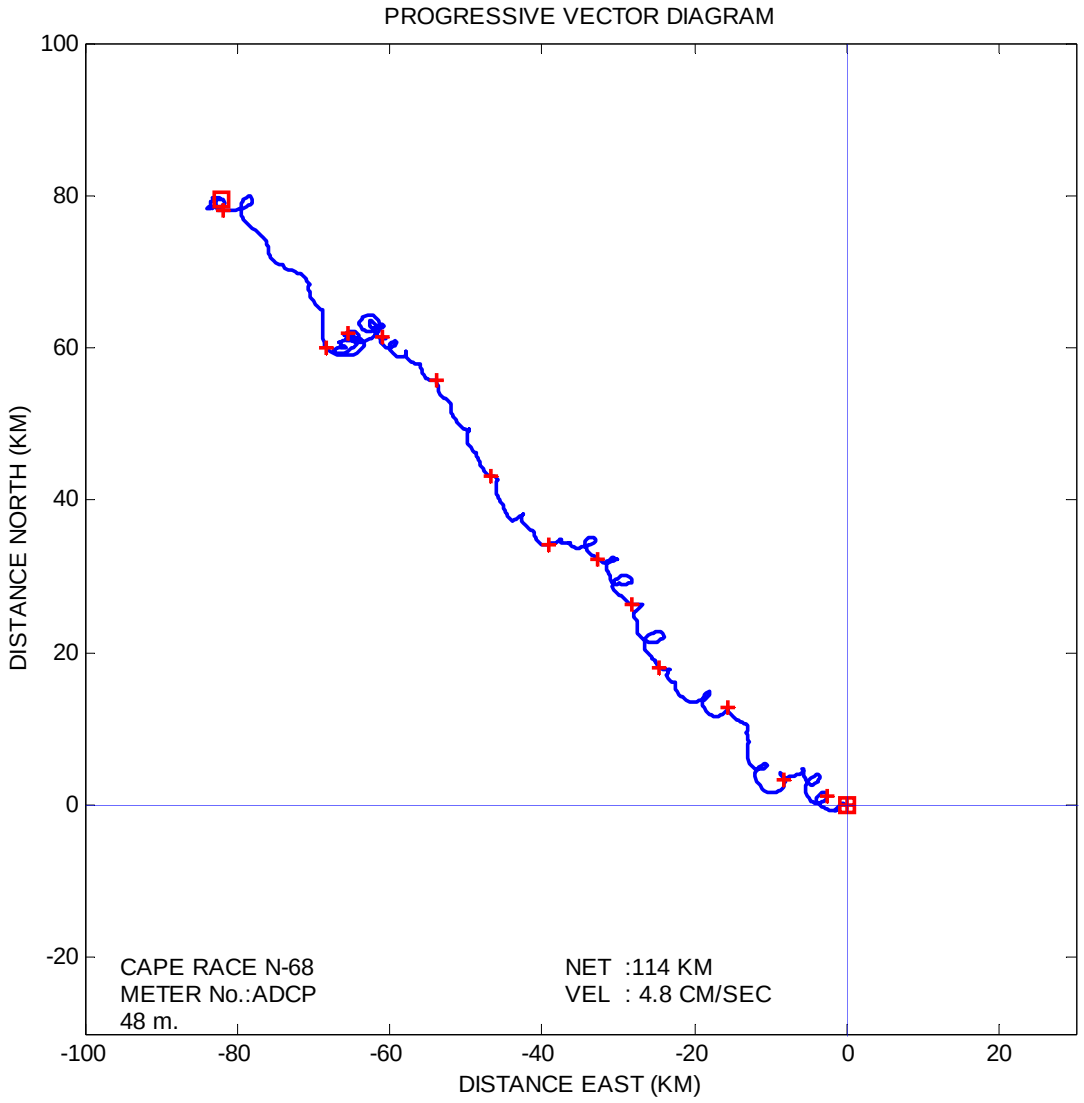

Figure C.11 Mid-depth Currents during July and August, 2000 at Cape Race N-68.

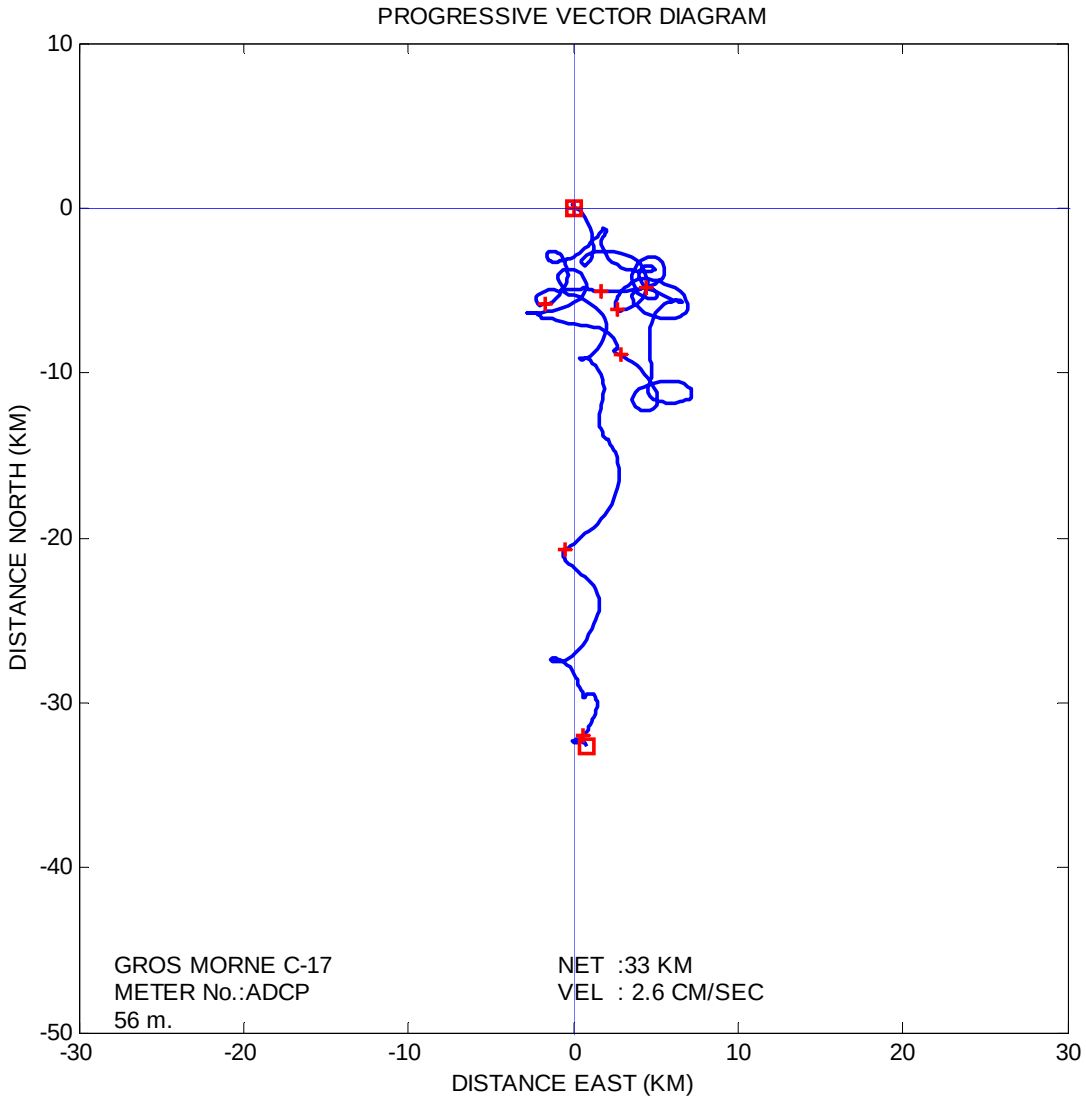

Figure C.12 Mid-depth Currents during September, 2002 at Gros Morne C-17.

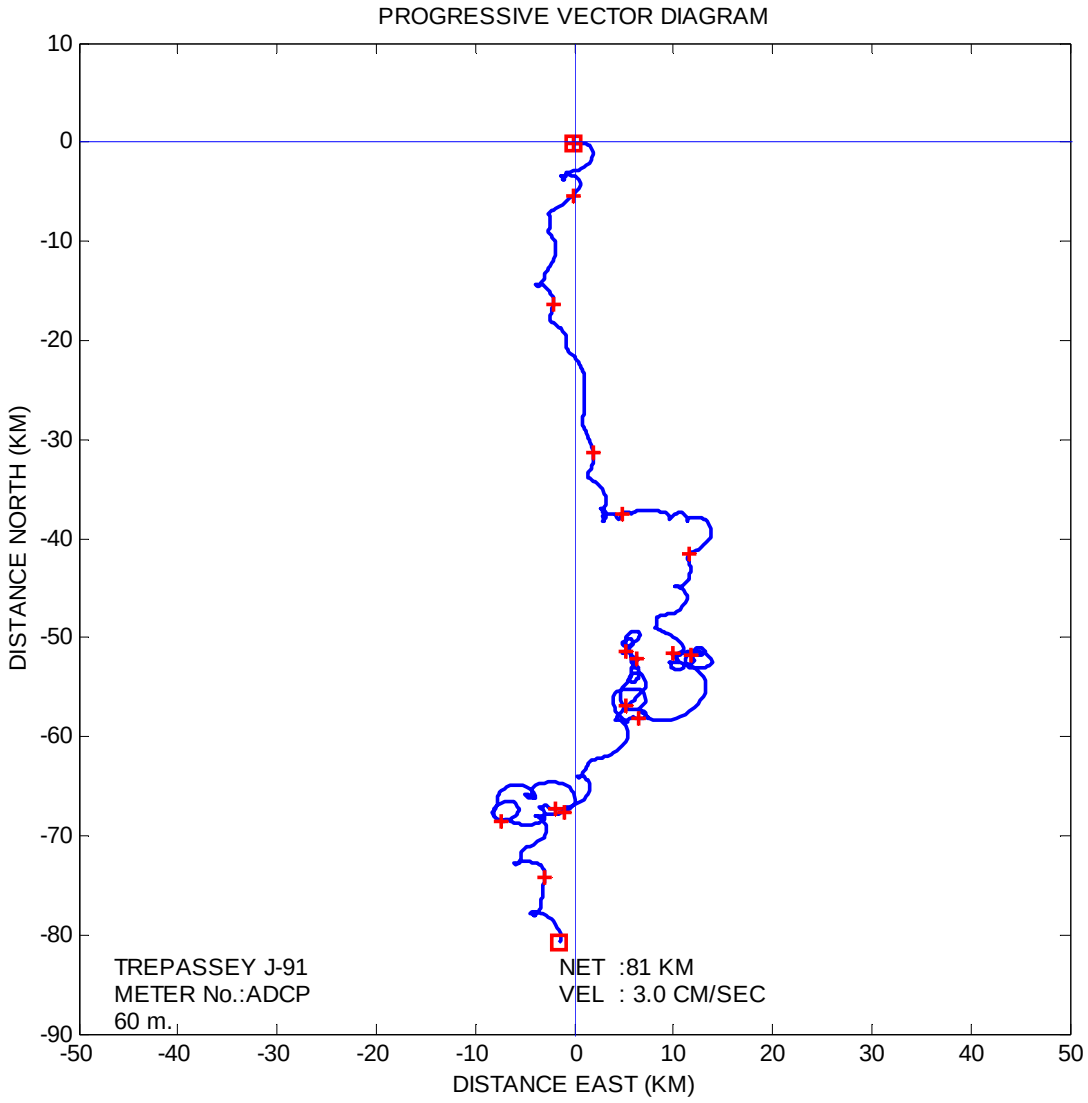

Figure C.13 Mid-depth Currents during July and August, 2002 at Trepassey J-91.

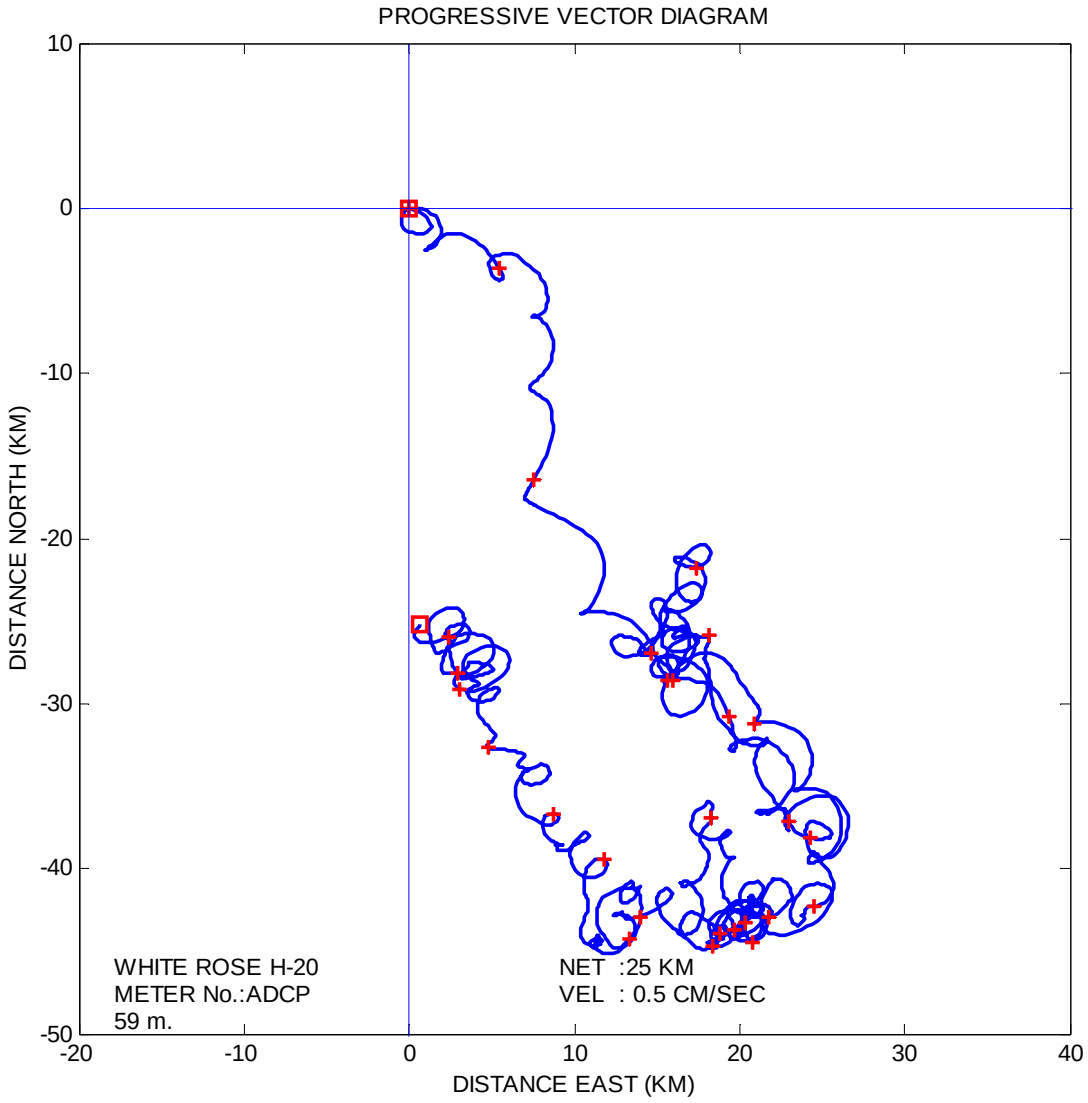

Figure C.14 Mid–depth Currents from May to July, 2000 at White Rose H-20.

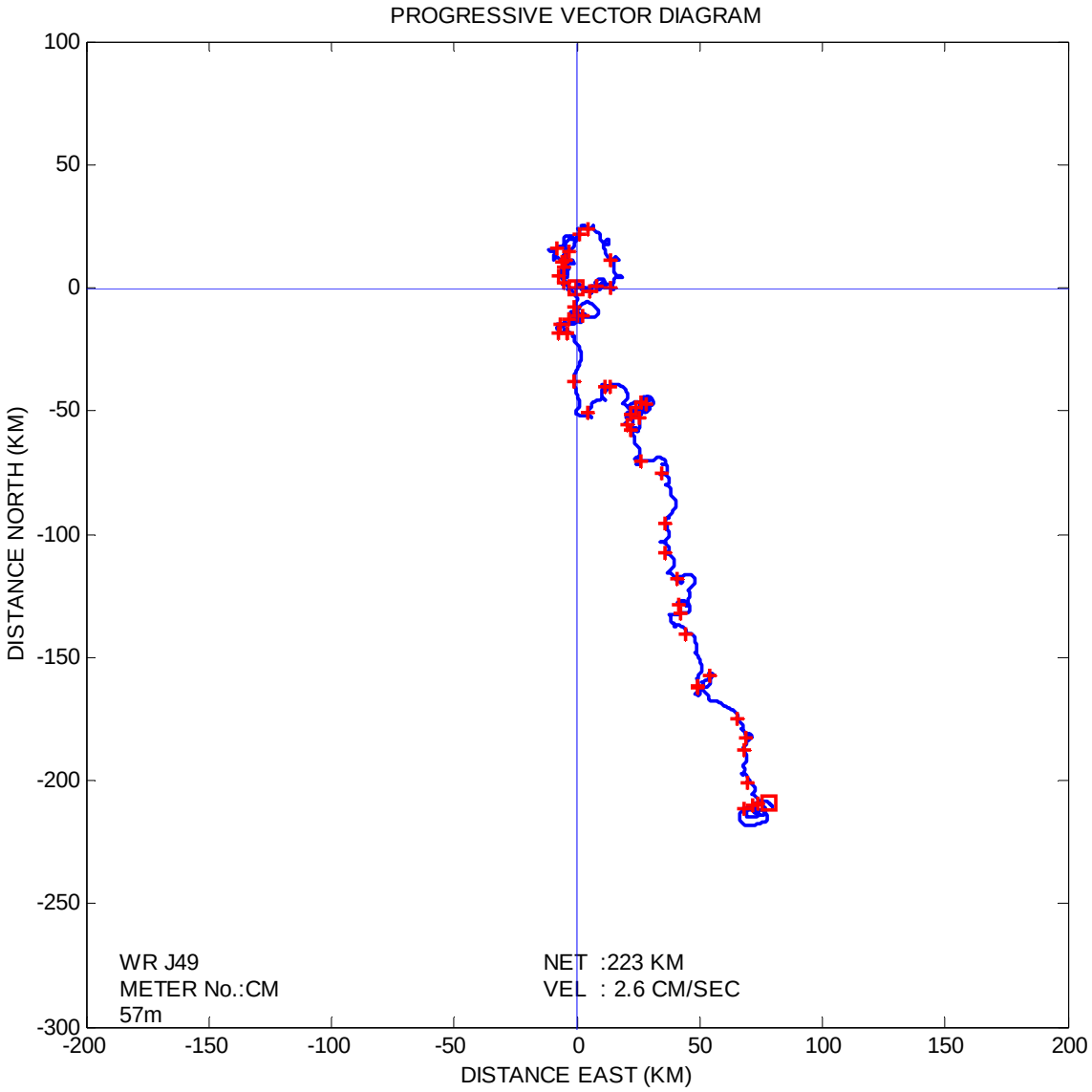

Figure C.15 Mid-depth Currents from August to November, 1985 at White Rose J-49.

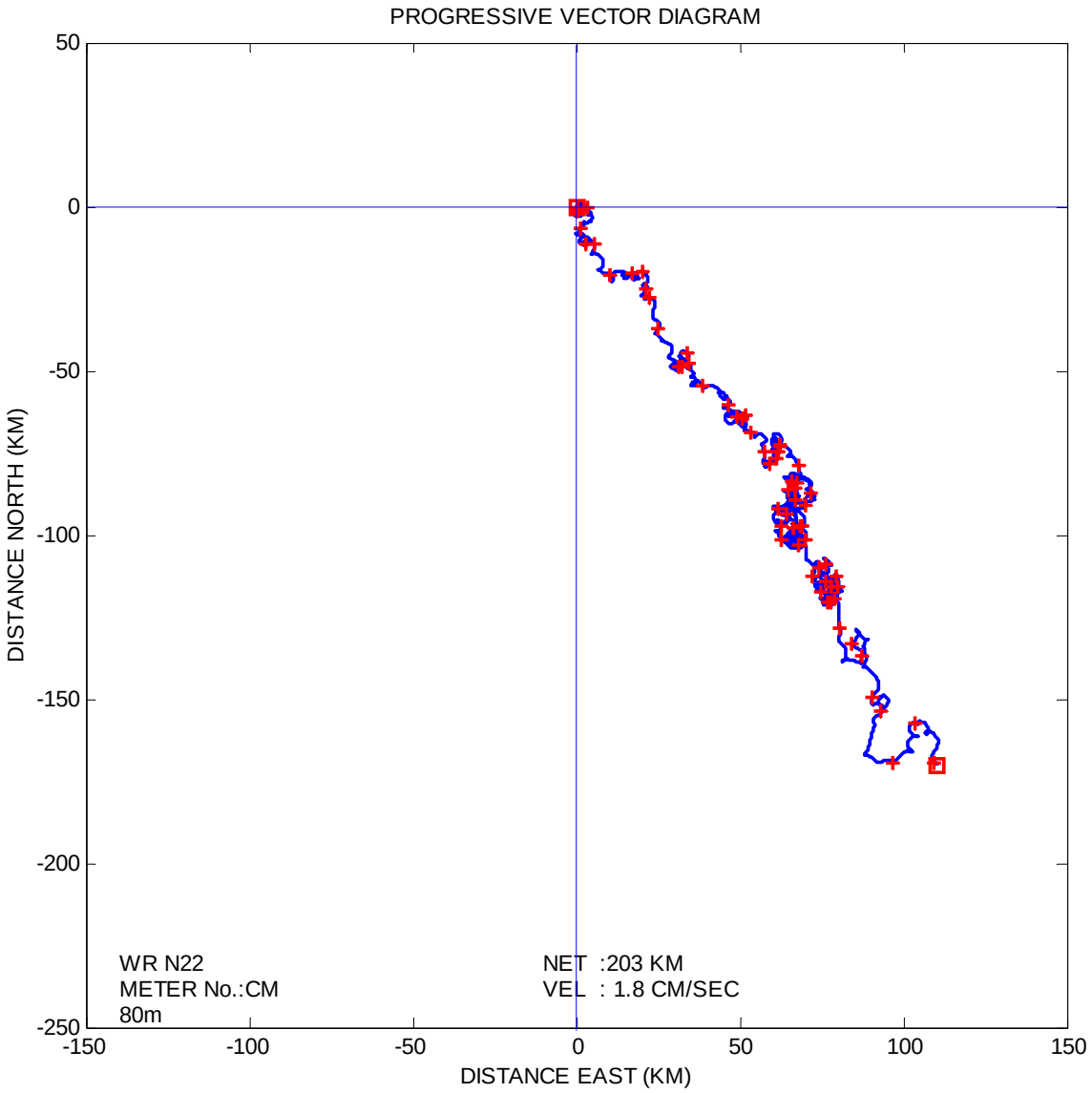

Figure C.16 Mid-depth Currents from July to November, 1988 at White Rose N-22.

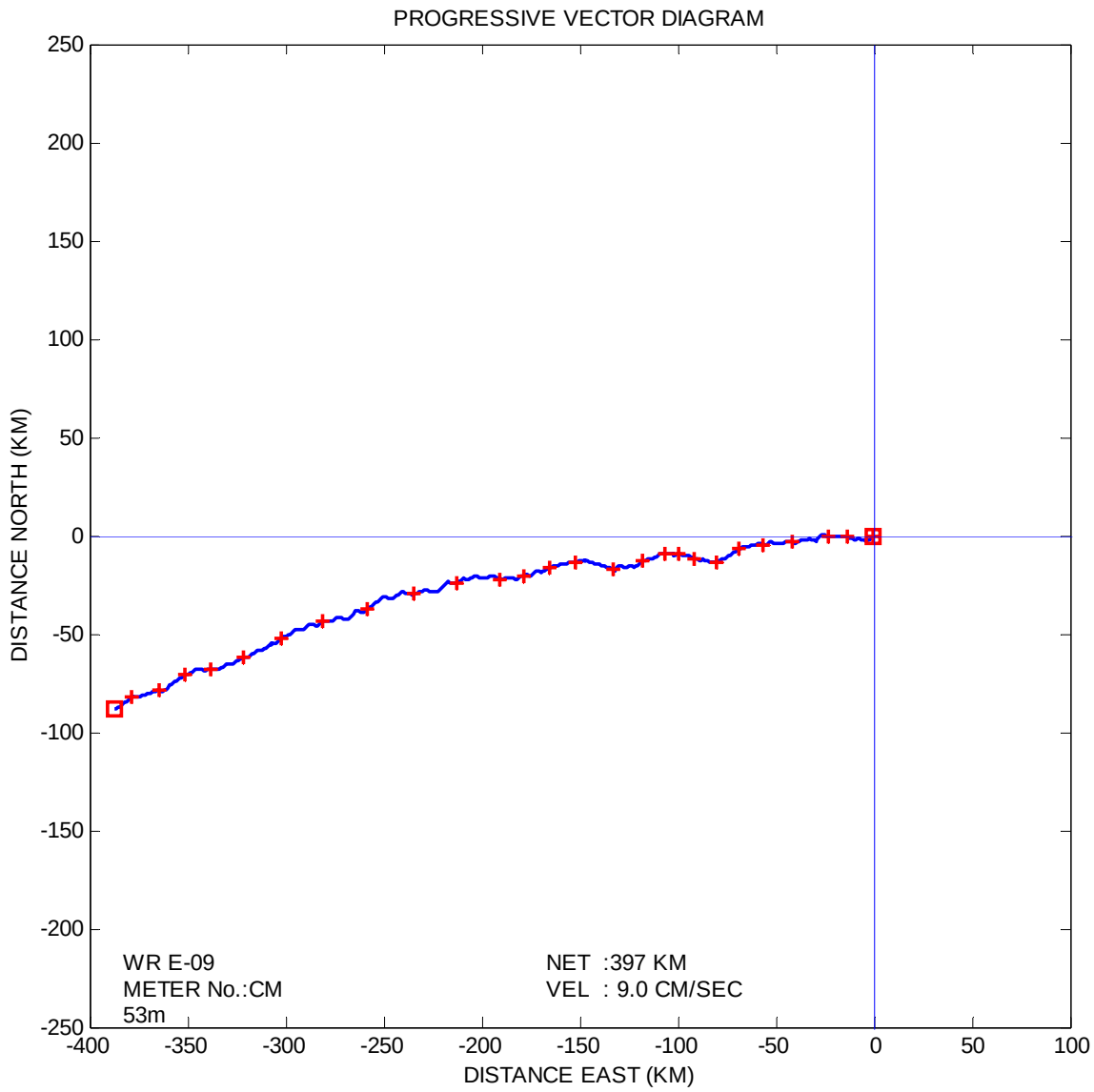

Figure C.17 Mid-depth Currents during September and October, 1987 at White Rose E-09.

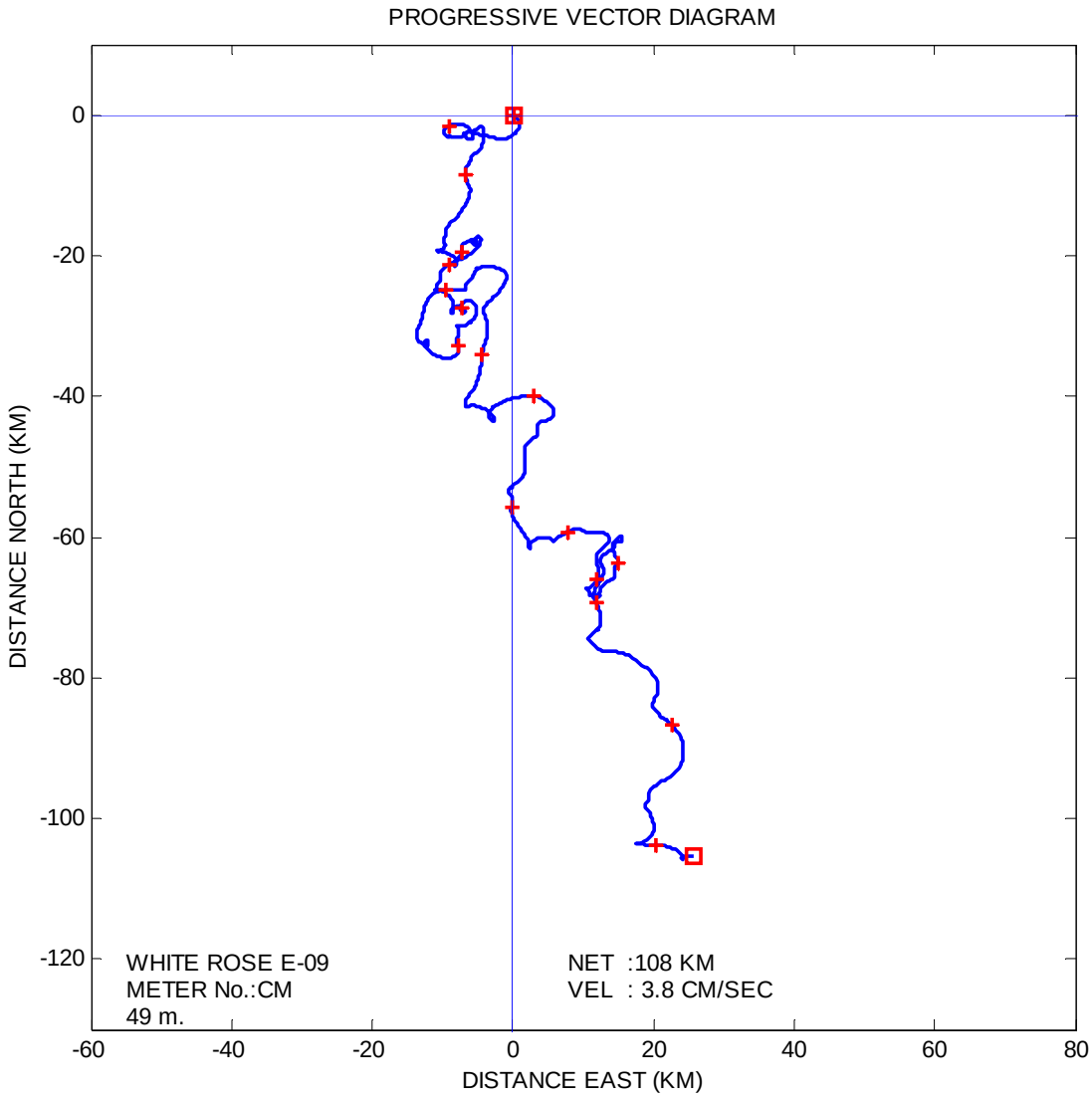

Figure C.18 Mid-depth Currents during January and February, 1988 at White Rose E-09.

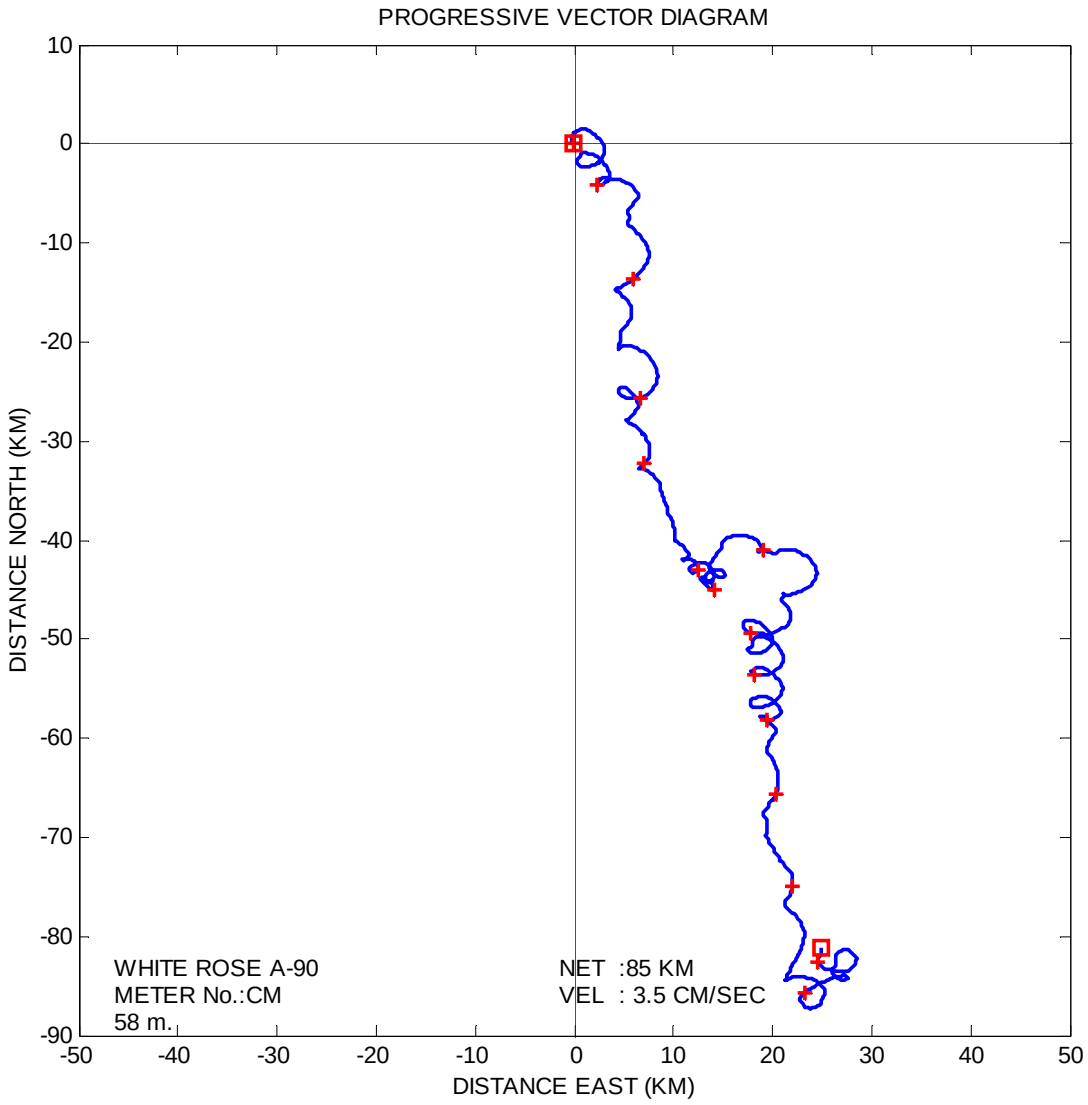

Figure C.19 Mid-depth Currents during July and August, 1988 at White Rose A-90.

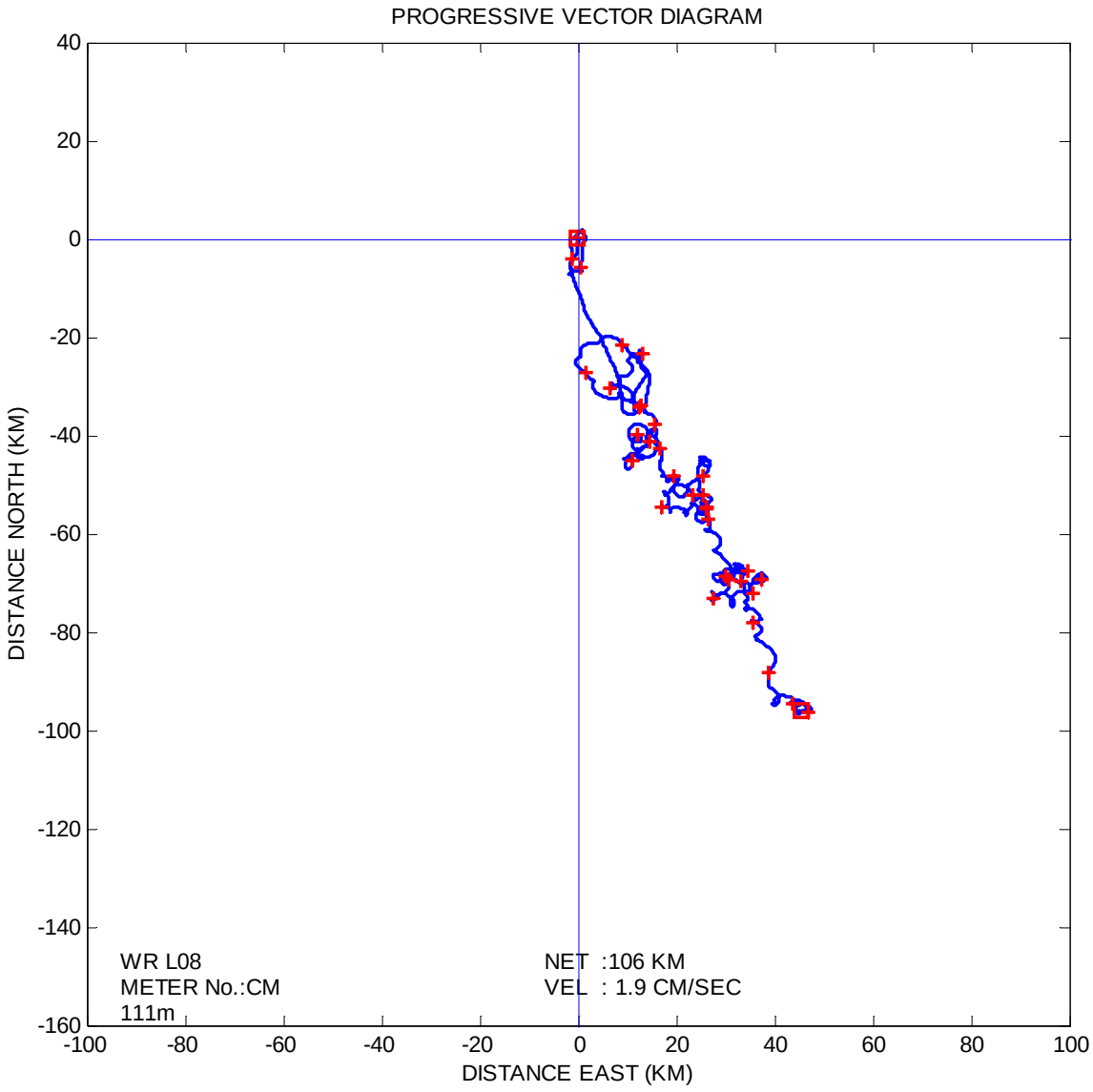

Figure C.20 Near-bottom Currents from March to June, 1999 at White Rose L-08.

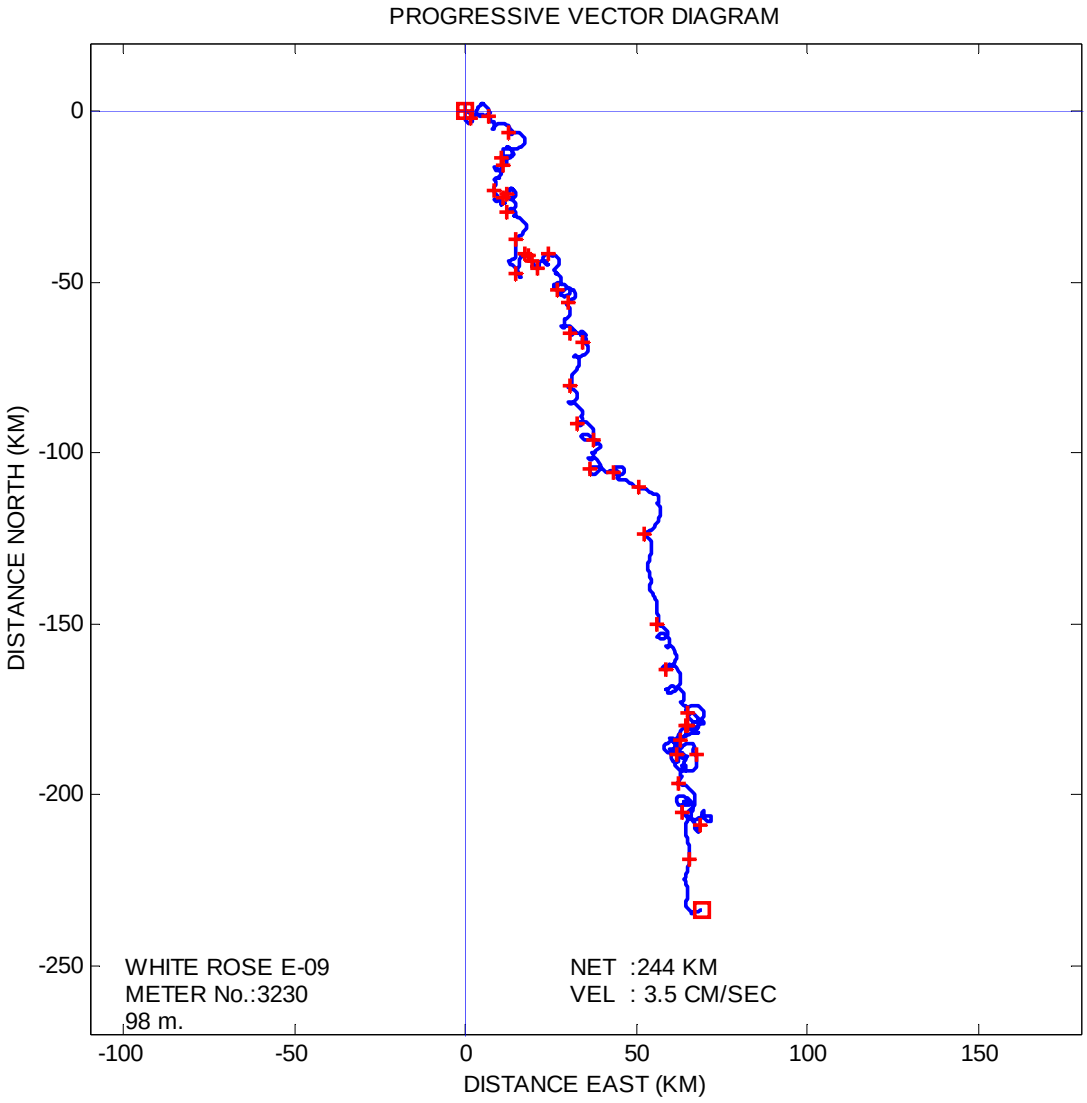

Figure C.21 Near-bottom Currents during May to July, 1988 at White Rose E-09.

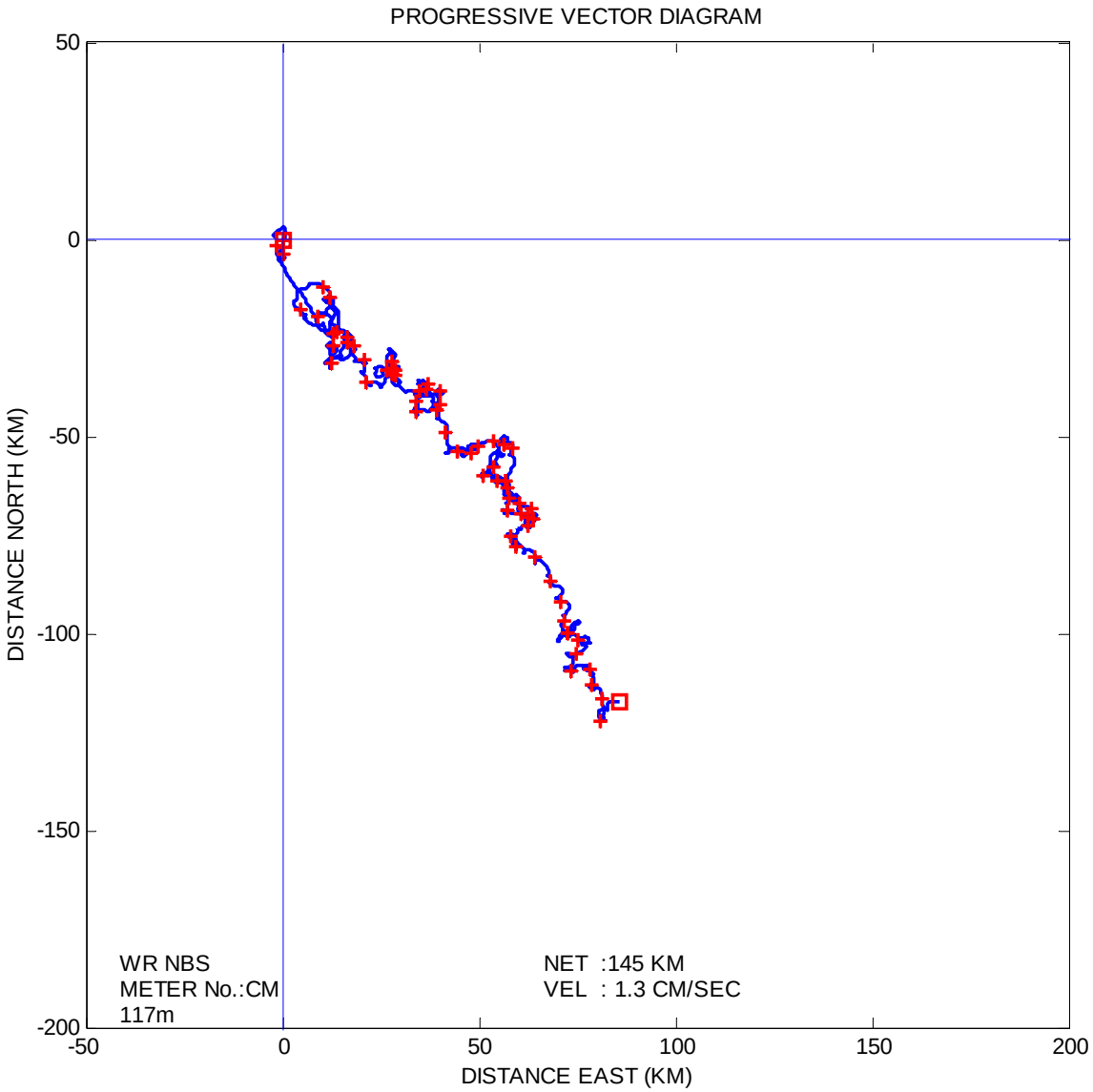

Figure C.22 Near-bottom Currents from April to August, 2002 at White Rose.

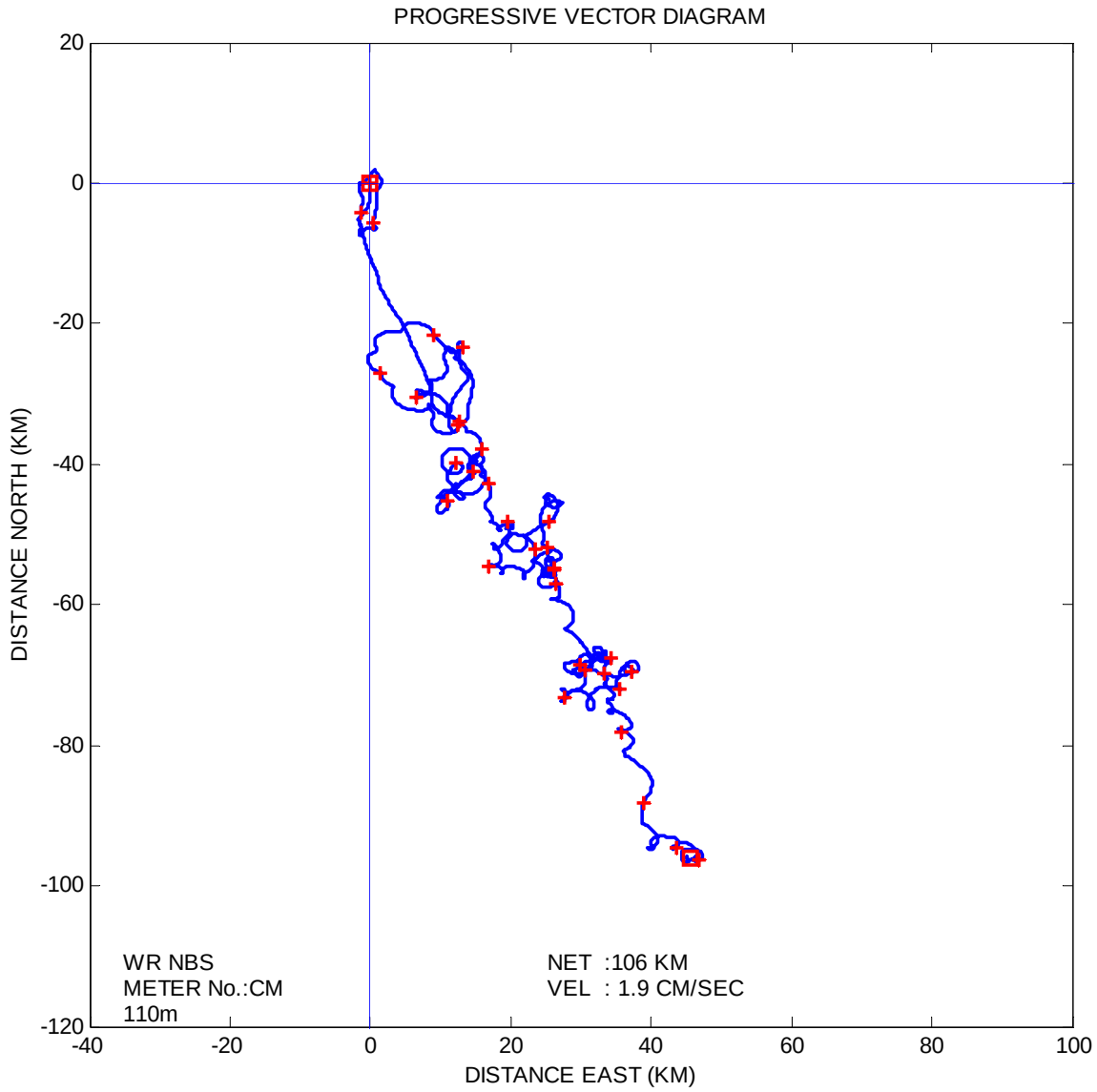

Figure C.23 Near-bottom Currents from April to June, 2002 at White Rose.

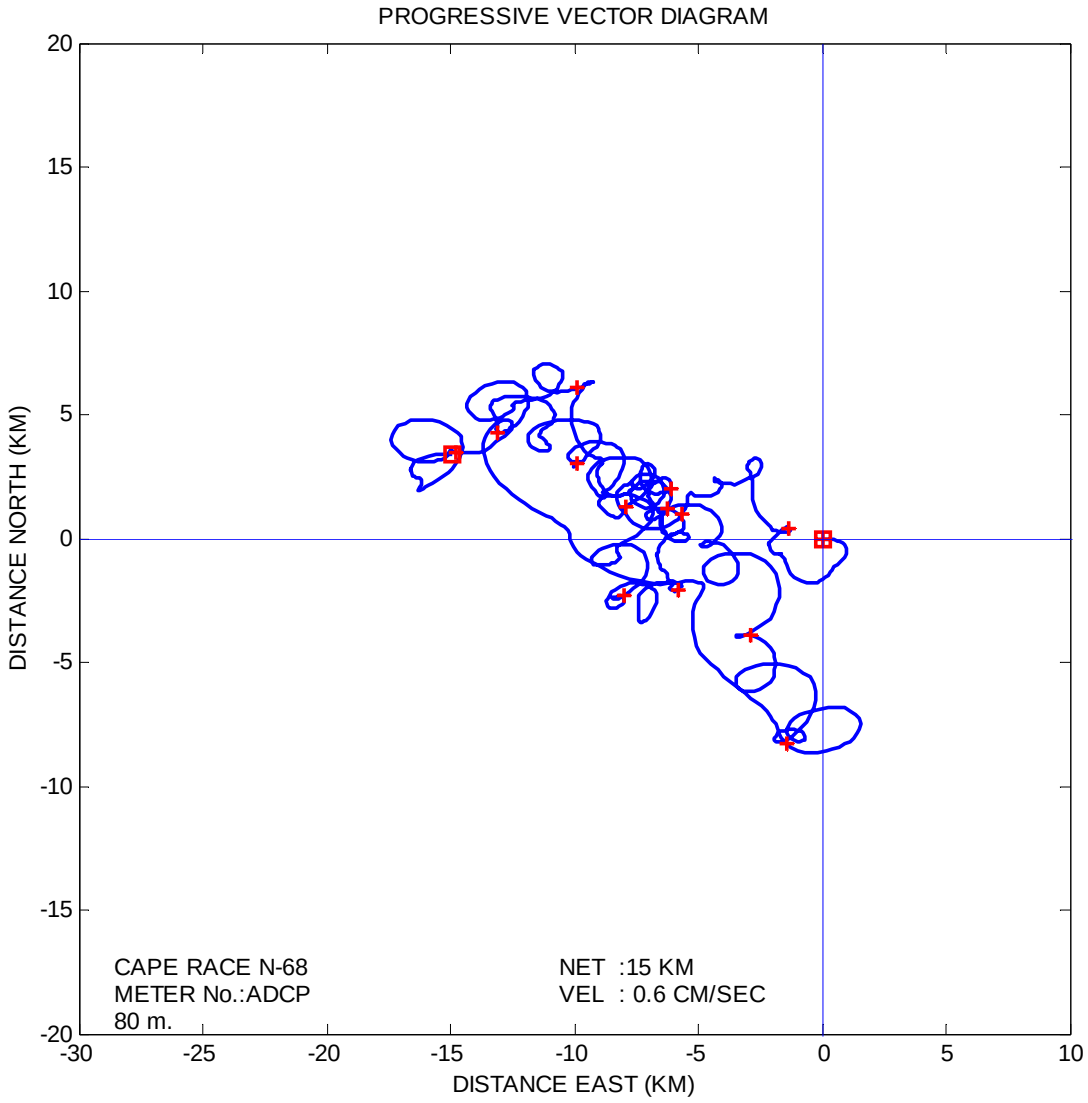

Figure C.24 Near-bottom Currents during July at Cape Race N-68.

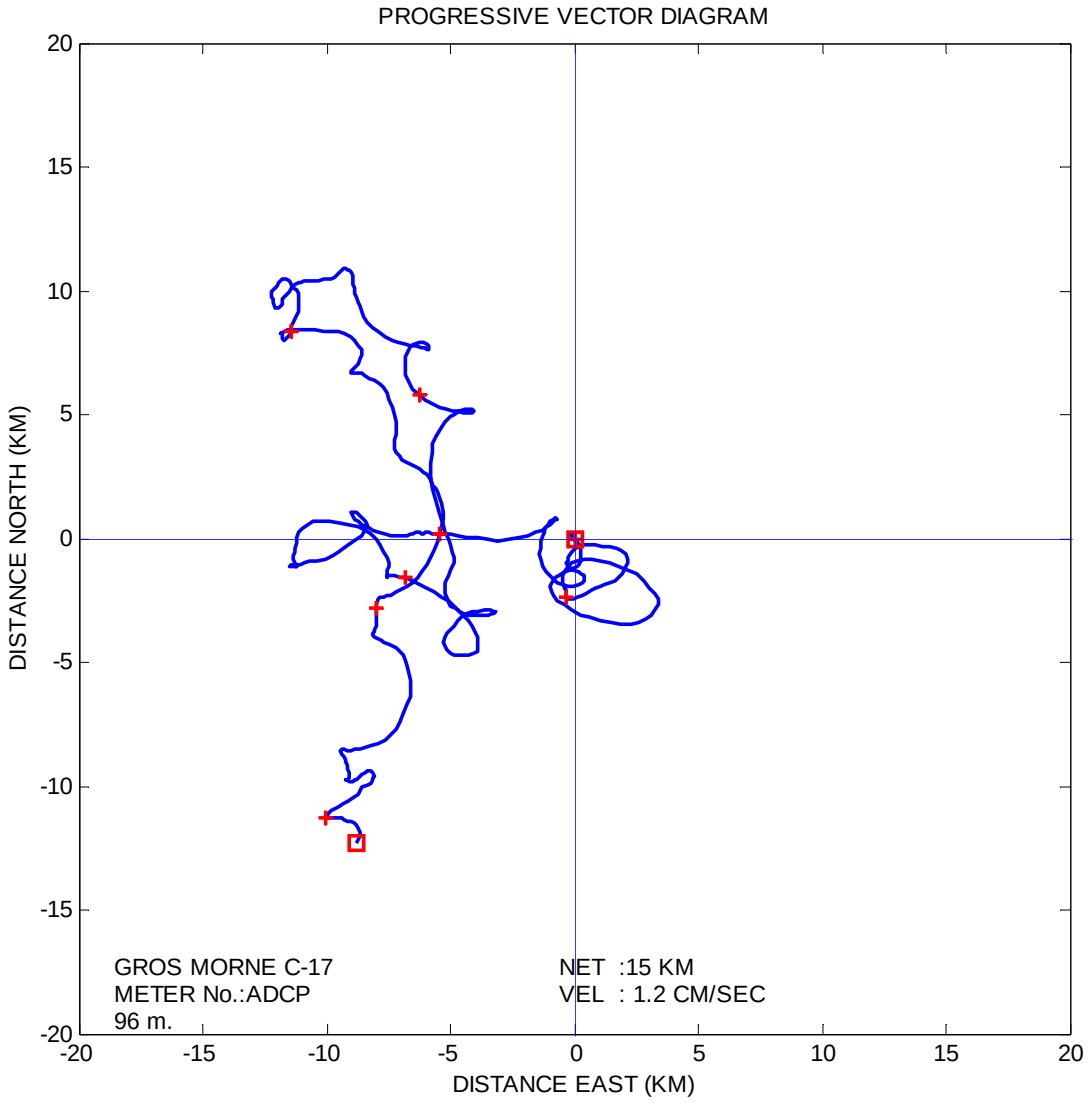

Figure C.25 Near-bottom Currents during September, 2002 at Gros Morne C-17.

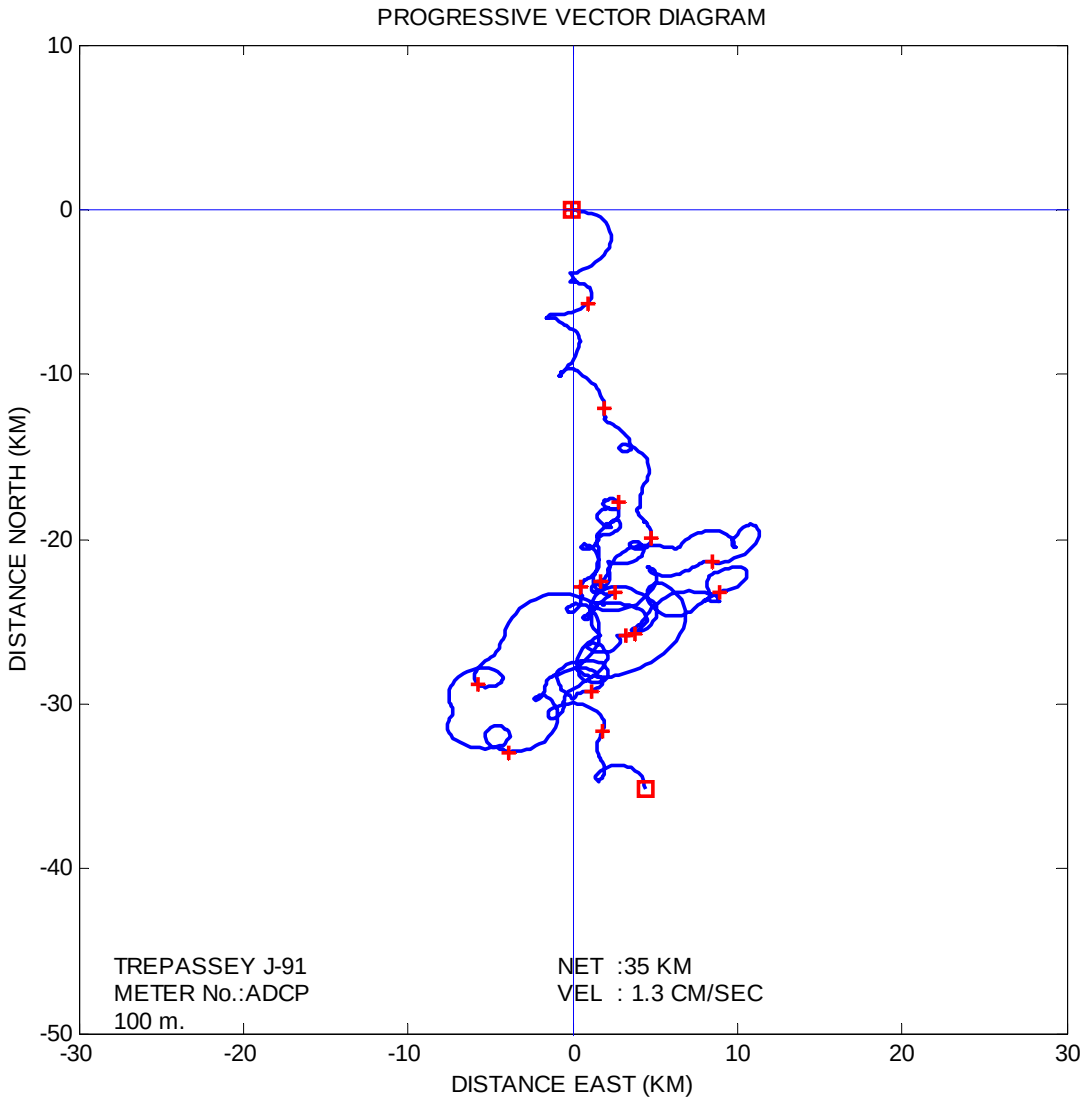

Figure C.26 Near-bottom Currents during August. 2002 at Trepassey J-91.

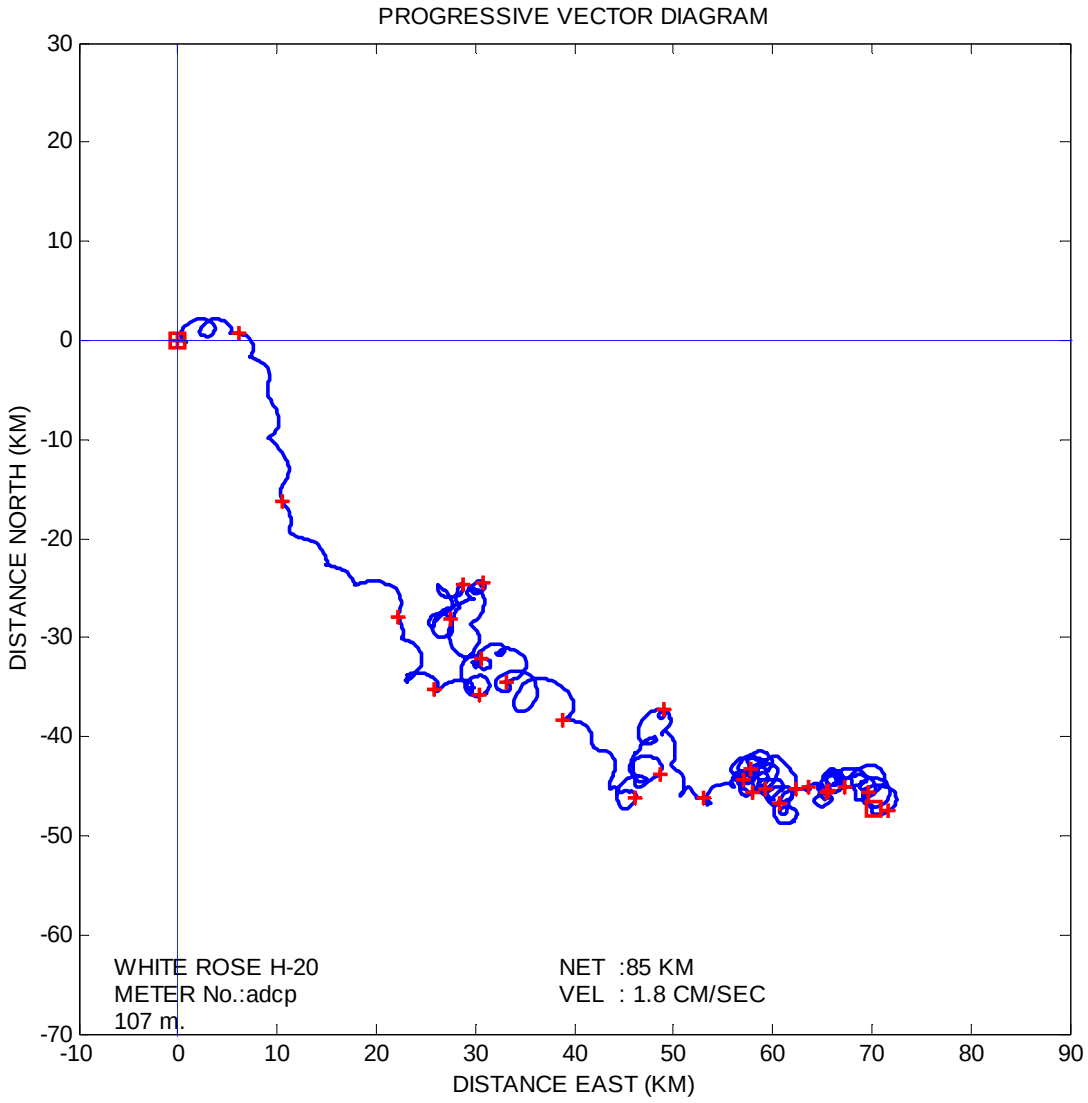

Figure C.27 Near-bottom Currents from May to July, 2000 at White Rose H-20.

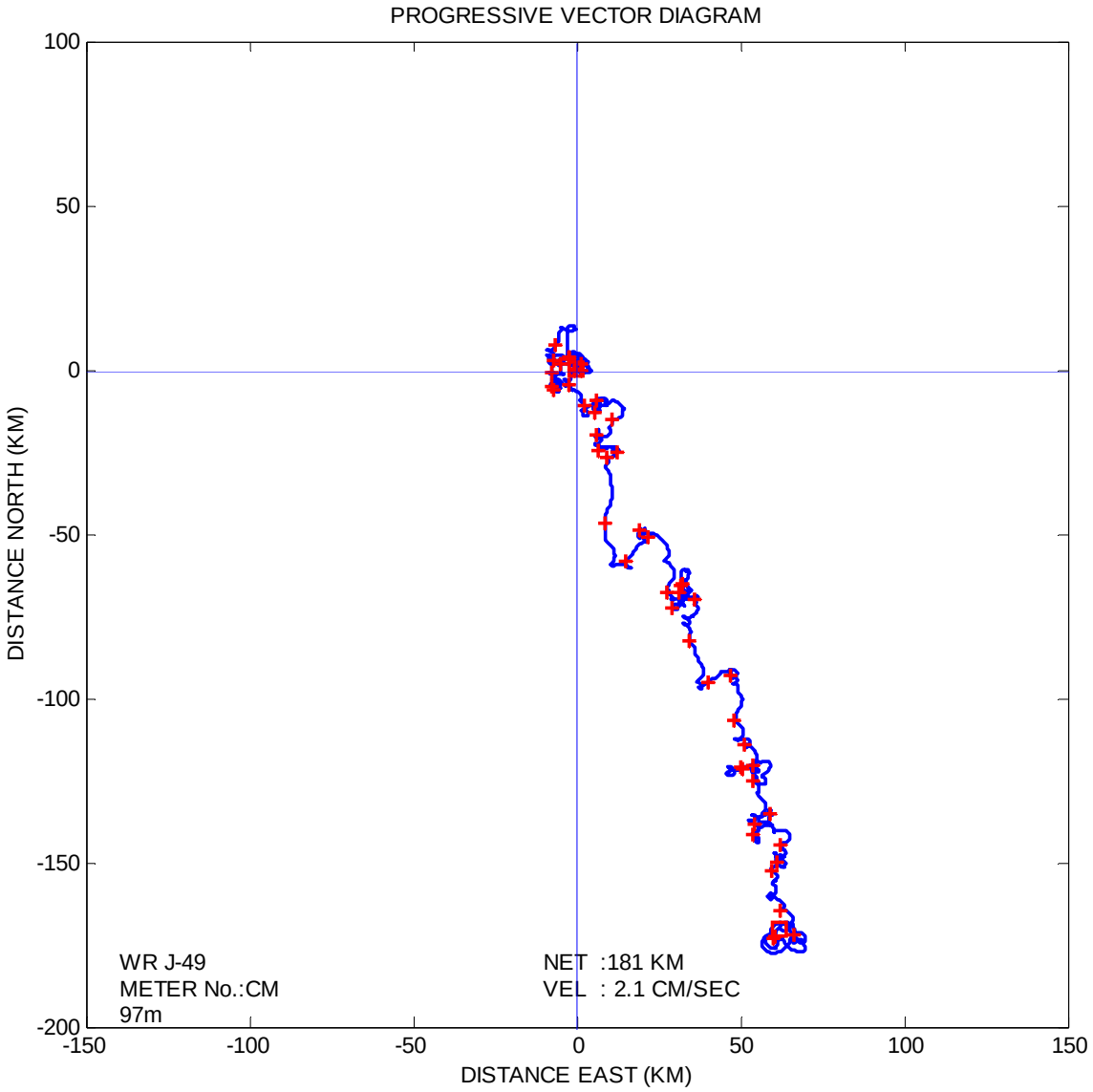

Figure C.28 Near-bottom Currents from August to November, 1985 at White Rose J-49.

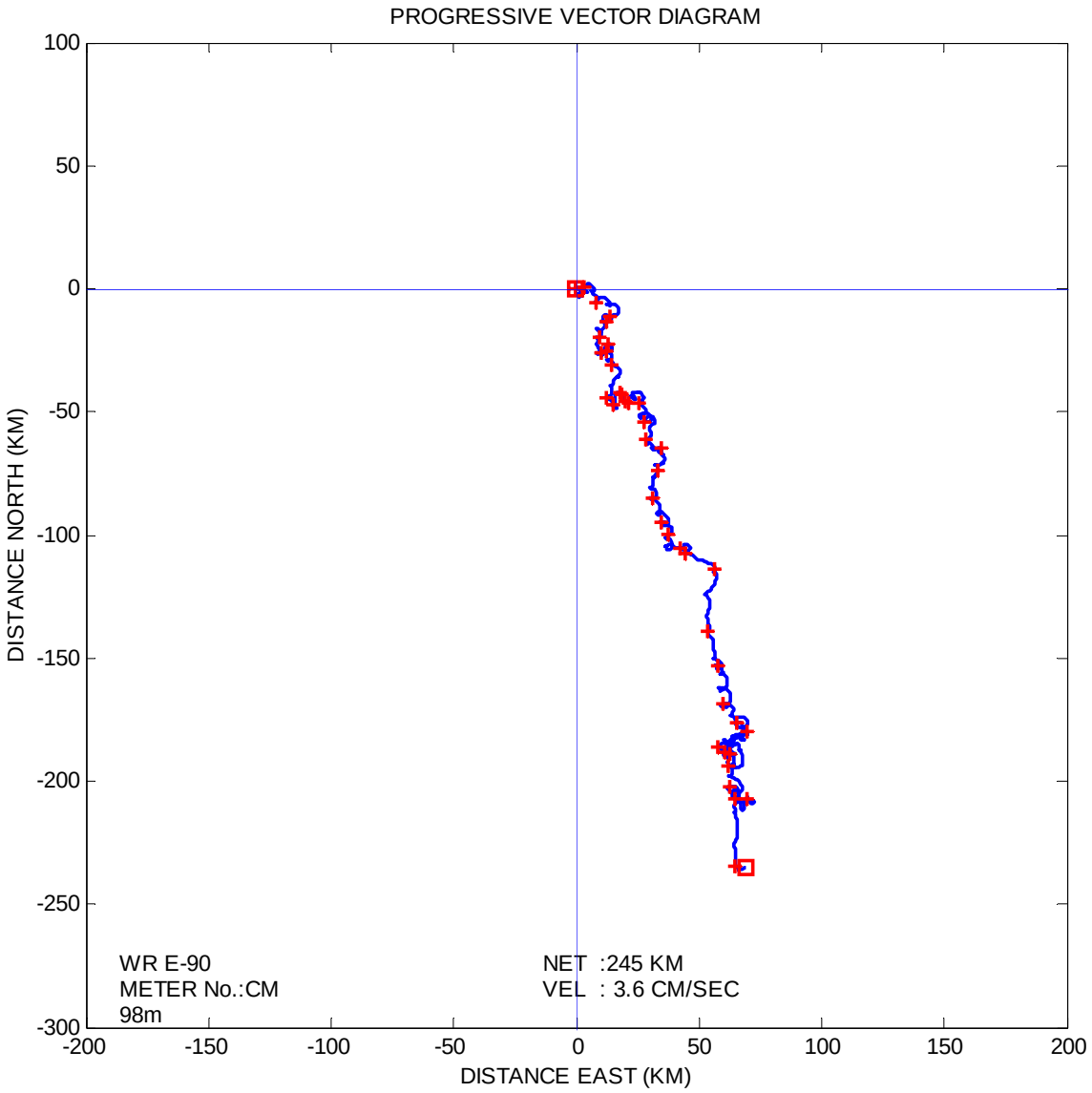

Figure C.29 Near-bottom Currents from September to November, 1987 at White Rose E-09.

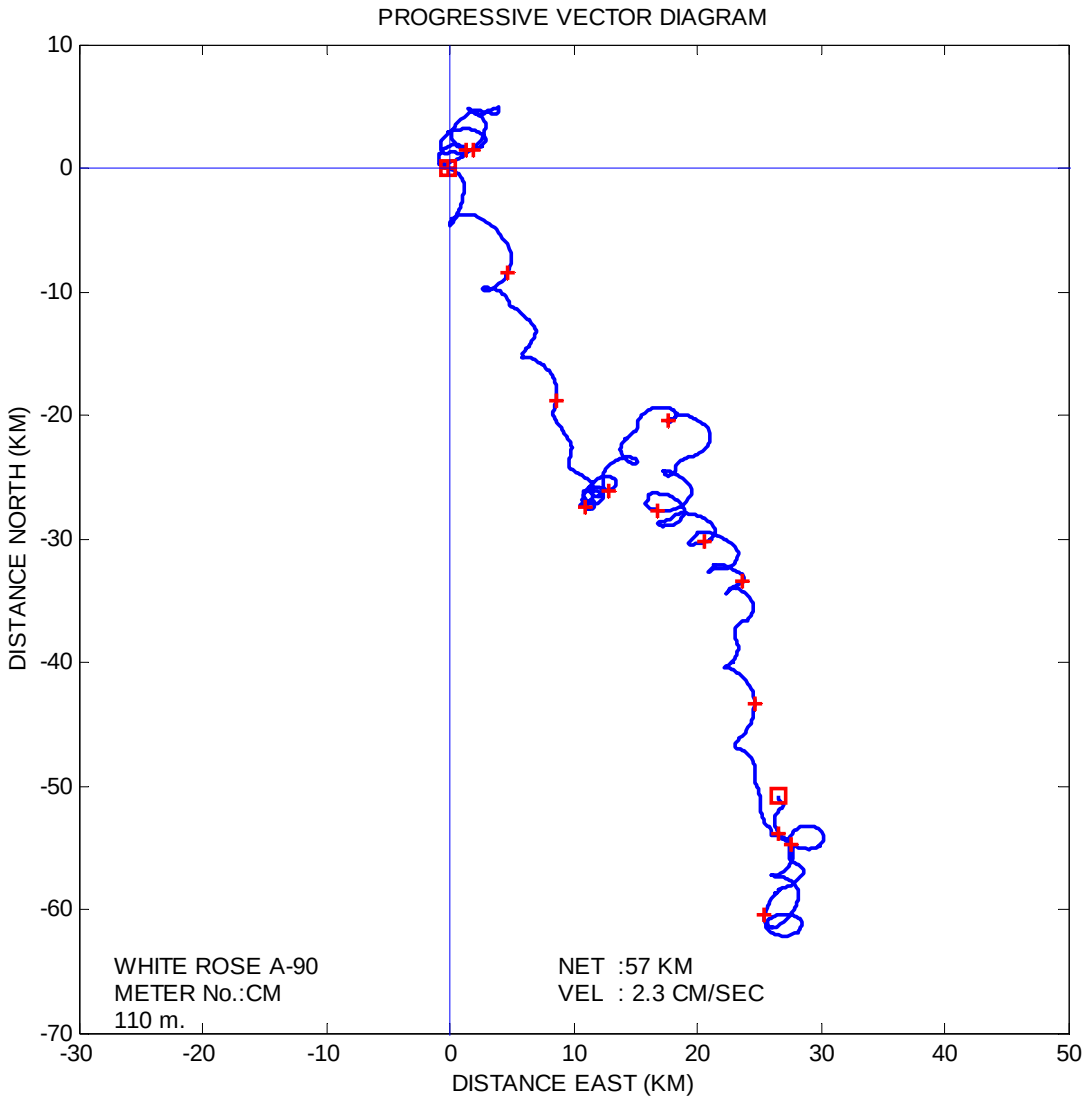

Figure C.30 Bottom Currents during January and February, 1988 at White Rose E-09.

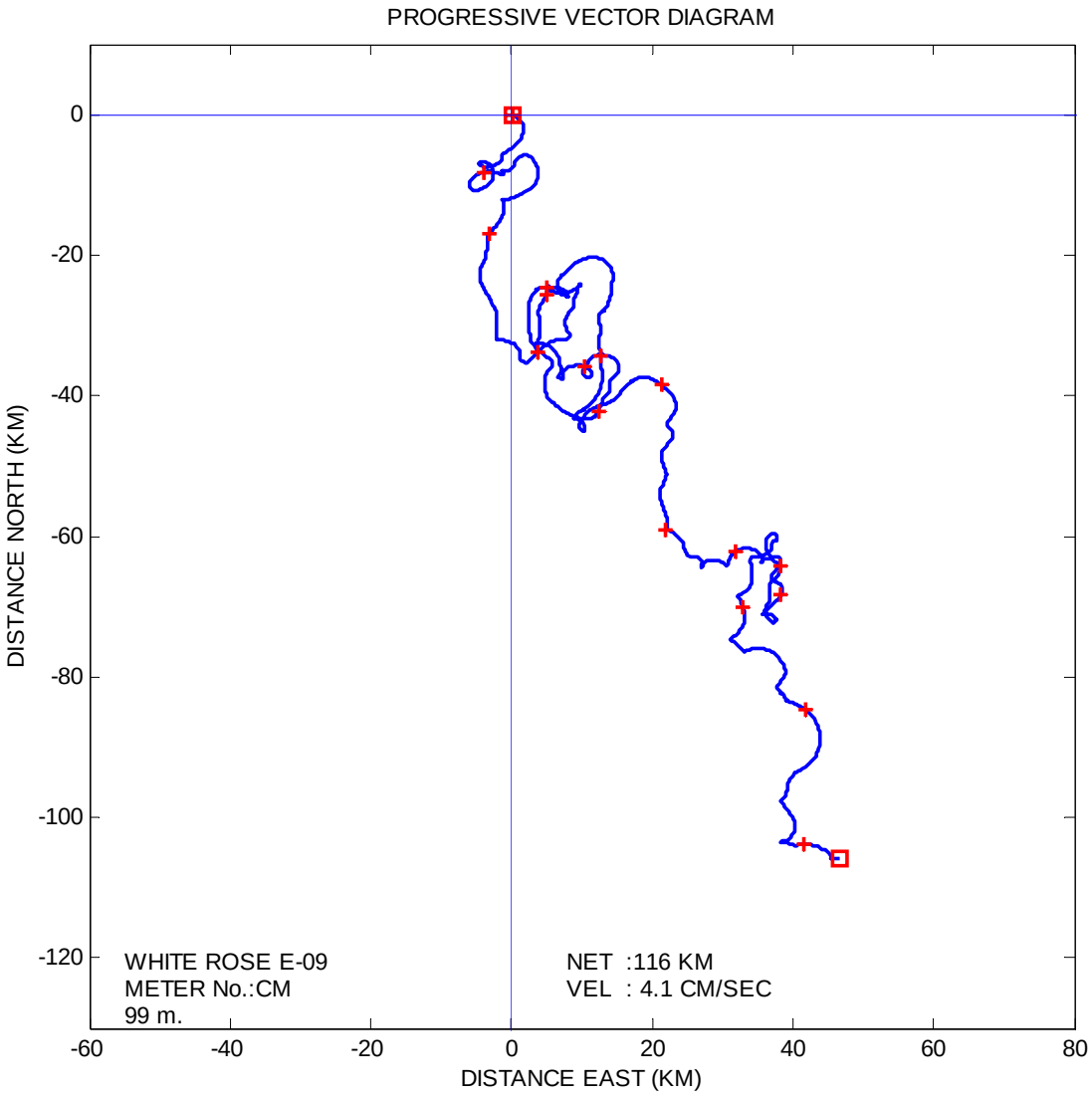

Figure C.30 Bottom Current during July and August, 1988 at White rose A-90.